Chapter 1

Background and Significance

How does pH modulate the solution-to-membrane conformational change of Bcl-X_LΔTM *in vitro*? This is the central question that has been addressed in this research project. The regulation of the solution-to-membrane conformational change of Bcl-X_LΔTM is critical for the process of programmed cell death. This introductory chapter begins with a description of the programmed cell death and its biological significance, narrows the focus down to the roles of the Bcl-2 family proteins and finally draws attention to the roles of Bcl-X_L, a member of the Bcl-2 family in regulating programmed cell death. The chapter ends with a description of the specific goals of the research project and the rationale behind the design of the research plan.

The process of programmed cell death

The genetically programmed method of cell death (death "from inside out") was well known since the 1960s but it wasn't until later that it was recognized as a fundamentally different process from necrosis. The characterization of programmed cell death due to a breakdown of cellular energy supply and failure of homeostasis wasn't appreciated until later. The term apoptosis is of Greek origin and literally means "the falling of a petal from a flower or a leaf from a tree". In the biological context, it refers to the cells dying by programmed cell death falling off the supporting tissue structures to which they belong to. The term apoptosis describes the programmed cell death process characterized based on the following morphological observations (Wyllie, 1994):

(i) shrinkage of cell volume

(ii) disruption of the cytoskeleton

(iii) progressive chromatin condensation

(iv) fragmentation of the DNA

(v) membrane blebbing

(vi) loss of mitochondrial function

(vii) exposure of cell surface signals for removal of the dying cell by phagocytes.

The interval between commitment to programmed cell death and the appearance of the morphological hallmarks is variable depending on the cell type but from the initial appearance of these morphological changes to removal by phagocytosis could be complete in 1 or 2 hours (Wyllie, 1994).

Apoptosis is essential to the survival of the multicellular organism, critical for maintaining homeostasis. It also plays a significant role during development. Dysregulation of cell death, developmental or damage-induced, has been shown to contribute to various diseased states (Green and Kroemer, 2004). The delicate balance between cell death and cell survival is carefully regulated and is essential for proper homeostasis (Rathmell and Thompson, 2002). Too much cell death has been shown to result in degenerative diseases like Alzheimer's, muscular dystrophy, amyotrophic lateral sclerosis (ALS) and AIDS (Nijhawan et al., 2000; Rudin and Thompson, 1997). On the other hand, too little cell death contributes to diseases of over proliferation such as cancer and AIDS (Reed, 1999).

In the invertebrate nematode *Caenorhabditis elegans*, during the development of the adult hermaphrodite worm, 131 cells undergo apoptosis leaving the adult with 959 cells (Hengartner and Horvitz, 1994; Liu and Hengartner, 1999). As in invertebrates, developmental cell death is regulated at the transcriptional level in vertebrates, in the regression of the tadpole tail and in the classical example of interdigital cell death (Meier

et al., 2000). The general mechanism for developmental biology in metazoans can be described as follows: an over-production of cells followed by apoptotic culling of unwanted cells to form the end product, the functioning adult organism (Hengartner, 2000). Having shown the importance of apoptosis for development, homeostasis and survival, I will now review the current understanding of the molecular pathways of apoptosis.

The pathways of apoptosis

Most of the morphological changes defining apoptotic cell death are caused by the action of the downstream effector molecules called caspases. Caspases are cysteine dependent aspartic proteases that cleave target proteins at specific sites typically next to aspartate residues (Earnshaw et al., 1999). Caspases involved in apoptosis are present as zymogens which are activated when cell death is triggered. The activation of caspases and their action on cellular substrates like nuclear lamins and nucleases results in the manifestation of the morphological hallmarks ascribed to an apoptotic cell death. This has led to the downstream caspases to be viewed as the executioners in the process of programmed cell death.

In the mitochondrial pathway of apoptosis shown in Figure 1.1, it is thought that the critical step that commits a cell to undergo cell death is the release of a small globular protein, cytochrome c into the cytosol (Liu et al., 1996). Cytochrome c is localized in the intermitochondrial membrane space and functions in oxidative phosphorylation. When cytochrome c is released into the cytosol during apoptosis, it forms a protein complex with an adaptor protein, Apaf-1 and procaspase-9 (Li et al., 1997). This complex

formation results in the activation of procaspase-9 (Li et al., 1997). The activation of procaspase-9 to form caspase-9 leads to the activation of other downstream caspases in an amplification process that ultimately results in cell death (Earnshaw et al., 1999; Li et al., 1997).

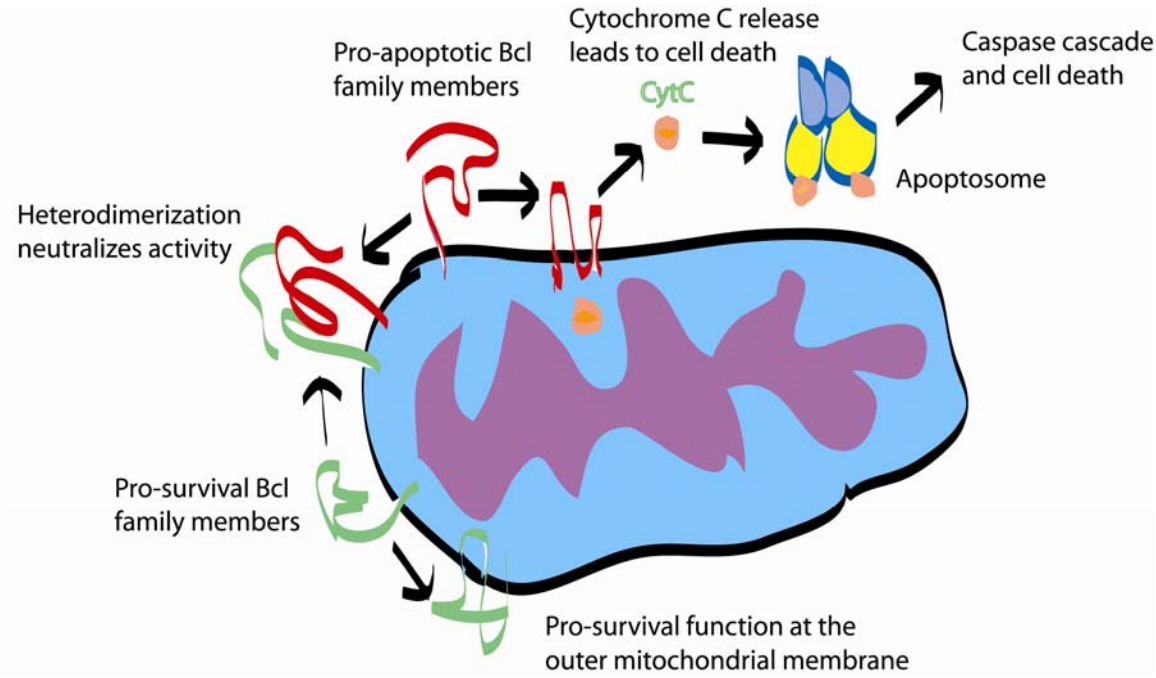

Figure 1.1 A schematic representation of the mitochondrial pathway of apoptosis. The release of cytochrome c into the cytosol results in the formation of the apoptosome that triggers the caspase cascade and ultimately cell death.

Stress signals like DNA damage, UV irradiation, withdrawal of growth factors, presence of toxic drugs like staurosporine, dexamethasone etc. cause apoptosis by triggering cytochrome c release by interacting with sensor molecules that respond to these stress factors (Kuwana and Newmeyer, 2003). The diverse signals are then integrated at a central location in the mitochondria where the critical step of commitment to apoptosis takes place (Green and Reed, 1998). The maintenance of the integrity of the

mitochondrial outer membrane assumes a great importance in the regulation of apoptosis since the disruption of the outer membrane either by specific proteins or by a swelling and rupture of the mitochondria could cause a release of cytochrome c that activates the downstream effectors and causes cell death (Jacotot et al., 1999). The important role in the regulation of mitochondrial membrane permeabilization is carried out by the Bcl-2 family of proteins that are discussed in detail in the next section.

The Bcl-2 family and the regulation of the mitochondrial pathway

The Bcl-2 family of proteins shares one or more of the conserved motifs, short 10-15 residue regions called BH regions, BH1 through BH4 (Adams and Cory, 1998; Chao and Korsmeyer, 1998; Cory et al., 2003; Gross et al., 1999; Kelekar and Thompson, 1998; Kuwana and Newmeyer, 2003; Reed, 1997a). There are three different classes into which the Bcl-2 family members may be classified (Figure 1.2) :

1. The sensors which have only the BH3 region, also known as the BH3 only proteins Bik, Bid, Bad and Bim that sense the different stress signals and transmit the information onto the effectors and protectors.
2. The effectors, the pro-apoptotic members of the family like Bax and Bak which have the BH1, BH2 and BH3 regions. These proteins cause mitochondrial membrane permeabilization, release of cytochrome c and cell death.
3. The protectors, the pro-survival members of the Bcl-2 family including Bcl-X_L and Bcl-2 act both in the cytosol and at the mitochondria to prevent cytochrome c release into the cytosol. Bcl-2 and Bcl-X_L share all the Bcl-2 homology regions, BH1-4 and function to prevent cell death.

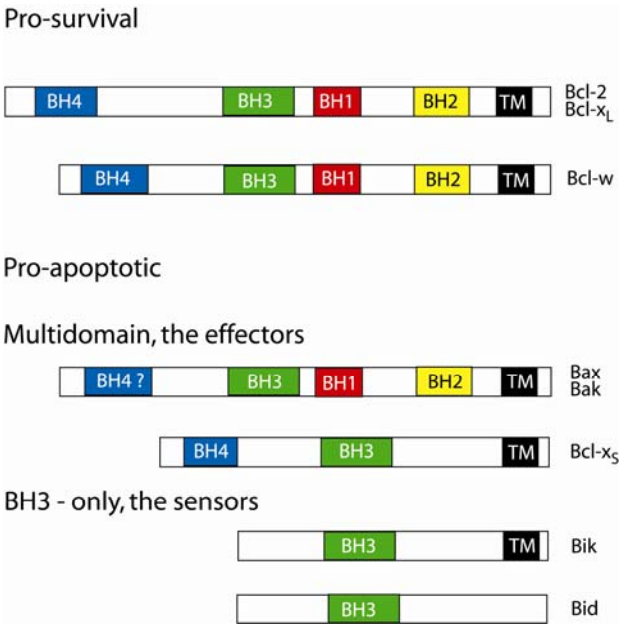

Figure 1.2 Conserved sequence features of the Bcl-2 family proteins. The three classes of the Bcl-2 family members are represented. One class of proteins that are pro-survival and two classes that are pro-apoptotic. The pro-apoptotic proteins include the multidomain proteins that act as effectors and the BH3-only proteins that act as sensors.

Insights from the structure of Bcl-2 proteins

The structure of some Bcl-2 family proteins like Bcl-2, Bcl-X_L, Bax, CED-9 and Bid are known (Aritomi et al., 1997; Chou et al., 1999; Muchmore et al., 1996; Petros et al., 2001; Suzuki et al., 2000a; Woo et al., 2003; Yan et al., 2004). Remarkably, Bcl-X_L and Bax though being implicated in opposing roles in apoptosis are structurally quite similar, both displaying helical bundle topologies and displaying common molecular features like the structurally conserved hydrophobic helical hairpin that forms the hydrophobic core of the protein (Figure 1.3) (Muchmore et al., 1996; Suzuki et al., 2000a). Although they exhibit a 30% sequence identity, the structural similarity is surprising considering the opposing roles they play in programmed cell death. Although they share the same basic structural fold, the difference in their activity could still stem from the subtle differences in the details of the sequence in critical regions of the molecule.

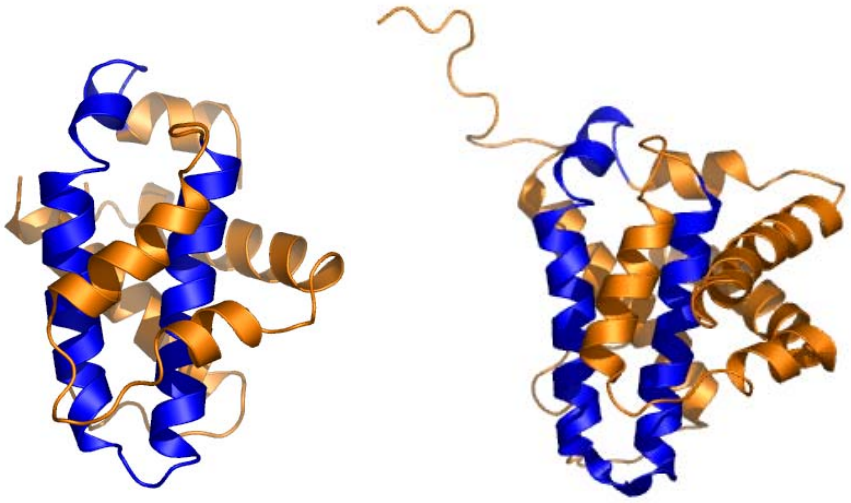

Figure 1.3 Structural similarity between Bcl-2 proteins that have opposing functions in apoptosis. The crystal structure of Bcl-$X_L\Delta$TM that lacks the C-terminal TM segment (from 1MAZ.pdb) is shown on the left. The solution structure of Bax (from 1F16.pdb) is shown on the right. The conserved structural feature, the hydrophobic helical hairpin is highlighted in blue.

Highly conserved sequence features and three-dimensional structures, yet completely opposite functional roles provide the motivation, in part, for the current study. In an attempt to understand the biological activity of Bcl-2 proteins, I have concentrated my efforts on understanding in detail the mechanism of action of one of the important Bcl-2 family members, Bcl-X_L.

Bcl-X_L functions to prevent apoptosis in vivo

The bcl-x gene was initially identified from a low stringency Southern blotting of chicken genomic DNA with a murine bcl-2 cDNA probe (Boise et al., 1993). Further experiments also identified the two different forms of the gene that were expressed, a long version called bcl-xl and the short, alternatively spliced version, bcl-xs (Boise et al., 1993). The two forms of the bcl-x gene were observed to have opposing functions: bcl-xl rescues cells from IL-3 withdrawal induced apoptosis as well as another pro-survival

protein bcl-2; bcl-xs inhibits ability of bcl-2 to rescue cells from apoptosis (Boise et al., 1993). Studies on the characterization of gene products from the mouse bcl-x gene indicated that apart from the Bcl-X_L and Bcl-X_S form, there was an additional alternatively spliced form that is expressed, Bcl-$X_L\Delta$TM which lacks the C-terminal transmembrane tail(Fang et al., 1994). This form was localized to the cytosol but was still able to rescue cells from apoptosis. The human form of Bcl-X_L lacking the C-terminal transmembrane segment was also shown to exhibit almost 86% of the ability of the full length form in a rescue assay of cells from cell death following IL-3 withdrawal (Muchmore et al., 1996).

Bcl-$X_L\Delta$TM – structure and features

The first structure of a Bcl-2 family member to be determined was that of Bcl-X_L, and in a remarkable effort, both the crystal (Figure 1.3) and solution structures (Figure 1.4) of the molecule were solved (Muchmore et al., 1996). The constructs used for structure determination by NMR and X-ray crystallography, lacked the putative transmembrane segment at the C-terminus(residues 210-233). The solution structure closely matches the crystal structure with an RMSD of 1.6 Å showing an all α-helical fold with 7 α-helices (Muchmore et al., 1996). The structure consists of a hydrophobic helical hairpin formed by the helices α5 and α6, which forms the hydrophobic core of the protein. The helical hairpin is surrounded by amphipathic helices α3 and α4 on one side and α1, α2 and α7 on the other.

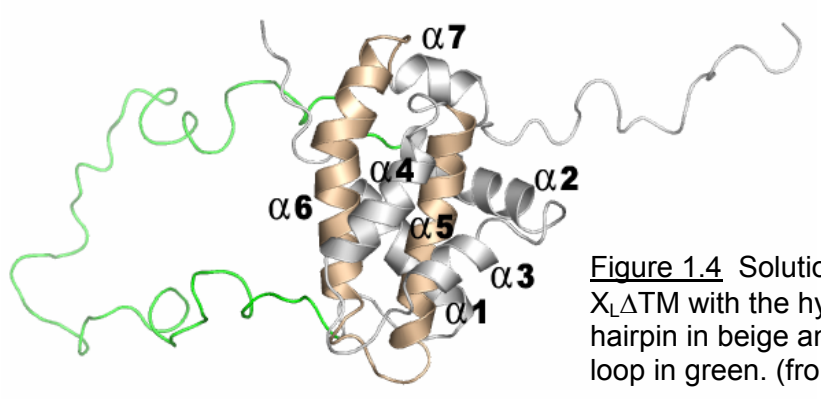

Figure 1.4 Solution structure of Bcl-$X_L\Delta TM$ with the hydrophobic helical hairpin in beige and the unstructured loop in green. (from 1 LXL.pdb)

Residues 26-83 form an unstructured loop that is poorly defined by the lack of long-range NOEs in the NMR structure and for which no electron density was observed in the crystallography study, presumably because of its high degree of disorder. Residues from the highly conserved regions, BH1, BH2 and BH3 in Bcl-X_L form a binding cleft that was shown to bind peptides derived from the BH3 region of a number of pro-apoptotic Bcl-2 family proteins. The C-terminal segment of 25 residues is hydrophobic suggesting that it could anchor the protein in the mitochondrial outer membrane. The C-terminal end of the protein with the sequence SRK has two basic residues which help in targeting the protein to the mitochondria (Kaufmann et al., 2003).

The structural similarity between Bcl-X_L and bacterial pore-forming toxins like colicin A provided clues to its possible role at the mitochondrial outer membrane (Figure 1.5) (Muchmore et al., 1996). These proteins share the central, hydrophobic helical hairpin which is known to mediate insertion into membranes in a pH-dependent manner. This suggests that Bcl-X_L can adopt multiple conformations, a globular solution conformation and a membrane inserted conformation with different functions attributed to different forms.

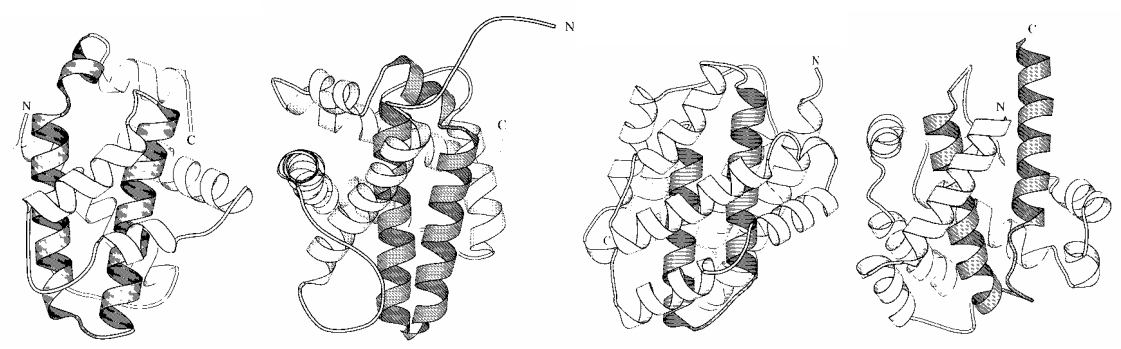

Bcl-X_L **Bax** **Colicin A** **DTX-T domain**

Figure 1.5 The structural similarity between Bcl-2 proteins like Bcl-X_L(1MAZ.pdb)/Bax(1F16.pdb) and bacterial pore forming toxins like colicinA (1COL.pdb) / diphtheria toxin T domain (1DDT.pdb) shown above in the same order left to right. The hydrophobic helical hairpin motif that is conserved among these proteins is shown in a darker shade of gray.

How does Bcl-X_L prevent apoptosis?

Evidence suggests that Bax and Bak act as antagonists of the pro-survival proteins like Bcl-2 and Bcl-X_L (Chittenden et al., 1995; Oltvai et al., 1993). The "heterodimerization" model describes the pro-death molecules acting as effectors of cell death and the pro-survival molecules acting by binding, sequestering and inhibiting the activity of the pro-death molecules in the cell death process. The structure of a Bcl-X_L / Bak BH3 peptide complex was determined. The features of the binding pocket that define the interaction with the BH3 peptides suggest that the formation of a hydrophobic cleft with properly positioned charged residues is essential for this interaction (Sattler et al., 1997). It is interesting to note that the peptide derived from the sequence of Bak bound the tightest to Bcl-X_L suggesting that Bak might be the cognate partner to Bcl-X_L *in vivo*. The binding of the Bak BH3 derived peptide was found to be almost 40 times stronger than that of the Bax-derived peptide with K_D of 0.34 and 13 μM respectively (Sattler et al., 1997). However, this "sequestration model" for Bcl-X_L activity was found

to be incomplete since mutants of Bcl-X_L that were unable to bind Bax and Bak were still able to elicit the biological function of preventing cell death (Cheng et al., 1996).

These findings led to alternative hypotheses that focus on Bcl-X_L acting at the mitochondrial outer membrane. The motivation for these hypotheses were two-fold: (i) Bcl-X_L was found to be localized to the mitochondrial outer membrane during apoptosis (Hsu et al., 1997), (ii) the structural similarity between Bcl-X_L and the bacterial toxins that insert into membranes (Muchmore et al., 1996). Experimental investigation into the role of Bcl-X_L on the mitochondrial outer membrane resulted in observations that Bcl-X_L can form ion channels in synthetic lipid vesicles and membrane bilayers *in vitro* (Minn et al., 1997).

These observations lead to a fundamental question: Is the solution conformation of Bcl-X_L the biologically relevant form or is it the membrane conformation? Or is it possible that both forms have definite roles to play in the regulation of programmed cell death? An answer to these questions was provided in a remarkable study where Minn et al. showed that there were multiple roles that Bcl-X_L could play in eliciting its activity including heterodimerization dependent and heterodimerization independent roles (Minn et al., 1999). In this study, Bcl-X_L with a mutation in the Bax binding cleft, Y101K was unable to bind Bax but able to rescue cells from apoptosis although not as efficiently as the wild-type molecule. Another mutant, Bcl-X_L-XB (with the residues E153 to R165 replaced by an identical region from Bax) possessing altered ion channel activity but normal binding to Bax, also showed partially impaired function indicating that membrane activity might be essential for function. The most important observation was the double mutant that combined the Y101K and the XB mutations that showed complete abrogation

of the ability of Bcl-X_L to rescue cells from apoptosis (Minn et al., 1999). This study confirmed the importance of both the solution conformation and the membrane inserted conformation of Bcl-X_L in promoting cell survival.

The physiological role of Bcl-X_L in the membrane

Evidence indicates that Bcl-X_L has multiple roles in the membrane. Exactly how the membrane conformation of Bcl-X_L regulates cell death is unknown. Several hypotheses have been proposed:

1. **Ion channel activity:** It has been hypothesized that Bcl-X_L functions as an ion channel on the mitochondrial outer membrane to maintain ion homeostasis and preserve mitochondrial outer membrane integrity. The initial studies to examine the membrane insertion property of Bcl-$X_L\Delta$TM monitored the efflux of Cl^- ions from KCl-solute loaded lipid vesicles, which is a typical assay that is used for testing the pore-forming property of bacterial toxins (Minn et al., 1997). Similar to bacterial toxins, Bcl-X_L (both ΔTM and ΔloopΔTM versions) caused an efflux of Cl^- ions through the membrane bilayer in a pH-dependent manner. Although no significant efflux was observed above pH 5.5, efflux increased in proportion to a pH decrease below pH 5.5 (Minn et al., 1997). The efflux was found to be dependent on the presence of anionic lipids in the lipid vesicles (Minn et al., 1997). These observations were confirmed by single channel measurements using planar bilayers. In this work, Bcl-$X_L\Delta$TM readily formed ion channels at pH 4.0 that exhibited multiple conductance levels. Even at physiological pH conditions, pH 7.2, Bcl-$X_L\Delta$TM formed ion channels albeit at much slower rates (Minn et al., 1997). This seminal work illuminated the features that ion channels of Bcl-$X_L\Delta$TM

share with those of diphtheria toxin in the following observations: (i) an increased specificity for cations at physiological pH compared to low pH and (ii) increase in ion conductance at low pH.

2. **Modulation of VDAC:** Bcl-X_L modulates the activity of the Voltage Dependent Anion Channel (VDAC), a component of the Permeability Transition Pore Complex (PTPC), a large, multi-protein complex spanning both the outer and inner mitochondrial membranes (Vander Heiden et al., 2001). The PTPC is fundamentally composed of two proteins, namely the VDAC on the outer membrane, and the Adenine Nucleotide Translocase (ANT) on the inner membrane (Vander Heiden and Thompson, 1999). These proteins have been shown to interact with the Bcl-2 family of proteins, both physically and functionally. Bax has been observed to regulate the permeability transition (PT) by interacting with VDAC and ANT, resulting in the disruption of anionic metabolite transport and homeostasis (Brenner et al., 2000; Marzo et al., 1998; Narita et al., 1998). This disruption has been hypothesized to result in an osmotic swelling of the mitochondria, and eventual rupture releasing cytochrome c into the cytosol (Vander Heiden et al., 2001). However, the pro-survival protein, Bcl-X_L promotes the open configuration of VDAC, and is thought to maintain anionic metabolite transport across the mitochondrial outer membrane, thereby maintaining mitochondrial membrane integrity (Vander Heiden et al., 2001). Whether the effect of Bcl-X_L on VDAC arises from a direct effect or an indirect effect is unknown.

3. **Sequestration of Apaf-1:** Bcl-X_L in its membrane inserted form can prevent cell death by sequestering Apaf-1, which is an essential component of the Apoptosome. The current hypothesis for this negative regulatory role is based on the evidence that the BH4

region, which is presumably exposed in the membrane inserted form may be essential for Bcl-2 / Bcl-X_L to bind to Apaf-1, and to function as an inhibitor of Apaf-1 to prevent apoptosome formation (Huang et al., 1998; Pan et al., 1998). The presence of an N-terminal conserved region, termed BH4 in only the pro-survival proteins and the lack of it in structurally similar pro-death proteins like Bax and Bak suggested a negative role was played by this BH4 region in inducing cells towards apoptosis. Deletion of the BH4 region abrogated the activity of Bcl-2 in preventing cell death but did not affect its binding to pro-death proteins like Bax and Bak. The activity was regained when the BH4 region of Bcl-X_L was inserted into Bcl-2(ΔBH4) (Huang et al., 1998). These observations strongly supported the negative regulatory role for the BH4 region in preventing cell death.

Modulation of Bcl-X_L activity

The activity of the solution and membrane conformations of Bcl-X_L is tightly regulated *in vivo*. Besides regulation at the transcriptional level, the activity of Bcl-X_L has been observed to be modulated in a number of ways:

1. **Post-translational modification of Bcl-X_L**: This includes the phosphorylation of the loop region and potential deamidation of Asn residues in the protein. Deletion of the loop region (residues 26-83) enhances the ability of Bcl-X_L to rescue FL5.12 cells from IL-3 withdrawal induced apoptosis (Chang et al., 1997). This has been attributed to the possible phosphorylation dependent suppression of the pro-survival activity of Bcl-X_L (Bassik et al., 2004). Deamidation of Asn residues was observed in rat Bcl-X_L, suggesting a potential means of regulation although

the biological relevance of deamidation in apoptosis still remains unclear (Aritomi et al., 1997).

2. **Caspase cleavage of Bcl-X_L** at D61 and D76 produces ΔN61 and ΔN76 Bcl-X_L, which convert the protein from pro-survival to pro-apoptotic. Bcl-X_L has caspase cleavage sites located in the long, unstructured loop region, cleavage of which results in ΔN61 and ΔN76 Bcl-X_L. The ΔN61 and ΔN76 forms of Bcl-X_L are surprisingly pro-apoptotic and they act to promote cell death(Basanez et al., 2001b). This could result from their ability to bind and insert into membranes much more readily to form a membrane conformation that is essentially different from that formed by full length Bcl-X_L. The membrane inserted forms of the ΔN versions of Bcl-X_L were able to form pores large enough for cytochrome c to pass through. This property is reminiscent of Bax which forms large, oligomeric pores on the membrane that aid in cytochrome c release. The solution structure of Bax is similar to that of Bcl-X_L and the functional similarity of Bax with ΔN61 and ΔN76 suggest that their membrane forms might be similar with both forming large oligomeric pores in the mitochondrial outer membrane (Basanez et al., 2002; Basanez et al., 2001b). In this model of regulation, caspase load and activity determine the ultimate role of Bcl-X_L, to either promote cell survival or cell death.

Besides the above methods of modulation, a change in localization of Bcl-X_L from the cytosol to the mitochondrial membrane might play a role in its regulation. This change in localization is coupled with the solution-to-membrane conformational change

with both conformations of Bcl-X_L being essential for its biological activity. In an interesting study, Hsu et al. showed that there was a relocalization of the protein inside the cell during the initial stages in apoptosis. In healthy murine thymocytes, Bcl-X_L was partly localized to the cytosol and partly to the intracellular membrane fraction. Upon induction of apoptosis by dexamethasone treatment or γ-irradiation, Bcl-X_L relocalized to the membrane with all of it becoming membrane bound (Hsu et al., 1997). This relocalization hints at the possibility that there is an apoptosis-triggered relocalization of Bcl-X_L to the mitochondrial outer membrane that regulates the anti-apoptotic activity of Bcl-X_L.

The various mechanisms of action hypothesized above are represented in Figure 1.6. The presence of two biologically active conformations of Bcl-X_L (solution and membrane conformations) and the transition from one to the other *in vivo* might be an important mechanism of regulation of the activity of Bcl-X_L.

The observation that there is a pH triggered conformational change from solution to membrane *in vitro* suggests that pH could be the trigger that is used during the regulation of apoptosis. It has also been observed that there is a change in the cytosolic pH that is associated with the initial stages of apoptosis induction (Matsuyama and Reed, 2000). This pH change ranging between 0.6 and 0.9 units could be the trigger that drives the transition of Bcl-X_L from the cytosol to the membrane (Li and Eastman, 1995; Matsuyama et al., 2000).

If intracellular acidification is indeed the trigger that mediates the conformational change of Bcl-X_L *in vivo*, the understanding of the pH-mediated change from a solution

conformation to a membrane-inserted conformation of Bcl-X_LΔTM will reveal the mechanism of Bcl-X_L's biological activity.

Significance of the pH-dependent conformational change

Besides the biological relevance, an understanding of the pH-dependent conformational solution-to-membrane conformational change of Bcl-X_LΔTM *in vitro* will provide insights into:

1. how an amino acid sequence is able to adopt two different and thermodynamically stable conformations in two different environments.
2. how Bax and Bcl-X_L, which share the same solution fold, could adopt two potentially different membrane structures resulting in opposing functions in the cell death process.
3. potential intermediates along the soluble-to-membrane conformational change that might provide critical targets for therapeutic intervention.
4. how similar pH-dependent processes in biology are regulated.

Specific aims of the project

The central question that this research aims to answer is how pH modulates the solution-to-membrane conformational change of Bcl-X_LΔTM *in vitro* (Figure 1.6). To address this question, we proposed the following specific aims:

1. Is the mechanism of insertion into membranes similar to that of structurally similar proteins like diphtheria toxin and colicins?

2. What does pH modulate and how does it modulate to mediate transition of Bcl-X_L from solution to the membrane?

3. Are there other factors besides pH that modulate this transition?

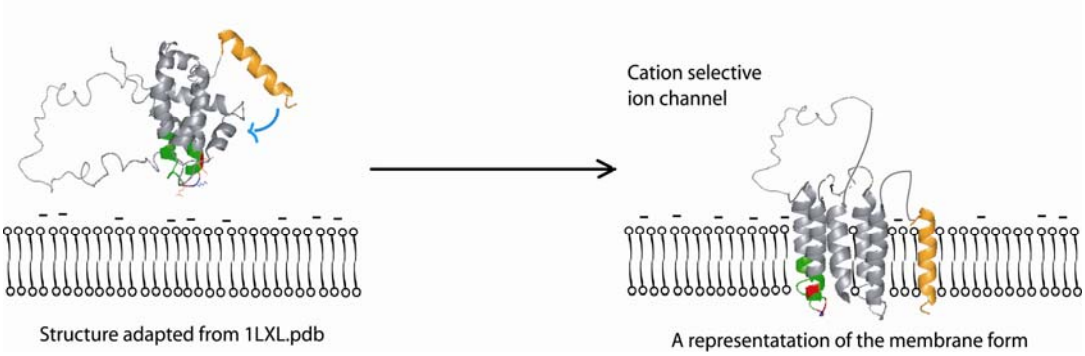

Figure 1.6 The pH-dependent conformational change from the solution conformation to a membrane-inserted conformation defines the central question that is addressed by this project.

A detailed description of the existing knowledge to answer these questions is discussed in the following section.

1. **Lessons learnt from the bacterial toxins**

Many proteins share significant structural similarity with Bcl-X_L and these include the bacterial toxins like colicins and diphtheria toxin (Lesieur et al., 1997; Muchmore et al., 1996). The central hydrophobic helical hairpin (HHH) that is common between Bcl-X_L and the pore-forming toxins is thought to mediate their insertion into membranes (Lesieur et al., 1997; Muchmore et al., 1996). It has been postulated that in the case of colicin A, for example, an acid-induced molten globule formation mediates the pH-dependent insertion into the membrane (van der Goot et al., 1991). However, such a mechanism has not been observed for colicin E1 which inserts by the pH-dependent local unfolding of a "pH-trigger" helix that drives a conformational change and electrostatic interactions with the membrane surface modulated by pH (Merrill et al.,

1997; Musse and Merrill, 2003; Zakharov and Cramer, 2002a; Zakharov and Cramer, 2002b; Zakharov et al., 1996). It has been observed that membrane insertion is a complex process that is mediated by a number of different mechanisms each playing their part in the transition from the solution conformation to the membrane conformation (Zakharov and Cramer, 2002a; Zakharov and Cramer, 2002b).

Some colicins and diphtheria toxin use a "cloak and dagger" strategy for insertion with the hydrophobic helical hairpin forming the dagger for insertion (Lakey et al., 1992; Lesieur et al., 1997; Zakharov and Cramer, 2002a; Zakharov and Cramer, 2002b). Evidence suggests that bacterial toxins like diphtheria toxin and colicins (colicin A, E1 and Ia) insert into membranes in a multi-step process, the critical step of which is the initial insertion of the helical hairpin into the membrane and the other helices lying on top of the membrane forming an "umbrella like intermediate" (Lakey et al., 1992; Lesieur et al., 1997; Zakharov and Cramer, 2002a; Zakharov and Cramer, 2002b). These observations aid us in investigating the pH-dependent solution-to-membrane conformational change of Bcl-$X_L\Delta$TM.

2. How does pH modulate the protein and the membrane?

In the simple *in vitro* system with purified protein and lipid vesicles made from synthetic lipids, a decrease in the pH of the system will affect the electrostatic character of the protein as well as that of the membrane surface. A decrease in pH from 7.4 to 5.0 will result in the protonation of ionizable residues like histidines with a pKa ~ 6.0 and other charged residues with altered pKa values (Creighton, 1993). A decrease in pH could also change the electrostatic character of the surface of the lipid vesicle due to the protonation of ionizable groups on the membrane surface. It is also important to note that

besides the acidic pH conditions, the presence of anionic lipids in the membrane is essential for the association of Bcl-X_L with membranes (Basanez et al., 2001b; Minn et al., 1997). It has been observed in certain cases, that electrostatic interactions between charged protein surfaces and charged membrane surfaces mediate association and insertion of proteins into membranes (Heymann et al., 1996).

3. **Does Ca^{2+} help regulate the solution to membrane conformational change of Bcl-X_L?**

It has been observed that in purified systems, with just purified Bcl-X_L and lipid vesicles composed of synthetic lipids, the insertion does indeed occur in a pH-dependent manner. In this defined system *in vitro*, there appears to be no need for other protein mediators. In the *in vivo* system, however, there might be other factors that trigger this conformational change and thereby regulate apoptosis. For example, the ion channel activity of Bcl-X_L was found to be reversibly inhibited by divalent calcium with a dissociation constant of ~60 μM(Lam et al., 1998). This suggests a role for calcium in the regulation of apoptosis. Indeed, the release of Ca^{2+} from the intracellular stores in the ER appears to be a critical step in the timing of programmed cell death (Scorrano, 2003; Scorrano et al., 2003).

It is interesting to note that in certain cases, Ca^{2+} bridges the interaction between proteins and membranes (Verdaguer et al., 1999; Huang et al., 2003; Nelsestuen and Ostrowski, 1999). We tested the hypothesis that Ca^{2+} might be important in the case of Bcl-X_L, considering the requirement for anionic lipids for the solution-to-membrane conformational change. The electrostatic surface of the protein is predominantly anionic at physiological pH conditions and Ca^{2+} being positively charged could bridge the

interaction between Bcl-X_L and the membrane and thereby mediate the solution to membrane conformational change.

Based on these observations, we hypothesized three models for the solution-to-membrane conformational change as shown in Figure 1.7. These models might not be mutually exclusive and it is possible that the solution-to-membrane conformational change of Bcl-$X_L\Delta$TM requires a contribution from more than one mechanism.

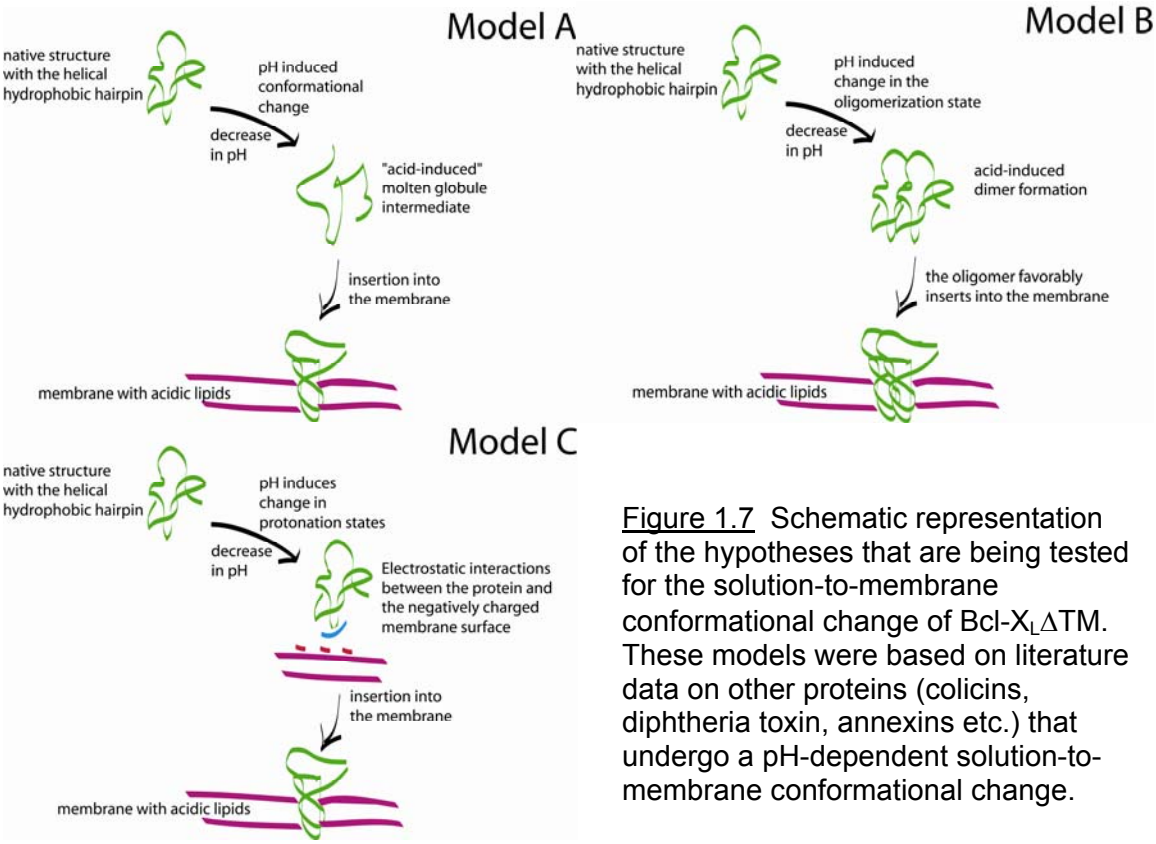

Figure 1.7 Schematic representation of the hypotheses that are being tested for the solution-to-membrane conformational change of Bcl-$X_L\Delta$TM. These models were based on literature data on other proteins (colicins, diphtheria toxin, annexins etc.) that undergo a pH-dependent solution-to-membrane conformational change.

In order to address these questions, we have to investigate the pH-dependence of the biophysical properties of the protein in the absence and presence of the membrane. In our simple system for experimental investigation, we have the protein Bcl-$X_L\Delta$TM, lipid vesicles composed of synthetic lipids (that mimic the composition of the mitochondrial outer membrane) and a buffering system (Figure 1.8).

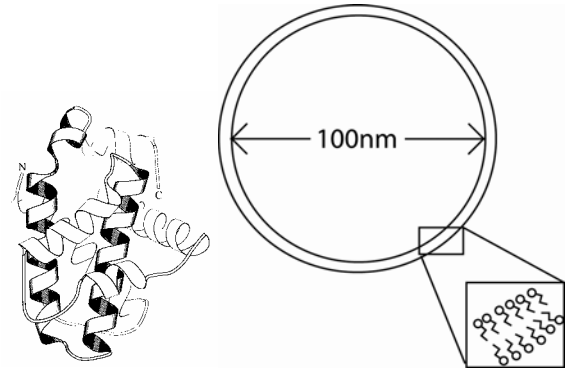

Figure 1.8 A schematic representation of the two component system that is used for the study of the pH-dependent solution-to-membrane conformational change of Bcl-$X_L\Delta$TM. The protein is represented by a representation of the crystal structure adapted from 1MAZ.pdb and the membrane is represented by large, unilamellar lipid vesicles composed of 60% DOPC and 40% DOPG.

The surface of the mitochondrial outer membrane is negatively charged due to the presence of a significant number of anionic lipids such as phosphatidyl glycerol, phosphatidyl serine, phosphatidic acid and cardiolipin interspersed among zwitterionic lipids such as phosphatidyl choline and phosphatidyl ethanolamine. Of the anionic lipids, PG, PS and PA carry a net charge of -1 while cardiolipin carries a charge of -2 per phospholipid molecule. PG and CL are found in all bacterial membranes but are found primarily in the mitochondria in eukaryotic cells (Dowhan, 1997; Hovius et al., 1990; Hovius et al., 1993). These lipids contribute significantly to the negative surface potential on the mitochondria (McLaughlin, 1989). It is presumed that this negative surface potential is critical to the insertion of Bcl-X_L into the mitochondria and influences the conformational change in a number of ways. Therefore, the lipid vesicles used in various studies of membrane interactions of Bcl-2 family proteins used the following composition: 60% DOPC and 40% DOPG which is what was primarily used in our studies unless noted otherwise (Basanez et al., 2001b; Minn et al., 1997).

An outline for the thesis

To restate the fundamental question, I want to unravel the mechanism of the pH-dependent solution to membrane conformational change of Bcl-X_L, and reveal insights into the molecular features that define this conformational change.

The initial chapters, Chapters 1 and 2 are devoted towards understanding the effects of pH on Bcl-$X_L\Delta$TM in solution in an attempt to identify any insights it might provide towards the pH-dependent solution to membrane conformational change. In Chapter 1, I test the hypothesis that Bcl-$X_L\Delta$TM forms an "acid-induced" molten-globule that is known to mediate pH-induced solution-to-membrane conformational changes for many bacterial toxins (Model A in Figure 1.7). The oligomerization-dependent conformational change hypothesis is also tested by observing the pH-dependent quarternary structural changes of Bcl-$X_L\Delta$TM in solution (Model B in Figure 1.7). Besides pH-dependent structural changes, the effect of pH-dependent changes in the dynamics of Bcl-X_L are investigated in Chapter 2. The latter half of Chapter 2 contains work on GB1, a model system used to explore the accuracy and precision of the novel relaxation compensated CPMG experiments used to determine conformational dynamics during protein folding. Chapter 3 details the investigations of the pH dependent changes in Bcl-$X_L\Delta$TM in the presence of a membrane in the form of lipid vesicles. The first half of Chapter 3 describes the characterization of the pH-dependent interaction between Bcl-X_L and lipid vesicles. This is followed by experiments that test the hypothesis that electrostatic interactions drive the pH-dependent association of Bcl-X_L with the lipid vesicles (Model C in Figure 1.7). This chapter concludes with the evaluation of a Ca^{2+} mediated conformational change. Chapter 4 tests the hypothesis that electrostatic

interactions could mediate the solution to membrane conformational change. At the end of Chapter 4, I summarize the current understanding of the system in terms of a structural and a thermodynamic model that is formulated to provide a framework for further exploration.

References

Adams, J.M., and S. Cory. 1998. The Bcl-2 protein family: arbiters of cell survival. *Science* 281(5381):1322-1326.

Aritomi, M., N. Kunishima, N. Inohara, Y. Ishibashi, S. Ohta, and K. Morikawa. 1997. Crystal structure of rat Bcl-xL. Implications for the function of the Bcl-2 protein family. *J Biol Chem* 272(44):27886-27892.

Basanez, G., J.C. Sharpe, J. Galanis, T.B. Brandt, J.M. Hardwick, and J. Zimmerberg. 2002. Bax-type apoptotic proteins porate pure lipid bilayers through a mechanism sensitive to intrinsic monolayer curvature. *J Biol Chem* 277(51):49360-49365.

Basanez, G., J. Zhang, B.N. Chau, G.I. Maksaev, V.A. Frolov, T.A. Brandt, J. Burch, J.M. Hardwick, and J. Zimmerberg. 2001. Pro-apoptotic cleavage products of Bcl-xL form cytochrome c-conducting pores in pure lipid membranes. *J Biol Chem* 276(33):31083-31091.

Bassik, M.C., L. Scorrano, S.A. Oakes, T. Pozzan, and S.J. Korsmeyer. 2004. Phosphorylation of BCL-2 regulates ER Ca2+ homeostasis and apoptosis. *Embo J* 23(5):1207-1216.

Boise, L.H., M. Gonzalez-Garcia, C.E. Postema, L. Ding, T. Lindsten, L.A. Turka, X. Mao, G. Nunez, and C.B. Thompson. 1993. bcl-x, a bcl-2-related gene that functions as a dominant regulator of apoptotic cell death. *Cell* 74(4):597-608.

Brenner, C., H. Cadiou, H.L. Vieira, N. Zamzami, I. Marzo, Z. Xie, B. Leber, D. Andrews, H. Duclohier, J.C. Reed, and G. Kroemer. 2000. Bcl-2 and Bax regulate the channel activity of the mitochondrial adenine nucleotide translocator. *Oncogene* 19(3):329-336.

Chang, B.S., A.J. Minn, S.W. Muchmore, S.W. Fesik, and C.B. Thompson. 1997. Identification of a novel regulatory domain in Bcl-X(L) and Bcl-2. *Embo J* 16(5):968-977.

Chao, D.T., and S.J. Korsmeyer. 1998. BCL-2 family: regulators of cell death. *Annu Rev Immunol* 16:395-419.

Cheng, E.H., B. Levine, L.H. Boise, C.B. Thompson, and J.M. Hardwick. 1996. Bax-independent inhibition of apoptosis by Bcl-XL. *Nature* 379(6565):554-556.

Chittenden, T., E.A. Harrington, R. O'Connor, C. Flemington, R.J. Lutz, G.I. Evan, and B.C. Guild. 1995. Induction of apoptosis by the Bcl-2 homologue Bak. *Nature* 374(6524):733-736.

Chou, J.J., H. Li, G.S. Salvesen, J. Yuan, and G. Wagner. 1999. Solution structure of BID, an intracellular amplifier of apoptotic signaling. *Cell* 96(5):615-624.

Cory, S., D.C. Huang, and J.M. Adams. 2003. The Bcl-2 family: roles in cell survival and oncogenesis. *Oncogene* 22(53):8590-8607.

Creighton, T.E. 1993. Proteins: Structures and Molecular Properties. W.H.Freeman and Company.

Dowhan, W. 1997. Molecular basis for membrane phospholipid diversity: why are there so many lipids? *Annu Rev Biochem* 66:199-232.

Earnshaw, W.C., L.M. Martins, and S.H. Kaufmann. 1999. Mammalian caspases: structure, activation, substrates, and functions during apoptosis. *Annu Rev Biochem* 68:383-424.

Fang, W., J.J. Rivard, D.L. Mueller, and T.W. Behrens. 1994. Cloning and molecular characterization of mouse bcl-x in B and T lymphocytes. *J Immunol* 153(10):4388-4398.

Green, D.R., and G. Kroemer. 2004. The pathophysiology of mitochondrial cell death. *Science* 305(5684):626-629.

Green, D.R., and J.C. Reed. 1998. Mitochondria and apoptosis. *Science* 281(5381):1309-1312.

Gross, A., J.M. McDonnell, and S.J. Korsmeyer. 1999. BCL-2 family members and the mitochondria in apoptosis. *Genes Dev* 13(15):1899-1911.

Hengartner, M.O. 2000. The biochemistry of apoptosis. *Nature* 407(6805):770-776.

Hengartner, M.O., and H.R. Horvitz. 1994. The ins and outs of programmed cell death during C. elegans development. *Philos Trans R Soc Lond B Biol Sci* 345(1313):243-246.

Heymann, J.B., S.D. Zakharov, Y.L. Zhang, and W.A. Cramer. 1996. Characterization of electrostatic and nonelectrostatic components of protein--membrane binding interactions. *Biochemistry* 35(8):2717-2725.

Hovius, R., H. Lambrechts, K. Nicolay, and B. de Kruijff. 1990. Improved methods to isolate and subfractionate rat liver mitochondria. Lipid composition of the inner and outer membrane. *Biochim Biophys Acta* 1021(2):217-226.

Hovius, R., J. Thijssen, P. van der Linden, K. Nicolay, and B. de Kruijff. 1993. Phospholipid asymmetry of the outer membrane of rat liver mitochondria. Evidence for the presence of cardiolipin on the outside of the outer membrane. *FEBS Lett* 330(1):71-76.

Hsu, Y.T., K.G. Wolter, and R.J. Youle. 1997. Cytosol-to-membrane redistribution of Bax and Bcl-X(L) during apoptosis. *Proc Natl Acad Sci U S A* 94(8):3668-3672.

Huang, D.C., J.M. Adams, and S. Cory. 1998. The conserved N-terminal BH4 domain of Bcl-2 homologues is essential for inhibition of apoptosis and interaction with CED-4. *Embo J* 17(4):1029-1039.

Huang, M., A.C. Rigby, X. Morelli, M.A. Grant, G. Huang, B. Furie, B. Seaton, and B.C. Furie. 2003. Structural basis of membrane binding by Gla domains of vitamin K-dependent proteins. *Nat Struct Biol* 10(9):751-756.

Jacotot, E., P. Costantini, E. Laboureau, N. Zamzami, S.A. Susin, and G. Kroemer. 1999. Mitochondrial membrane permeabilization during the apoptotic process. *Ann N Y Acad Sci* 887:18-30.

Kaufmann, T., S. Schlipf, J. Sanz, K. Neubert, R. Stein, and C. Borner. 2003. Characterization of the signal that directs Bcl-x(L), but not Bcl-2, to the mitochondrial outer membrane. *J Cell Biol* 160(1):53-64.

Kelekar, A., and C.B. Thompson. 1998. Bcl-2-family proteins: the role of the BH3 domain in apoptosis. *Trends Cell Biol* 8(8):324-330.

Kuwana, T., and D.D. Newmeyer. 2003. Bcl-2-family proteins and the role of mitochondria in apoptosis. *Curr Opin Cell Biol* 15(6):691-699.

Lakey, J.H., J.M. Gonzalez-Manas, F.G. van der Goot, and F. Pattus. 1992. The membrane insertion of colicins. *FEBS Lett* 307(1):26-29.

Lam, M., M.B. Bhat, G. Nunez, J. Ma, and C.W. Distelhorst. 1998. Regulation of Bcl-xl channel activity by calcium. *J Biol Chem* 273(28):17307-17310.

Lesieur, C., B. Vecsey-Semjen, L. Abrami, M. Fivaz, and F. Gisou van der Goot. 1997. Membrane insertion: The strategies of toxins (review). *Mol Membr Biol* 14(2):45-64.

Li, J., and A. Eastman. 1995. Apoptosis in an interleukin-2-dependent cytotoxic T lymphocyte cell line is associated with intracellular acidification. Role of the Na(+)/H(+)-antiport. *J Biol Chem* 270(7):3203-3211.

Li, P., D. Nijhawan, I. Budihardjo, S.M. Srinivasula, M. Ahmad, E.S. Alnemri, and X. Wang. 1997. Cytochrome c and dATP-dependent formation of Apaf-1/caspase-9 complex initiates an apoptotic protease cascade. *Cell* 91(4):479-489.

Liu, Q.A., and M.O. Hengartner. 1999. The molecular mechanism of programmed cell death in C. elegans. *Ann N Y Acad Sci* 887:92-104.

Liu, X., C.N. Kim, J. Yang, R. Jemmerson, and X. Wang. 1996. Induction of apoptotic program in cell-free extracts: requirement for dATP and cytochrome c. *Cell* 86(1):147-157.

Marzo, I., C. Brenner, N. Zamzami, J.M. Jurgensmeier, S.A. Susin, H.L. Vieira, M.C. Prevost, Z. Xie, S. Matsuyama, J.C. Reed, and G. Kroemer. 1998. Bax and adenine nucleotide translocator cooperate in the mitochondrial control of apoptosis. *Science* 281(5385):2027-2031.

Matsuyama, S., J. Llopis, Q.L. Deveraux, R.Y. Tsien, and J.C. Reed. 2000. Changes in intramitochondrial and cytosolic pH: early events that modulate caspase activation during apoptosis. *Nat Cell Biol* 2(6):318-325.

Matsuyama, S., and J.C. Reed. 2000. Mitochondria-dependent apoptosis and cellular pH regulation. *Cell Death Differ* 7(12):1155-1165.

McLaughlin, S. 1989. The electrostatic properties of membranes. *Annu Rev Biophys Biophys Chem* 18:113-136.

Meier, P., A. Finch, and G. Evan. 2000. Apoptosis in development. *Nature* 407(6805):796-801.

Merrill, A.R., B.A. Steer, G.A. Prentice, M.J. Weller, and A.G. Szabo. 1997. Identification of a chameleon-like pH-sensitive segment within the colicin E1 channel domain that may serve as the pH-activated trigger for membrane bilayer association. *Biochemistry* 36(23):6874-6884.

Minn, A.J., C.S. Kettlun, H. Liang, A. Kelekar, M.G. Vander Heiden, B.S. Chang, S.W. Fesik, M. Fill, and C.B. Thompson. 1999. Bcl-xL regulates apoptosis by heterodimerization-dependent and -independent mechanisms. *Embo J* 18(3):632-643.

Minn, A.J., P. Velez, S.L. Schendel, H. Liang, S.W. Muchmore, S.W. Fesik, M. Fill, and C.B. Thompson. 1997. Bcl-x(L) forms an ion channel in synthetic lipid membranes. *Nature* 385(6614):353-357.

Muchmore, S.W., M. Sattler, H. Liang, R.P. Meadows, J.E. Harlan, H.S. Yoon, D. Nettesheim, B.S. Chang, C.B. Thompson, S.L. Wong, S.L. Ng, and S.W. Fesik. 1996. X-ray and NMR structure of human Bcl-xL, an inhibitor of programmed cell death. *Nature* 381(6580):335-341.

Musse, A.A., and A.R. Merrill. 2003. The molecular basis for the pH-activation mechanism in the channel-forming bacterial colicin E1. *J Biol Chem* 278(27):24491-24499.

Narita, M., S. Shimizu, T. Ito, T. Chittenden, R.J. Lutz, H. Matsuda, and Y. Tsujimoto. 1998. Bax interacts with the permeability transition pore to induce permeability transition and cytochrome c release in isolated mitochondria. *Proc Natl Acad Sci U S A* 95(25):14681-14686.

Nelsestuen, G.L., and B.G. Ostrowski. 1999. Membrane association with multiple calcium ions: vitamin-K-dependent proteins, annexins and pentraxins. *Curr Opin Struct Biol* 9(4):433-437.

Nijhawan, D., N. Honarpour, and X. Wang. 2000. Apoptosis in neural development and disease. *Annu Rev Neurosci* 23:73-87.

Oltvai, Z.N., C.L. Milliman, and S.J. Korsmeyer. 1993. Bcl-2 heterodimerizes in vivo with a conserved homolog, Bax, that accelerates programmed cell death. *Cell* 74(4):609-619.

Pan, G., K. O'Rourke, and V.M. Dixit. 1998. Caspase-9, Bcl-XL, and Apaf-1 form a ternary complex. *J Biol Chem* 273(10):5841-5845.

Petros, A.M., A. Medek, D.G. Nettesheim, D.H. Kim, H.S. Yoon, K. Swift, E.D. Matayoshi, T. Oltersdorf, and S.W. Fesik. 2001. Solution structure of the antiapoptotic protein bcl-2. *Proc Natl Acad Sci U S A* 98(6):3012-3017.

Rathmell, J.C., and C.B. Thompson. 2002. Pathways of apoptosis in lymphocyte development, homeostasis, and disease. *Cell* 109 Suppl:S97-107.

Reed, J.C. 1997. Bcl-2 family proteins: regulators of apoptosis and chemoresistance in hematologic malignancies. *Semin Hematol* 34(4 Suppl 5):9-19.

Reed, J.C. 1999. Dysregulation of apoptosis in cancer. *J Clin Oncol* 17(9):2941-2953.

Rudin, C.M., and C.B. Thompson. 1997. Apoptosis and disease: regulation and clinical relevance of programmed cell death. *Annu Rev Med* 48:267-281.

Sattler, M., H. Liang, D. Nettesheim, R.P. Meadows, J.E. Harlan, M. Eberstadt, H.S. Yoon, S.B. Shuker, B.S. Chang, A.J. Minn, C.B. Thompson, and S.W. Fesik. 1997. Structure of Bcl-xL-Bak peptide complex: recognition between regulators of apoptosis. *Science* 275(5302):983-986.

Scorrano, L. 2003. Divide et impera: Ca^{2+} signals, mitochondrial fission and sensitization to apoptosis. *Cell Death Differ* 10(12):1287-1289.

Scorrano, L., S.A. Oakes, J.T. Opferman, E.H. Cheng, M.D. Sorcinelli, T. Pozzan, and S.J. Korsmeyer. 2003. BAX and BAK regulation of endoplasmic reticulum Ca^{2+}: a control point for apoptosis. *Science* 300(5616):135-139.

Suzuki, M., R.J. Youle, and N. Tjandra. 2000. Structure of Bax: coregulation of dimer formation and intracellular localization. *Cell* 103(4):645-654.

van der Goot, F.G., J.M. Gonzalez-Manas, J.H. Lakey, and F. Pattus. 1991. A 'molten-globule' membrane-insertion intermediate of the pore-forming domain of colicin A. *Nature* 354(6352):408-410.

Vander Heiden, M.G., X.X. Li, E. Gottleib, R.B. Hill, C.B. Thompson, and M. Colombini. 2001. Bcl-xL promotes the open configuration of the voltage-dependent anion channel and metabolite passage through the outer mitochondrial membrane. *J Biol Chem* 276(22):19414-19419.

Vander Heiden, M.G., and C.B. Thompson. 1999. Bcl-2 proteins: regulators of apoptosis or of mitochondrial homeostasis? *Nat Cell Biol* 1(8):E209-216.

Verdaguer, N., S. Corbalan-Garcia, W.F. Ochoa, I. Fita, and J.C. Gomez-Fernandez. 1999. $Ca(^{2+})$ bridges the C2 membrane-binding domain of protein kinase Calpha directly to phosphatidylserine. *Embo J* 18(22):6329-6338.

Woo, J.S., J.S. Jung, N.C. Ha, J. Shin, K.H. Kim, W. Lee, and B.H. Oh. 2003. Unique structural features of a BCL-2 family protein CED-9 and biophysical characterization of CED-9/EGL-1 interactions. *Cell Death Differ* 10(12):1310-1319.

Wyllie, A.H. 1994. Death from inside out: an overview. *Philos Trans R Soc Lond B Biol Sci* 345(1313):237-241.

Yan, N., L. Gu, D. Kokel, J. Chai, W. Li, A. Han, L. Chen, D. Xue, and Y. Shi. 2004. Structural, biochemical, and functional analyses of CED-9 recognition by the proapoptotic proteins EGL-1 and CED-4. *Mol Cell* 15(6):999-1006.

Zakharov, S.D., and W.A. Cramer. 2002a. Colicin crystal structures: pathways and mechanisms for colicin insertion into membranes. *Biochim Biophys Acta* 1565(2):333-346.

Zakharov, S.D., and W.A. Cramer. 2002b. Insertion intermediates of pore-forming colicins in membrane two-dimensional space. *Biochimie* 84(5-6):465-475.

Zakharov, S.D., J.B. Heymann, Y.L. Zhang, and W.A. Cramer. 1996. Membrane binding of the colicin E1 channel: activity requires an electrostatic interaction of intermediate magnitude. *Biophys J* 70(6):2774-2783.

Chapter 2

Evidence that Bcl-X_L inserts into membranes by a different mechanism than the structurally homologous, translocation domain from Diphtheria toxin

Summary

Regulation of programmed cell death by Bcl-X_L is dependent on both its solution and integral membrane conformations. A conformational change from solution to membrane is also important in this regulation. This conformational change shows a pH-dependence profile similar to the translocation domain of Diphtheria toxin, where an acid-induced molten globule conformation in the absence of lipid vesicles mediates the change from solution to membrane conformations. By contrast, Bcl-X_LΔTM in the absence of lipid vesicles exhibits no gross conformational changes upon acidification as monitored by near- and far-UV circular dichroism spectropolarimetry. Additionally, no significant local conformational changes upon acidification were observed by heteronuclear NMR spectroscopy of Bcl-X_LΔTM. Under conditions that favor the solution conformation (pH 7.4), the free energy of folding for Bcl-X_LΔTM (ΔG°) was determined to be 15.8 kcal·mol^{-1}. Surprisingly, under conditions that favor a membrane conformation (pH 4.9), ΔG° was 14.6 kcal·mol^{-1}. These results imply other contributions must be necessary to destabilize the solution conformation and favor the membrane conformation at pH 4.9. Such contributions might include the presence of a negatively-charged membrane or an electrostatic potential across the membrane. Thus, for proteins that adopt both solution and membrane conformations, an obligatory molten globule intermediate may not be necessary. The absence of a molten globule intermediate might have evolved to protect Bcl-X_L from intracellular proteases as it undergoes this conformational change essential for its activity.

Introduction

The Bcl-2 proteins regulate programmed cell death by acting in the cytosol and organellar membranes (Adams and Cory, 1998; Chao and Korsmeyer, 1998; Green and Reed, 1998; Harris and Thompson, 2000; Hengartner, 2000; Ng and Shore, 1998). Some Bcl-2 proteins act by adopting at least two different structural conformations: a solution conformation and an integral membrane conformation. For example, pro-apoptotic Bax is a monomeric, helical bundle protein localized in the cytosol until an apoptotic signal causes translocation to the mitochondrial outer membrane (Suzuki et al., 2000a). At the mitochondrial outer membrane, Bax inserts and folds into a large, multimeric integral membrane protein that is thought to regulate the release of cytochrome c (Antonsson et al., 2000; Antonsson et al., 2001a; Hsu et al., 1997; Saito et al., 2000; Shimizu et al., 1999; Wolter et al., 1997). Similar to Bax, the anti-apoptotic protein Bcl-X_L is a soluble primarily monomeric, helical bundle protein localized in part to the cytosol (Muchmore et al., 1996). However, in contrast to Bax, Bcl-X_L inserts into the mitochondrial outer membrane and folds into a small, integral membrane protein (Hsu et al., 1997; Minn et al., 1997). For both proteins, the solution-to-membrane conformational change has been reconstituted *in vitro* with only recombinant proteins and vesicles from synthetic lipids suggesting that this conformational change might not be receptor-mediated (Basanez et al., 2001b; Minn et al., 1997).

The dual structural nature of the Bcl-2 proteins allows for dual mechanisms for their biological activity. In the case of Bcl-X_L, the solution conformation acts by sequestering pro-apoptotic factors in the cytosol as a water-soluble helical bundle (Sattler

et al., 1997; Sedlak et al., 1995). By contrast, the membrane conformation acts as a small, moderately selective cationic channel in the mitochondrial outer membrane (Minn et al., 1997; Vander Heiden et al., 2001). The exact mechanism of Bcl-X_L activity in the membrane is still under debate, but mutants of Bcl-X_L that possess altered ion channel properties also have altered apoptotic activities confirming a biological role for the membrane conformation (Basanez et al., 2001b; Losonczi et al., 2000; Minn et al., 1999; Minn et al., 1997; Vander Heiden et al., 2001; Xie et al., 1998). These properties of Bcl-X_L were actually demonstrated with Bcl-$X_L\Delta TM$[1] that lacks the C-terminal hydrophobic anchor, which is not required for biological activity or ion channel activity (Minn et al., 1997; Muchmore et al., 1996).

The dual mechanisms for the anti-apoptotic activity of Bcl-$X_L\Delta TM$ in the cytosol and in the membrane raise the question of how a water-soluble protein undergoes a conformational change to become an integral membrane protein. This conformational change appears to have two requirements: acidic pH and presence of lipid vesicles (Basanez et al., 2001b). In fact, Bcl-$X_L\Delta TM$ is only weakly associated with lipid vesicles at pH 7.0 but is fully associated at pH 4.5 as measured by a sedimentation assay (Basanez et al., 2001b). The ion channel activity of Bcl-$X_L\Delta TM$ also shows a similar pH dependence with conductance occurring readily under acidic conditions but not readily at pH 7.0 (Minn et al., 1997). Because these experiments were performed *in vitro* with recombinant protein and vesicles derived from synthetic lipids, they suggest that the amino acid sequence alone can specify both solution and membrane conformations.

Many bacterial toxins also undergo a pH-dependent conformational change from solution to membrane conformations including the translocation domain from diphtheria

toxin and the colicin family of pore-forming toxins (Lacy and Stevens, 1998; Lakey et al., 1992; London, 1992; Parker et al., 1990). The solution structures of many of these proteins are known and they share a common helical bundle topology (Choe et al., 1992; Parker et al., 1989; Parker et al., 1992). In fact, the motivation to explore ion channel properties of Bcl-$X_L\Delta TM$ arose, in part, from the structural similarity it shares with the translocation domain of diphtheria toxin (Figure 2.1), which also binds to lipid vesicles in a pH-dependent manner (Muchmore et al., 1996; Sandvig and Olsnes, 1980). Some of these helical bundles retain a helical conformation in the membrane (Chenal et al., 2002; Oh et al., 1996; Zakharov and Cramer, 2002b), but no high-resolution structure of a membrane conformation of these proteins has been determined. The topology of this helical membrane conformation must be quite different from the solution conformation, because the polar or charged residues on the surface of the solution conformation would need to be sequestered from the hydrophobic milieu of the membrane bilayer. Based on these considerations, the solution to membrane conformational change has been referred to folding inside-out (Lesieur et al., 1997). However, recent work also indicates that the presence of charged residues in the membrane environment is tolerated in certain cases depending on the amino acid context in which the charged residues are present (Hessa et al., 2005; Jiang et al., 2003a; Jiang et al., 2003b).

A change in the solution conformation in the absence of lipid vesicles is known for many proteins to lower the activation energy for the solution to membrane conformational change. This change in the solution conformation can be large, such as a change in quaternary structure, or it can be small, such as a change in the tertiary structure commonly referred to as a molten globule conformation. A molten globule

conformation is characterized by native-like secondary structure without the well-packed hydrophobic core found in native-like proteins (Ptitsyn, 1995; Ptitsyn et al., 1990; van der Goot et al., 1991). For example, an acid-induced conformational change in the pore-forming toxin of Colicin A, even in the absence of lipid vesicles, results in formation of a molten globule conformation that more readily associates with lipid vesicles than the solution conformation that predominates at pH 7.4 (van der Goot et al., 1991). In fact, an acid-induced molten globule formation is the dominant mechanism for membrane insertion of many other proteins that undergo a solution to membrane conformational change including annexin 6, TRAIL, StAR, diphtheria toxin (DT) and other toxins (Blewitt et al., 1985; Bychkova et al., 1996; Chenal et al., 2002; Nam and Choi, 2002; Song et al., 2001; van der Goot et al., 1991).

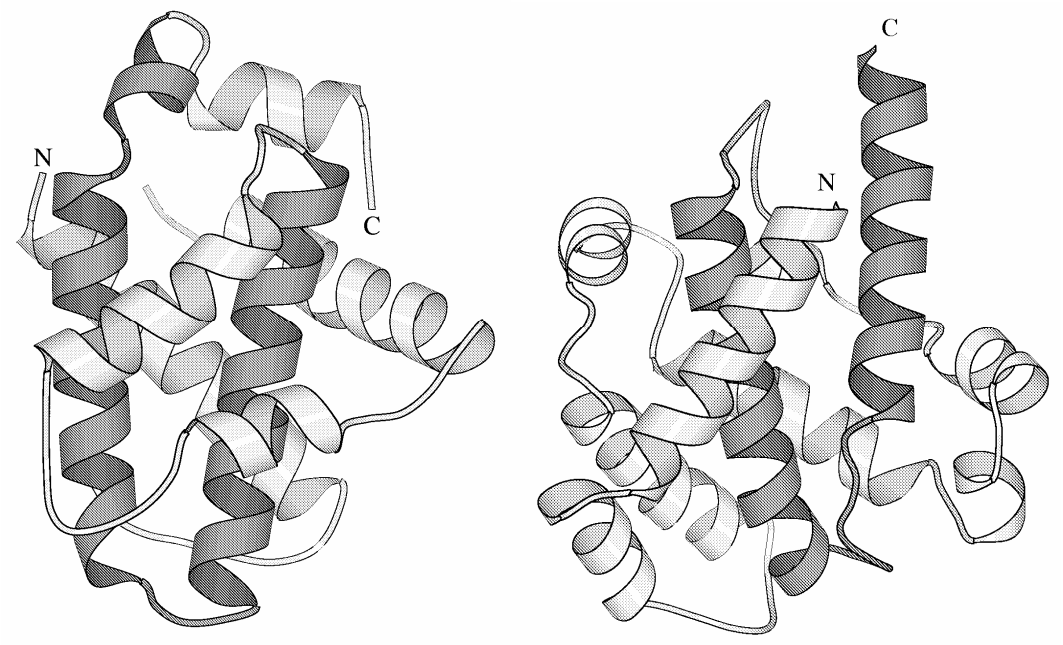

Figure 2.1 Bcl-X_L (left, from 1MAZ.pdb) and the translocation domain of Diphtheria toxin (right, from 1DDT.pdb) share the hydrophobic helical hairpin motif. The hydrophobic helical hairpin motifs, helices 5,6 of Bcl-X_L and helices 8,9 of diphtheria toxin T-domain are represented by a darker shade of grey. These figures were generated using MOLSCRIPT (Kraulis, 1991).

For Bcl-$X_L\Delta$TM, a mechanism for the solution to membrane conformational change is not known beyond the requirement for lipid vesicles and acidic conditions. Therefore, we first asked what changes are occurring to this protein under acidic conditions in the absence of lipid vesicles. Specifically we tested whether lowering the pH induces a change in the tertiary or quaternary structure by examining changes in the thermodynamic stability and structural properties of Bcl-$X_L\Delta$TM.

Materials and Methods

Protein Expression and Purification

Human Bcl-X_L(1-209) that lacks the C-terminal hydrophobic 24 amino acids was sub-cloned into pHis-GB vector using EcoRI and SalI restriction sites by standard procedures (Sambrook, 2001). This construct is an N-terminal fusion of the B1 domain from streptococcal protein G and was selected to improve expression and solubility of Bcl-X_L. The GB1 domain itself contains an N-terminal 6xHis tag for purification by Ni^{2+} affinity chromatography. 6xHis-GB1 is separated from Bcl-$X_L\Delta$TM by a 15-residue linker that contains a recognition site for cleavage by TEV protease, which allows for the liberation of Bcl-$X_L\Delta$TM from the fusion construct upon incubation with 6xHis-TEV protease. Success of the sub-cloning procedure was confirmed by nucleotide sequencing and the resulting plasmid transformed into *E. coli* Rosetta cells (Novagen) for protein overexpression.

To increase the yield of protein in the soluble fraction, cells were grown at 37 ˚C in 2 liters of LB media to a OD_{600} of ~0.7, collected by centrifugation, and gently resuspended in 0.5 L of M9 minimal media and continued to grow at 37 ˚C(Marley et al., 2001). After one hour, protein expression was induced by the addition of 0.5 mM IPTG. The cells were harvested by centrifugation after 5-6 hours at 37˚C and resuspended in Buffer A (20 mM Tris, 0.5 M NaCl, pH 8.0), lysed by three passes through a French press. The protein present in the soluble fraction was then purified by affinity purification on a Ni^{2+} affinity column (His-Trap, GE Healthcare), followed by dialysis into TEV protease cleavage buffer (50 mM Tris, 50 mM NaCl, 5 mM β-mercaptoethanol,

pH 8.0). The fusion protein was then treated overnight at 4˚C with recombinant 6xHis-TEV protease (1:50 w/w ratio) to release Bcl-X_LΔTM from the GB1 domain. The reaction mixture was loaded onto the His-Trap column again and the flow-through fraction containing Bcl-X_LΔTM was collected, concentrated and quantitated using UV-absorbance (ε_{280} = 41820 $M^{-1}cm^{-1}$ in 6 M GdnHCl). The yield of pure protein was approximately 10 mg/L. The purity was greater than 95% as judged by Coomassie-stained gel electrophoresis and the identity of the protein was further confirmed by MALDI-TOF mass spectrometry. ^{15}N labeled samples were prepared in a similar manner in the presence of $^{15}NH_4Cl$ in the M9 minimal medium. All the proteins were stored at 4 °C until used.

Chemical denaturation studies

The free energy of unfolding of Bcl-X_LΔTM was determined by chemical denaturation titration experiments using GdnHCl. The unfolding reaction was monitored by observing the changes in the ellipticity at 222 nm using a Jasco J-810 spectropolarimeter. The temperature was maintained at 25 °C and the scan speed was 10 nm/min. Each data point represents the average of 5 accumulations with a response time of 2 s. The data of ε_{222} vs [GdnHCl] were fit to a 2-state model using a non-linear least squares fit to the following equation using a script written in Igor Pro 4.04:

$$\varepsilon_{222} = \frac{((b_N + m_N \bullet [GdnHCl]) + (b_D + m_D \bullet [GdnHCl]) \bullet e^{-\frac{(\Delta G^0_{H_2O} - m_G \bullet [GdnHCl])}{RT}})}{(1 + e^{-\frac{(\Delta G^0_{H_2O} - m_G \bullet [GdnHCl])}{RT}})} \quad (2.1)$$

where b_N, m_N and b_D, m_D represent the ordinate and slope of the native and denatured baselines respectively (Santoro and Bolen, 1988). Values for the native and denatured state baselines were estimated by fits to the raw data to minimize the χ^2 of the fit. The global folding stability extrapolated to standard conditions is given by $\Delta G°_{H2O}$, and m_G is the slope of the linear extrapolation curve that represents the denaturant dependence of the Gibbs free energy.

Analytical Ultracentrifugation

Sedimentation equilibrium experiments were performed on Bcl-X_LΔTM at 25 °C in a Beckman XL-I analytical ultracentrifuge. 10 μM, 25 μM and 50 μM Bcl-X_LΔTM samples in 20 mM sodium phosphate buffer at pH 7.4 and in 20 mM sodium acetate buffer at pH 4.9 were subjected to centrifugation at the following speeds: 17000, 19000 and 22000 rpm. Equilibrium was achieved after 12 hours and the resulting data sets were globally fit to a modified Lamm-Svedberg equation as described (Hill et al., 2000b). Excellent fits were obtained by fitting to a single species using the Marquardt-Levenberg non-linear least square algorithm (Levenberg, 1944; Marquardt, 1963). The partial specific volume was estimated to be 0.7217 from the amino acid composition using the method of Cohn and Edsall (Cohn, 1943). The density of the buffers were estimated to be 0.99971 (phosphate) and 0.999723 (acetate) using the program Sednterp (www.jphilo.mailway.com).

Circular Dichroism Spectroscopy

The far-UV circular dichroism spectrum was collected on a 7 μM sample of Bcl-$X_L\Delta TM$ in 20 mM sodium phosphate at pH 7.4 or 20 mM sodium acetate at pH 4.9 using a JASCO Model 710 CD Spectropolarimeter. The far-UV spectra were collected from 260 to 190 nm at a scan rate of 10 nm/min. The near-UV spectra from 320 to 250 nm were collected at a scan rate of 10 nm/min with a protein concentration of 40 μM. All the spectra were collected at 25 °C, corrected for buffer ellipticity, and represent the signal average of five accumulations. The percent α-helicity was estimated by the method of Luo and Baldwin (Luo and Baldwin, 1997).

NMR Spectroscopy

Unlabeled or ^{15}N labeled NMR samples of Bcl-$X_L\Delta TM$ (0.5 mM) were prepared in 20 mM sodium phosphate buffer plus 10% D_2O at pH 7.4 (meter reading) and titrated down to pH 4.9 by the addition of small amounts of 0.1 N hydrochloric acid. The NMR experiments were performed at 25 °C either on a Varian INOVA 500 MHz or a Bruker AVANCE 600 MHz spectrometer equipped with a triple resonance probe with triple axis gradients. The ^{1}H-^{15}N heteronuclear single quantum coherence (HSQC) spectra were collected with 1024 × 128 complex points (acquisition times of 64 and 32 ms in the direct and indirect detected dimension, respectively) with the ^{15}N carrier offset at 117.5 ppm. The ^{1}H-^{13}C HSQC was collected at natural abundance (2048 transients) with 1024 × 40 complex points with acquisition times of 64 and 7.4 ms in ^{1}H and ^{13}C respectively with ^{13}C carrier offset placed at 17 ppm. The data were processed with nmrPipe (Delaglio et al., 1995) and displayed using NMRView (Johnson, 2004; Johnson, 1994a).

Results

No significant change in thermodynamic stability of Bcl-X_LΔTM upon acidification

Bcl-X_LΔTM is able to bind to lipid vesicles upon acidification(Basanez et al., 2001b; Minn et al., 1997). This process could be facilitated by a change in structure or dynamics, of the protein upon acidification even in the absence of lipid vesicles, which would be reflected in the thermodynamic stability of the protein. Therefore, the free energy of unfolding of Bcl-X_LΔTM was determined at pH 7.4 and 4.9 by chemical denaturation monitoring the circular dichroism signal at 222 nm as a function of increasing GdnHCl concentration (Figure 2.2). The data fit well to a 2-state model for the unfolding reaction. At pH 7.4, the change in free energy of unfolding (ΔG°) for Bcl-X_LΔTM was determined to be 15.8 ± 1.2 kcal·mol^{-1} while the corresponding value at pH 4.9 was 14.6 ± 1.0 kcal·mol^{-1}. Fits to a three state model resulted in variable values of ΔG° for the N to I and I to D transitions due to the difficulty in describing the intermediate state baselines.

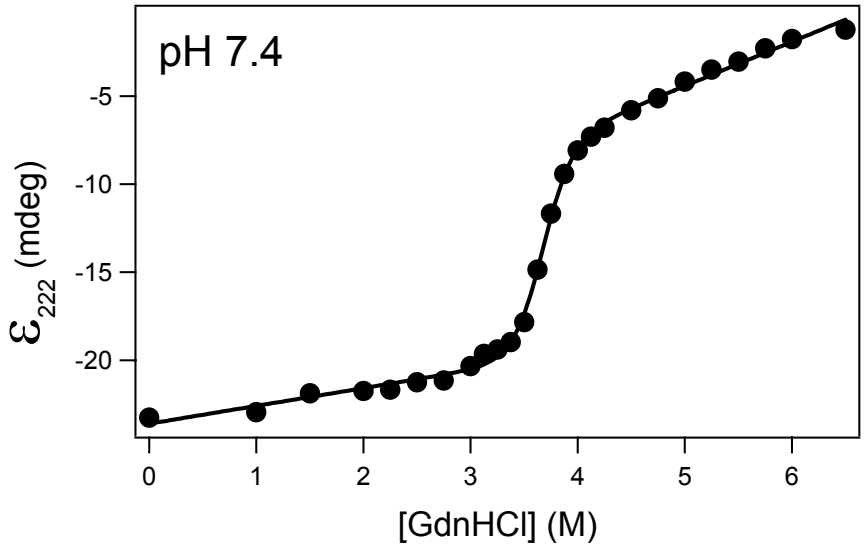

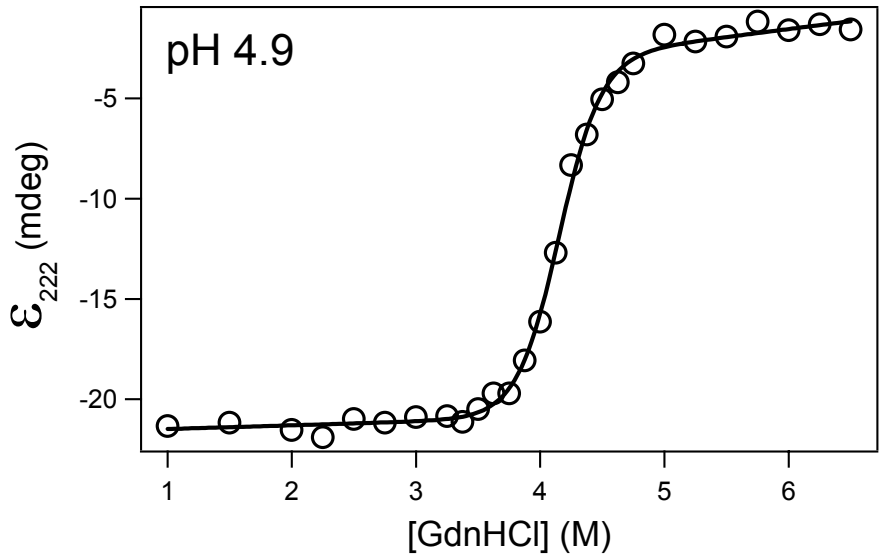

Figure 2.2 The thermodynamic stability of Bcl-X_LΔTM is slightly reduced upon acidification. The circular dichroic signal at 222nm of Bcl-X_LΔTM was monitored as a function of GdnHCl and the resulting data fit as described in the text. The free energy of folding, $\Delta G°(H_2O)$, under conditions that do not favor membrane insertion (pH 7.4, ●) is 15.8 ± 1.2 kcal·mol^{-1}. Under conditions that favor membrane insertion (pH 4.9, ○), $\Delta G°(H_2O)$ is 14.6 ± 1.0 kcal·mol^{-1}.

Chemical denaturation of Bcl-X_LΔTM monitored by the change in intrinsic tryptophan fluorescence also confirmed that there was no significant change in the thermodynamic stability upon acidification. The ΔG° of unfolding was estimated to be 14.3 ± 2.2 kcal·mol^{-1} and 15.8 ± 3.0 kcal·mol^{-1} at pH 7.4 and pH 4.9 respectively using fluorescence spectroscopy.

To determine the enthalpic contributions to the free energy of folding, we performed differential scanning calorimetry experiments at pH 7.4 and 4.9. The midpoint for the unfolding transition (T_m) is reduced upon acidification from 76 °C to 71 °C (data not shown). Unfortunately, the thermal unfolding transition was irreversible under these and other conditions; no further thermodynamic analysis was possible.

A decrease in pH does not induce a change in the quaternary structure

Given that the thermodynamic stability of Bcl-X_LΔTM at pH 4.9 is still quite high (14.6 kcal·mol^{-1}), we postulated that this protein might undergo a pH-dependent oligomerization as an intermediary step towards membrane insertion. We hypothesized that a decrease in pH might destabilize the monomer and favor oligomer formation providing the necessary free energy to achieve a membrane-insertion competent state and lead to the insertion of Bcl-X_LΔTM into the membrane. Previously, Bcl-X_LΔTM was reported to undergo dimerization although only in the presence of non-ionic detergents (Xie et al., 1998). To test for acid-induced formation of oligomers in solution, we used sedimentation equilibrium experiments. Six datasets collected using protein at 2 different concentrations and equilibrated at three different rotor speeds were globally fit to a modified Lamm-Svedberg equation. Analysis performed at pH 7.4 and pH 4.9 showed that there was no significant change in the oligomeric state of the protein as a function of pH (Figure 2.3). The data at both pH values were well described by a fit to a single monomeric species. The molecular weight estimates were 25.4 ± 0.2 kDa at pH 7.4, and 27.3 ± 0.2 kDa at pH 4.9. The actual molecular weight of Bcl-X_L ΔTM is 23.8 kDa. The slight discrepancies in the molecular weights most likely are due to the uncertainty in the estimate for the partial specific volume (Kharakoz, 1997), because fits of the data to a monomer-dimer equilibrium gave unreasonable values for K_D (10^2 M). Therefore, Bcl-X_L ΔTM is monomeric at both conditions.

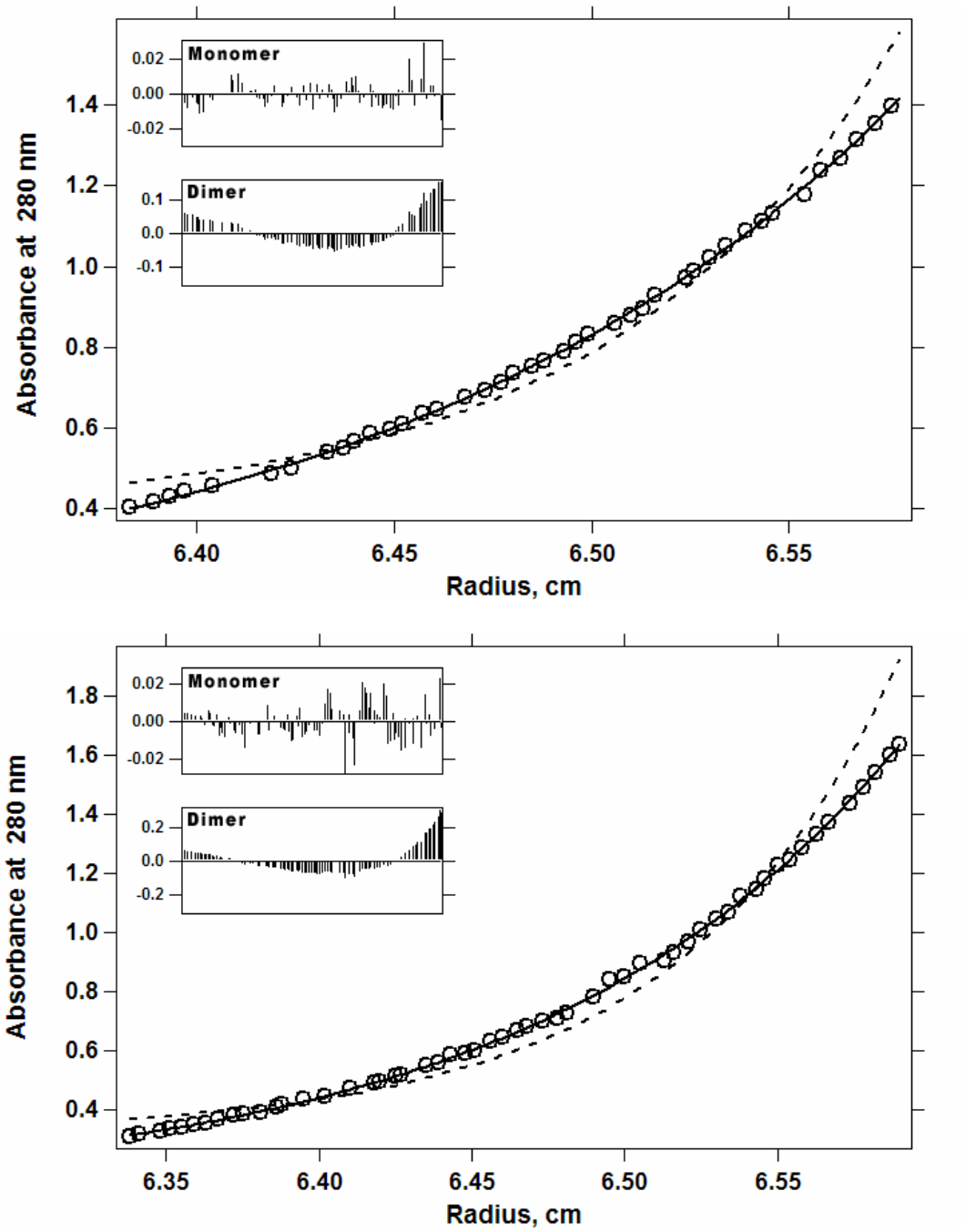

Figure 2.3 Bcl-X_LΔTM is monomeric in solution upon acidification. Representative sedimentation equilibrium data is presented for 25 μM Bcl-X_LΔTM at a XLI rotor speed of 19000 rpm in solution at 25 °C collected at (a) pH 7.4 and (b) 4.9. The data are well described by fitting to a single species (—) that is the molecular weight of monomeric Bcl-X_LΔTM within experimental uncertainty. Every second data point is displayed (○) but all data were globally fit. The fit to the molecular weight of the dimer of Bcl-X_LΔTM (- - -) and the residuals to the fits are also displayed. The results from the global fit of the data from three concentrations and XLI rotor speeds of 17000, 19000, and 22000 rpm, carried out using a modified Lamm-Svedberg equation are described in the text.

No global changes in backbone structure of Bcl-X_L ΔTM upon acidification

To test for any pH-dependent conformational change of the backbone of Bcl-X_L ΔTM, we recorded the far-UV circular dichroism spectrum as a function of pH (Figure 2.4). The far-UV CD spectrum reports primarily on the secondary structure of a protein and for Bcl-X_LΔTM at pH 7.4 is typical of a well-folded helical bundle protein with approximately 36% α-helicity. At pH 4.9, the spectrum was very similar to pH 7.4 (33% α-helicity) indicating no significant changes in the backbone structure occur upon acidification.

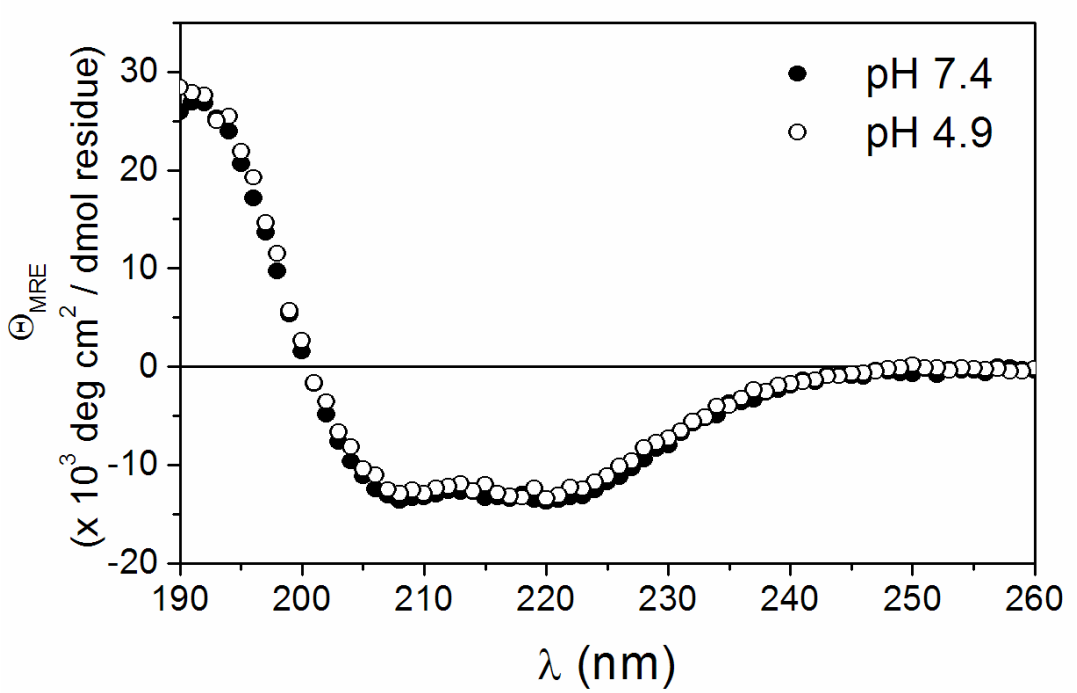

Figure 2.4 Secondary structure of Bcl-X_LΔTM is conserved upon acidification. The far-UV circular dichroism spectra were collected at pH 7.4 (●) and pH 4.9 (○).

The helical content from the circular dichroism spectra is slightly smaller than the values of 41.5% or 48.6% as calculated from the solution structure (1LXL.pdb) or the crystal structure (1MAZ.pdb). The difference could be attributed to the dynamics of the protein with the average helical content being slightly lower as measured using circular dichroism.

No local structural changes in backbone structure of Bcl-X_L ΔTM upon acidification

The circular dichroism spectrum measures mean residue ellipticity that is unable to report on site specific changes in the backbone structure of Bcl-X_LΔTM as a function of pH, whereas NMR spectroscopy can provide more detailed information. Therefore, to gain such information and to determine that the CD results did not arise from a concomitant loss and gain of helicity in the protein upon acidification, we examined the $^{1}H-^{15}N$ HSQC NMR spectrum as a function of pH (Figure 2.5a).

$^{1}H-^{15}N$ HSQC experiments provide residue-specific information primarily of the backbone structure of a protein. Upon lowering the pH, no significant change in the chemical shifts of the backbone amides of Bcl-X_LΔTM were observed in either the ^{1}H (Figure 2.5b-d) or ^{15}N data (not shown), which is consistent with the CD results. These results suggest that no significant structural changes, local or global, occur in the backbone structure of Bcl-X_LΔTM from pH 7.4 to 4.9.

In the case of many bacterial toxins, membrane insertion upon acidification is aided by the formation of a molten globule intermediate. In a "native-like" molten globule, the secondary structure of the protein is similar to the native state and the general tertiary fold is retained while in a "disordered" molten globule, the tertiary structure is not retained (Creighton, 1992; Ptitsyn, 1995; Ptitsyn et al., 1990). However, in both cases, the structural integrity of the hydrophobic core of a molten globule is compromised with the hydrophobic core becoming more fluid. This would result in the apolar sidechains becoming free to adopt more rotameric positions than in the native state (Creighton, 1992).

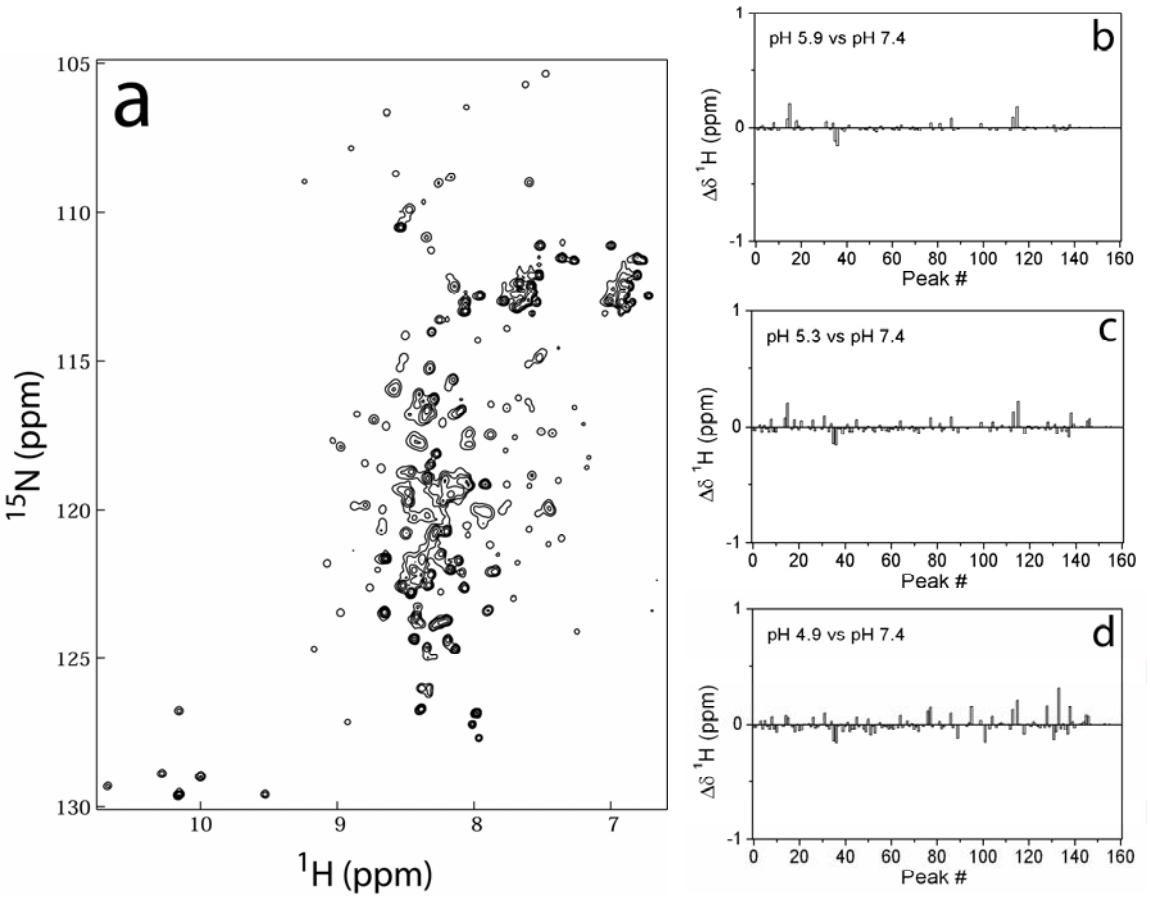

Figure 2.5 The backbone structure of Bcl-X_LΔTM does not undergo significant conformational change upon acidification. ^{1}H-^{15}N HSQC spectra of Bcl-X_LΔTM were collected on a 0.6 mM sample of uniformly ^{15}N labeled protein as a function of pH. (a) A representative ^{1}H-^{15}N HSQC spectrum for Bcl-X_LΔTM at pH 7.4 is shown. The differences in amide proton chemical shift between pH 7.4 and pH 5.9(b), pH 5.3 (c), and pH 4.9 (d) are displayed. Note that some minor differences are expected due to the salt dependence of the chemical shift(Schaller and Robertson, 1995). Differences in amide nitrogen chemical shift also showed no significant changes as function of pH (data not shown).

Therefore we tested whether the ability of Bcl-X_LΔTM to insert into membranes upon acidification arises from the formation of a molten globule that could be detected by observing changes in the hydrophobic core. The near-UV CD signal can report on the structural integrity of the aromatic residues in the hydrophobic core of the protein. In the case of a molten globule state, the aromatic residues are no longer well-packed in an asymmetric environment resulting in a loss of signal in this region of the spectrum. Bcl-

$X_L\Delta TM$ has about 15 aromatic residues in the hydrophobic core of the protein suggesting that changes in the fluidity of the hydrophobic core would be reflected in the near-UV CD signal. However, at pH 4.9, we observed no change in the near-UV CD signal from that observed at pH 7.4 (Figure 2.6) suggesting the lack of an acid-induced molten globule state of Bcl-X_L ΔTM.

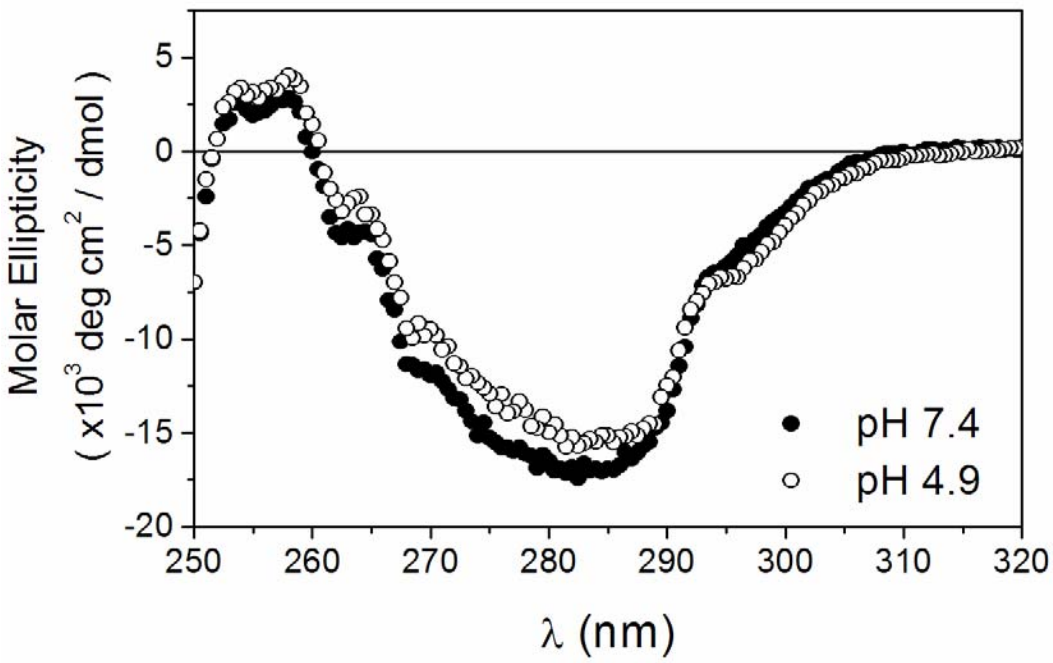

Figure 2.6. The integrity of the hydrophobic core packing in Bcl-$X_L\Delta TM$ is conserved upon acidification. Near-UV spectra were collected at pH 7.4 (●) and pH 4.9 (○).

A hallmark of a molten globule state is the ability to bind hydrophobic dyes such as 8-anilino-1-naphthalene sulfonic acid (ANS). In fact, Bcl-X_L ΔTM has been reported in the past to bind ANS (Xie et al., 1998). However, the solution conformation of Bcl-X_L ΔTM reveals a hydrophobic cleft that would be expected to bind ANS without molten globule formation. For this reason, we measured the pH dependence of the methyl carbon chemical shifts, which are a more direct measure of the integrity of the hydrophobic core. These chemical shifts arise from methyl sidechains of residues found primarily in the hydrophobic core of a protein. The spectrum collected at pH 7.4 showed

well dispersed resonances in the methyl region indicative of a well packed hydrophobic core and typical of a native protein (Figure 2.7a). Upon lowering the pH to 4.9, these methyl resonances were still well-dispersed indicating that the protein retained a well packed hydrophobic core consistent with the absence of a molten globule state (Figure 2.7b). The absence of any gross structural change in Bcl-X_LΔTM between pH 7.4 and 4.9 argues for either subtle structural or dynamical changes in solution that we were unable to detect by these CD or NMR experiments, or the requirement of lipids for its pH-dependent solution-to-membrane conformational change.

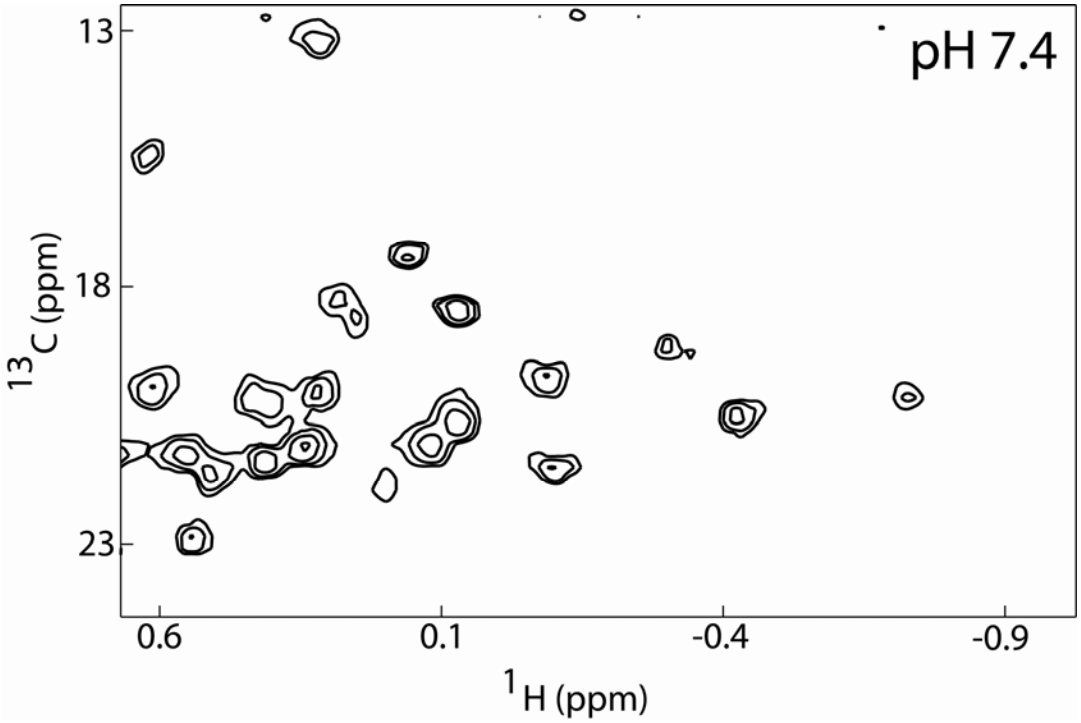

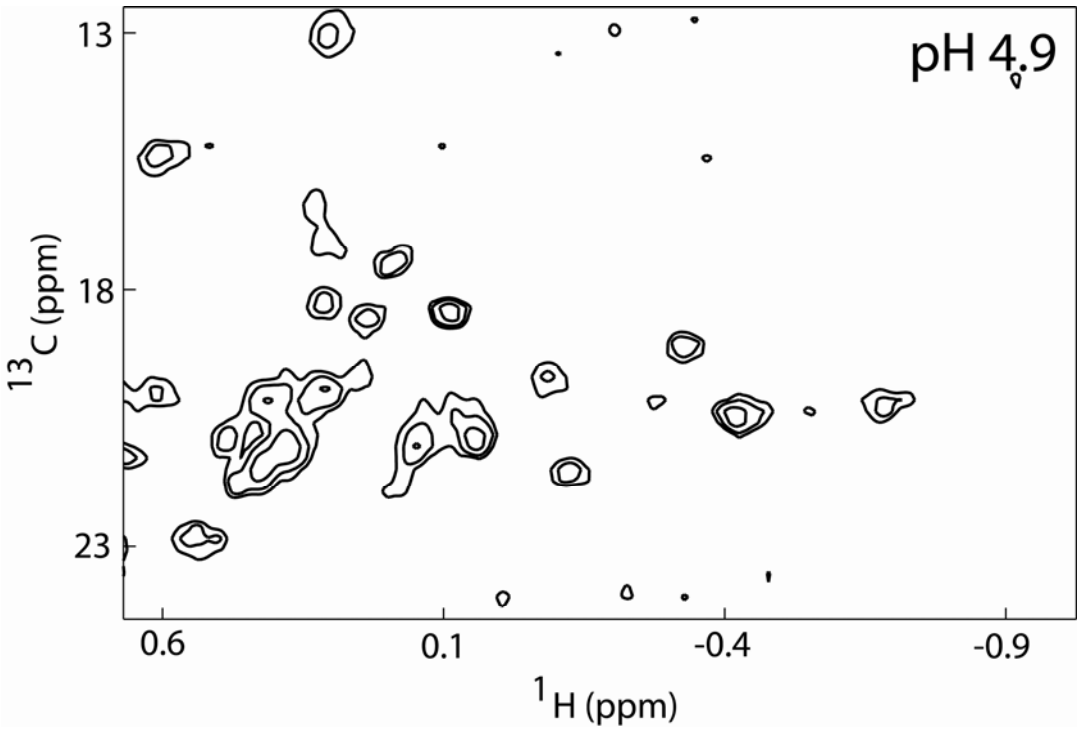

Figure 2.7 No indication of molten-globule formation upon acidification of Bcl-X_L ΔTM. ^{1}H-^{13}C HSQC spectra of Bcl-X_LΔTM were collected on a 0.8 mM unlabeled protein sample (natural abundance ^{13}C) as a function of pH. Data shown only for (a) pH 7.4 and (b) pH 4.9.

Discussion

Here we present data that suggests Bcl-X_L undergoes a solution to membrane conformational change by a different mechanism than the translocation domain from Diphtheria toxin by examining the thermodynamic and structural properties of Bcl-$X_L\Delta$TM as a function of pH in the absence of lipid vesicles. We find little change in the thermodynamic stability or structure of Bcl-$X_L\Delta$TM from pH 7.4 to 4.9 while in the presence of lipid vesicles this pH change results in complete association of Bcl-$X_L\Delta$TM with lipid vesicles - data not shown). The results presented here suggest that this protein does not insert through an obligatory molten globule intermediate, as has been observed for other membrane-insertable proteins such as cytochrome c, TRAIL, StAR, diphtheria toxin (DT) and other toxins (Blewitt et al., 1985; Bychkova et al., 1996; Chenal et al., 2002; Nam and Choi, 2002; Song et al., 2001; van der Goot et al., 1991).

The absence of significant structural changes in solution led us to alternative models that included the possibility of oligomer formation facilitating membrane insertion such as that which occurs for the annexin family of proteins (Beermann et al., 1998). An oligomeric insertion mechanism is also common for many β-barrel toxins (Gouaux, 1997; Heuck et al., 2001). However, no changes in oligomerization state were observed for Bcl-$X_L\Delta$TM as the data were best described by a fit to a monomeric species at both pH 7.4 and 4.9. Our data cannot exclude the possibility of oligomerization in the presence of the membrane, and evidence for monomeric and dimeric states of Bcl-$X_L\Delta$TM in the presence of detergents has been reported (Xie et al., 1998).

The difference in the free energy of folding ($\Delta\Delta G°$) of Bcl-$X_L\Delta TM$ between the pH 7.4 and 4.9 in the absence of lipid vesicles is only 1.2 kcal·mol^{-1}, which is within the uncertainty in the measurements and is small relative to its thermodynamic stability (14.6 kcal·mol^{-1} at pH 4.9). To confirm these observations, we repeated these measurements several times on different preparations of the protein. Therefore, even at a pH that favors the solution to membrane conformational change, the solution conformation of Bcl-$X_L\Delta TM$ is still quite stable. Therefore, we conclude that acid-induced destabilization of the solution conformation does not contribute to the energetics of the solution to membrane conformational change.

However, we did observe a pH-dependence to the denaturant dependence to the free energy of folding as reflected by the m_G value. The m_G value decreases from 4.3 ± 0.3 kcal·mol^{-2} at pH 7.4 to 3.5 ± 0.2 kcal·mol^{-2} at pH 4.9. Typically, such a decrease in m_G is interpreted as the presence of an intermediate that is stabilized at acidic pH conditions, leading to a decrease in 2-state character and a lower m_G value (Whitten et al., 2001). In our case, we do not explicitly observe the presence of an equilibrium intermediate, but it is certainly possible that such an intermediate is populated yet not detected by our methods.

The notable lack of difference in the free energy of folding ($\Delta\Delta G°$) of Bcl-$X_L\Delta TM$ between pH 7.4 and 4.9 is unlike other proteins that undergo an acid-induced solution to membrane conformational change. For example, the difference in the free energy of folding of diphtheria toxin is ten-fold from 6.9 kcal·mol^{-1} at pH 8 to 0.6 kcal·mol^{-1} at pH 2.5. In the case of diphtheria toxin, the large pH-dependence to the free energy of folding is presumably harnessed to provide the necessary free energy for the

solution to membrane conformational change (London, 1992; Ramsay et al., 1989). At low pH, the destabilization of the native structure of the diphtheria toxin translocation domain by 6.3 kcal·mol^{-1} favors insertion to a membrane conformation. Such a mechanism cannot be possible for Bcl-X_L given the lack of pH-dependence to the thermodynamic stability of the solution conformation.

This result with Bcl-X_L is somewhat surprising given the results with another pore-forming toxin, Colicin A. In this case, the rate limiting step for the solution to membrane conformational change was the acid-induced unfolding rate of the solution conformation, and not membrane binding (van der Goot et al., 1991). By contrast, the thermodynamic stability of a different colicin, Colicin B, has a smaller pH dependence that is more similar to Bcl-X_LΔTM than Colicin A. However, in the case of colicin B the small acid-induced change in free energy is accompanied by structural changes not observed in Bcl-X_LΔTM by our measurements.

While no pH-dependent change is observed in the thermodynamic stability for Bcl-X_LΔTM, the relative enthalpic and entropic contributions to the free energy of folding might exhibit a pH-dependence that would inform on the mechanism of the solution to membrane conformational change. Presumably the enthalpy of folding does have a pH-dependence because certain residues will become protonated from pH 7.4 to 5.0, and the enthalpy of protonation for these residues will contribute to the enthalpic contributions to the free energy of folding (Petrosian and Makhatadze, 2000; Pfeil and Privalov, 1976). To detect such enthalpy-entropy compensation to the overall free energy, we attempted to measure the enthalpy of unfolding for Bcl-X_LΔTM by

differential scanning calorimetry, but the thermal transition was irreversible under a variety of conditions and no further data analysis was possible.

If the enthalpy changed as anticipated based on expected values for the enthalpy of protonation, then the entropic contributions to the free energy would also change. NMR spin relaxation measurements that are sensitive to protein dynamics might be able to detect such a change in entropy (Palmer, 2001b; Wand, 2001; Yang et al., 1997), but the simple heteronuclear correlation experiments presented here are not. In our experiments, chemical exchange with a small population is difficult to detect (Thuduppathy and Hill, 2004a). Thus, the relative enthalpic and entropic contributions to the lack of pH dependence of the thermodynamic stability for Bcl-X_LΔTM await further investigation.

Our results with Bcl-X_LΔTM have implications for the full length molecule. The requirement for acidic pH conditions *in vitro* for the solution to membrane conformational change of Bcl-X_LΔTM in the presence of lipid vesicles is to potentially increase the likelihood that the protein lacking the C-terminal transmembrane anchor will associate with the membrane (Schendel et al., 1998). This acidic pH requirement might not be necessary for full length molecule. Or perhaps a lower decrease in pH is necessary for the full length molecule to drive the equilibrium from solution to the membrane conformations *in vivo*. Interestingly, a slight decrease in the pH of the cytosol from pH 7.4 to pH 6.6 has been observed during the initial phases of apoptosis (Matsuyama et al., 2000). Also, anionic lipids on the surface of a membrane, like the mitochondrial outer membrane, create a negative surface, increasing counter ion concentration near the membrane surface (McLaughlin, 1989; Menestrina et al., 1989; Murray et al., 1999; van

der Goot et al., 1991). It has been interpreted that the negative membrane surface also increases proton concentration near the surface, effectively lowering the local pH near the membrane surface, though this interpretation has been disputed (van der Goot et al., 1991).

Perhaps the reason for a difference in mechanism for the solution to membrane conformational changes of diphtheria toxin and Bcl-X_L relates to the biological process that triggers these conformational changes. While the exact trigger for Bcl-X_L is unknown, Diphtheria toxin enters the cell via a clathrin-coated endosome that becomes acidic during maturation of the endosome (Draper and Simon, 1980; Sandvig and Olsnes, 1980). By contrast, Bcl-X_L is exposed to a cytosolic environment that is more susceptible to intracellular proteases than the endosome. Therefore, the avoidance of a molten globule intermediate might have evolved to prevent unregulated degradation of Bcl-X_L by intracellular proteases that would cleave a molten globule intermediate state more efficiently than the native state of Bcl-X_L. Such proteases would not be present in the endosome, and might have allowed the evolution of a diphtheria toxin that capitalizes on the acidic nature of the endosome. Based upon the results presented here, Bcl-X_L must have evolved a different mechanism.

In summary, we find little change in the thermodynamic stability or solution conformation of Bcl-$X_L\Delta$TM upon acidification suggesting that the membrane conformation of this protein is not stabilized solely by acidification but requires the presence of membrane. Our results suggest that the solution to membrane conformational change for Bcl- X_L does not go through an obligatory molten globule intermediate which is the dominant mechanism for other proteins. Thus, the main driving

force behind this conformational change must be derived from the free energy of binding to the membrane or by coupling to another protein or peptide that assists in this conformational change *in vivo*.

References

Adams, J.M., and S. Cory. 1998. The Bcl-2 protein family: arbiters of cell survival. *Science* 281(5381):1322-1326.

Antonsson, B., S. Montessuit, S. Lauper, R. Eskes, and J.C. Martinou. 2000. Bax oligomerization is required for channel-forming activity in liposomes and to trigger cytochrome c release from mitochondria. *Biochem J* 345 Pt 2:271-278.

Antonsson, B., S. Montessuit, B. Sanchez, and J.C. Martinou. 2001. Bax is present as a high molecular weight oligomer/complex in the mitochondrial membrane of apoptotic cells. *J Biol Chem* 276(15):11615-11623.

Basanez, G., J. Zhang, B.N. Chau, G.I. Maksaev, V.A. Frolov, T.A. Brandt, J. Burch, J.M. Hardwick, and J. Zimmerberg. 2001. Pro-apoptotic cleavage products of Bcl-xL form cytochrome c-conducting pores in pure lipid membranes. *J Biol Chem* 276(33):31083-31091.

Beermann, B.B., H.J. Hinz, A. Hofmann, and R. Huber. 1998. Acid induced equilibrium unfolding of annexin V wild type shows two intermediate states. *FEBS Lett* 423(2):265-269.

Blewitt, M.G., L.A. Chung, and E. London. 1985. Effect of pH on the conformation of diphtheria toxin and its implications for membrane penetration. *Biochemistry* 24(20):5458-5464.

Bychkova, V.E., A.E. Dujsekina, S.I. Klenin, E.I. Tiktopulo, V.N. Uversky, and O.B. Ptitsyn. 1996. Molten globule-like state of cytochrome c under conditions simulating those near the membrane surface. *Biochemistry* 35(19):6058-6063.

Chao, D.T., and S.J. Korsmeyer. 1998. BCL-2 family: regulators of cell death. *Annu Rev Immunol* 16:395-419.

Chenal, A., P. Savarin, P. Nizard, F. Guillain, D. Gillet, and V. Forge. 2002. Membrane protein insertion regulated by bringing electrostatic and hydrophobic interactions into play. A case study with the translocation domain of diphtheria toxin. *J Biol Chem* 277(45):43425-43432.

Choe, S., M.J. Bennett, G. Fujii, P.M. Curmi, K.A. Kantardjieff, R.J. Collier, and D. Eisenberg. 1992. The crystal structure of diphtheria toxin. *Nature* 357(6375):216-222.

Cohn, E.J., and Edsall, J.T. 1943. Protein, Amino Acids, and Peptides as Ions and Dipolar Ions. Reinhold, New York.

Creighton, T.E. 1992. The Molten Globule State. *In* Protein Folding. W.H. Freeman and Company, New York. 243-300.

Delaglio, F., S. Grzesiek, G.W. Vuister, G. Zhu, J. Pfeifer, and A. Bax. 1995. NMRPipe: a multidimensional spectral processing system based on UNIX pipes. *J Biomol NMR* 6(3):277-293.

Draper, R.K., and M.I. Simon. 1980. The entry of diphtheria toxin into the mammalian cell cytoplasm: evidence for lysosomal involvement. *J Cell Biol* 87(3 Pt 1):849-854.

Gouaux, E. 1997. Channel-forming toxins: tales of transformation. *Curr Opin Struct Biol* 7(4):566-573.

Green, D.R., and J.C. Reed. 1998. Mitochondria and apoptosis. *Science* 281(5381):1309-1312.
Harris, M.H., and C.B. Thompson. 2000. The role of the Bcl-2 family in the regulation of outer mitochondrial membrane permeability. *Cell Death Differ* 7(12):1182-1191.
Hengartner, M.O. 2000. The biochemistry of apoptosis. *Nature* 407(6805):770-776.
Heuck, A.P., R.K. Tweten, and A.E. Johnson. 2001. Beta-barrel pore-forming toxins: intriguing dimorphic proteins. *Biochemistry* 40(31):9065-9073.
Hessa, T., S.H. White, and G. von Heijne. 2005. Membrane insertion of a potassium-channel voltage sensor. *Science* 307(5714):1427.
Hill, R.B., J.K. Hong, and W.F. DeGrado. 2000. Hydrogen bonded cluster can specify the native state of a protein. *J Am Chem Soc* 122(4):746-747.
Hsu, Y.T., K.G. Wolter, and R.J. Youle. 1997. Cytosol-to-membrane redistribution of Bax and Bcl-X(L) during apoptosis. *Proc Natl Acad Sci U S A* 94(8):3668-3672.
Jiang, Y., A. Lee, J. Chen, V. Ruta, M. Cadene, B.T. Chait, and R. MacKinnon. 2003a. X-ray structure of a voltage-dependent K+ channel. *Nature* 423(6935):33-41.
Jiang, Y., V. Ruta, J. Chen, A. Lee, and R. MacKinnon. 2003b. The principle of gating charge movement in a voltage-dependent K+ channel. *Nature* 423(6935):42-48.
Johnson, B.A. 2004. Using NMRView to visualize and analyze the NMR spectra of macromolecules. *Methods Mol Biol* 278:313-352.
Johnson, B.A., and Blevins, R. A. 1994. NMRView: A computer program for the visualization and analysis of NMR data. *Journal of Biomolecular NMR* 4(603-615).
Kharakoz, D.P. 1997. Partial volumes and compressibilities of extended polypeptide chains in aqueous solution: additivity scheme and implication of protein unfolding at normal and high pressure. *Biochemistry* 36(33):10276-10285.
Kraulis, P.J. 1991. MOLSCRIPT: A Program to Produce Both Detailed and Schematic Plots of Protein Structures. *Journal of Applied Crystallography* 24:946-950.
Lacy, D.B., and R.C. Stevens. 1998. Unraveling the structures and modes of action of bacterial toxins. *Curr Opin Struct Biol* 8(6):778-784.
Lakey, J.H., J.M. Gonzalez-Manas, F.G. van der Goot, and F. Pattus. 1992. The membrane insertion of colicins. *FEBS Lett* 307(1):26-29.
Lesieur, C., B. Vecsey-Semjen, L. Abrami, M. Fivaz, and F. Gisou van der Goot. 1997. Membrane insertion: The strategies of toxins (review). *Mol Membr Biol* 14(2):45-64.
Levenberg, K. 1944. A Method for the solution of certain problems in Least Squares. *Quart. Appl. Math.* 2:164-168.
London, E. 1992. Diphtheria toxin: membrane interaction and membrane translocation. *Biochim Biophys Acta* 1113(1):25-51.
Losonczi, J.A., E.T. Olejniczak, S.F. Betz, J.E. Harlan, J. Mack, and S.W. Fesik. 2000. NMR studies of the anti-apoptotic protein Bcl-xL in micelles. *Biochemistry* 39(36):11024-11033.
Luo, P., and R.L. Baldwin. 1997. Mechanism of helix induction by trifluoroethanol: a framework for extrapolating the helix-forming properties of peptides from trifluoroethanol/water mixtures back to water. *Biochemistry* 36(27):8413-8421.
Marley, J., M. Lu, and C. Bracken. 2001. A method for efficient isotopic labeling of recombinant proteins. *J Biomol NMR* 20(1):71-75.

Marquardt, D. 1963. An Algorithm for Least-Squares Estimation of Nonlinear Parameters. *SIAM J. Appl. Math.* 11:431-441.

Matsuyama, S., J. Llopis, Q.L. Deveraux, R.Y. Tsien, and J.C. Reed. 2000. Changes in intramitochondrial and cytosolic pH: early events that modulate caspase activation during apoptosis. *Nat Cell Biol* 2(6):318-325.

McLaughlin, S. 1989. The electrostatic properties of membranes. *Annu Rev Biophys Biophys Chem* 18:113-136.

Menestrina, G., S. Forti, and F. Gambale. 1989. Interaction of tetanus toxin with lipid vesicles. Effects of pH, surface charge, and transmembrane potential on the kinetics of channel formation. *Biophys J* 55(3):393-405.

Minn, A.J., C.S. Kettlun, H. Liang, A. Kelekar, M.G. Vander Heiden, B.S. Chang, S.W. Fesik, M. Fill, and C.B. Thompson. 1999. Bcl-xL regulates apoptosis by heterodimerization-dependent and -independent mechanisms. *Embo J* 18(3):632-643.

Minn, A.J., P. Velez, S.L. Schendel, H. Liang, S.W. Muchmore, S.W. Fesik, M. Fill, and C.B. Thompson. 1997. Bcl-x(L) forms an ion channel in synthetic lipid membranes. *Nature* 385(6614):353-357.

Muchmore, S.W., M. Sattler, H. Liang, R.P. Meadows, J.E. Harlan, H.S. Yoon, D. Nettesheim, B.S. Chang, C.B. Thompson, S.L. Wong, S.L. Ng, and S.W. Fesik. 1996. X-ray and NMR structure of human Bcl-xL, an inhibitor of programmed cell death. *Nature* 381(6580):335-341.

Murray, D., A. Arbuzova, G. Hangyas-Mihalyne, A. Gambhir, N. Ben-Tal, B. Honig, and S. McLaughlin. 1999. Electrostatic properties of membranes containing acidic lipids and adsorbed basic peptides: theory and experiment. *Biophys J* 77(6):3176-3188.

Nam, G.H., and K.Y. Choi. 2002. Association of human tumor necrosis factor-related apoptosis inducing ligand with membrane upon acidification. *Eur J Biochem* 269(21):5280-5287.

Ng, F.W., and G.C. Shore. 1998. Bcl-XL cooperatively associates with the Bap31 complex in the endoplasmic reticulum, dependent on procaspase-8 and Ced-4 adaptor. *J Biol Chem* 273(6):3140-3143.

Oh, K.J., H. Zhan, C. Cui, K. Hideg, R.J. Collier, and W.L. Hubbell. 1996. Organization of diphtheria toxin T domain in bilayers: a site-directed spin labeling study. *Science* 273(5276):810-812.

Palmer, A.G., 3rd. 2001. Nmr probes of molecular dynamics: overview and comparison with other techniques. *Annu Rev Biophys Biomol Struct* 30:129-155.

Parker, M.W., F. Pattus, A.D. Tucker, and D. Tsernoglou. 1989. Structure of the membrane-pore-forming fragment of colicin A. *Nature* 337(6202):93-96.

Parker, M.W., J.P. Postma, F. Pattus, A.D. Tucker, and D. Tsernoglou. 1992. Refined structure of the pore-forming domain of colicin A at 2.4 A resolution. *J Mol Biol* 224(3):639-657.

Parker, M.W., A.D. Tucker, D. Tsernoglou, and F. Pattus. 1990. Insights into membrane insertion based on studies of colicins. *Trends Biochem Sci* 15(4):126-129.

Petrosian, S.A., and G.I. Makhatadze. 2000. Contribution of proton linkage to the thermodynamic stability of the major cold-shock protein of Escherichia coli CspA. *Protein Sci* 9(2):387-394.

Pfeil, W., and P.L. Privalov. 1976. Thermodynamic investigations of proteins. III. Thermodynamic description of lysozyme. *Biophys Chem* 4(1):41-50.
Ptitsyn, O.B. 1995. How the molten globule became. *Trends Biochem Sci* 20(9):376-379.
Ptitsyn, O.B., R.H. Pain, G.V. Semisotnov, E. Zerovnik, and O.I. Razgulyaev. 1990. Evidence for a molten globule state as a general intermediate in protein folding. *FEBS Lett* 262(1):20-24.
Ramsay, G., D. Montgomery, D. Berger, and E. Freire. 1989. Energetics of diphtheria toxin membrane insertion and translocation: calorimetric characterization of the acid pH induced transition. *Biochemistry* 28(2):529-533.
Saito, M., S.J. Korsmeyer, and P.H. Schlesinger. 2000. BAX-dependent transport of cytochrome c reconstituted in pure liposomes. *Nat Cell Biol* 2(8):553-555.
Sambrook, J., and Russell, D.W. 2001. Molecular Cloning: A Laboratory Manual. Cold Spring Harbor Laboratory Press.
Sandvig, K., and S. Olsnes. 1980. Diphtheria toxin entry into cells is facilitated by low pH. *J Cell Biol* 87(3 Pt 1):828-832.
Santoro, M.M., and D.W. Bolen. 1988. Unfolding free energy changes determined by the linear extrapolation method. 1. Unfolding of phenylmethanesulfonyl alpha-chymotrypsin using different denaturants. *Biochemistry* 27(21):8063-8068.
Sattler, M., H. Liang, D. Nettesheim, R.P. Meadows, J.E. Harlan, M. Eberstadt, H.S. Yoon, S.B. Shuker, B.S. Chang, A.J. Minn, C.B. Thompson, and S.W. Fesik. 1997. Structure of Bcl-xL-Bak peptide complex: recognition between regulators of apoptosis. *Science* 275(5302):983-986.
Schaller, W., and A.D. Robertson. 1995. pH, ionic strength, and temperature dependences of ionization equilibria for the carboxyl groups in turkey ovomucoid third domain. *Biochemistry* 34(14):4714-4723.
Schendel, S.L., M. Montal, and J.C. Reed. 1998. Bcl-2 family proteins as ion-channels. *Cell Death Differ* 5(5):372-380.
Sedlak, T.W., Z.N. Oltvai, E. Yang, K. Wang, L.H. Boise, C.B. Thompson, and S.J. Korsmeyer. 1995. Multiple Bcl-2 family members demonstrate selective dimerizations with Bax. *Proc Natl Acad Sci U S A* 92(17):7834-7838.
Shimizu, S., M. Narita, and Y. Tsujimoto. 1999. Bcl-2 family proteins regulate the release of apoptogenic cytochrome c by the mitochondrial channel VDAC. *Nature* 399(6735):483-487.
Song, M., H. Shao, A. Mujeeb, T.L. James, and W.L. Miller. 2001. Molten-globule structure and membrane binding of the N-terminal protease-resistant domain (63-193) of the steroidogenic acute regulatory protein (StAR). *Biochem J* 356(Pt 1):151-158.
Suzuki, M., R.J. Youle, and N. Tjandra. 2000. Structure of Bax: coregulation of dimer formation and intracellular localization. *Cell* 103(4):645-654.
Thuduppathy, G.R., and R.B. Hill. 2004. Applications of NMR spin relaxation methods for measuring biological motions. *Methods Enzymol* 384:243-264.
van der Goot, F.G., J.M. Gonzalez-Manas, J.H. Lakey, and F. Pattus. 1991. A 'molten-globule' membrane-insertion intermediate of the pore-forming domain of colicin A. *Nature* 354(6352):408-410.
Vander Heiden, M.G., X.X. Li, E. Gottleib, R.B. Hill, C.B. Thompson, and M. Colombini. 2001. Bcl-xL promotes the open configuration of the voltage-

dependent anion channel and metabolite passage through the outer mitochondrial membrane. *J Biol Chem* 276(22):19414-19419.

Wand, A.J. 2001. Dynamic activation of protein function: a view emerging from NMR spectroscopy. *Nat Struct Biol* 8(11):926-931.

Whitten, S.T., J.O. Wooll, R. Razeghifard, B.G. E, and V.J. Hilser. 2001. The origin of pH-dependent changes in m-values for the denaturant-induced unfolding of proteins. *J Mol Biol* 309(5):1165-1175.

Wolter, K.G., Y.T. Hsu, C.L. Smith, A. Nechushtan, X.G. Xi, and R.J. Youle. 1997. Movement of Bax from the cytosol to mitochondria during apoptosis. *J Cell Biol* 139(5):1281-1292.

Xie, Z., S. Schendel, S. Matsuyama, and J.C. Reed. 1998. Acidic pH promotes dimerization of Bcl-2 family proteins. *Biochemistry* 37(18):6410-6418.

Yang, D., Y.K. Mok, J.D. Forman-Kay, N.A. Farrow, and L.E. Kay. 1997. Contributions to protein entropy and heat capacity from bond vector motions measured by NMR spin relaxation. *J Mol Biol* 272(5):790-804.

Zakharov, S.D., and W.A. Cramer. 2002. Insertion intermediates of pore-forming colicins in membrane two-dimensional space. *Biochimie* 84(5-6):465-475.

Chapter 3

Relaxation compensated CPMG experiments suggest that pH-dependent changes in protein dynamics contribute to the solution-to-membrane conformational change

Summary

No significant changes in the structural features of Bcl-X_L in solution upon a decrease in pH were observed (Chapter 2). The absence of secondary, tertiary and quarternary structural changes in solution suggested that (i) the presence of the membrane is essential for the solution to membrane conformational change and/or (ii) subtle pH-dependent changes in protein dynamics provide the initial thrust for the solution to membrane conformational change resulting in membrane insertion. Investigating the latter hypothesis further, data from novel relaxation compensated CPMG experiments revealed interesting differences in the conformational dynamics of Bcl-$X_L\Delta$TM between pH 7.4 and pH 4.9 in solution. The results from these experiments suggest pH-dependent differences in the μs-ms timescale dynamics that might initiate the solution to membrane conformational change. However, these NMR methods are new, and the extent of their accuracy and precision in measuring protein dynamics is only beginning to be determined (Palmer, 2001a; Palmer et al., 2005). To determine the accuracy and precision of these methods, we evaluated a model system that was well characterized like the B1 domain of Streptococcal protein G (GB1) to study the conformational change between the native and denatured state.

While we were unable to fully evaluate the robustness of the CPMG methods, we explicitly detected folding intermediates during GB1 folding using other NMR methods. Our results suggest that there is an initial hydrophobic collapse to form an intermediate state with a hydrophobic core that is identical to the native state. This result is significant as it resolves a current controversy as to whether or not the folding of GB1 is really two-

state. The results of the experiments on Bcl-X_L and GB1 highlight the advantages of NMR spectroscopy and specifically, the CPMG based techniques to study conformational dynamics during protein folding and conformational change.

Introduction

Proteins execute their biological activity via a number of mechanisms, protein-protein interactions and protein conformational change being two of them. Protein conformational changes have been observed to be the driving forces for essential biological process like oxygenation of hemoglobin, muscle contraction etc. As has been discussed in the introductory chapter, the transition of Bcl-X_L from solution to the membrane represents a dramatic conformational change. This conformational change is modulated by pH with the solution form favored at neutral pH conditions and the membrane form favored at acidic pH conditions. The structure of Bcl-$X_L\Delta$TM (Figure 3.1) was found to be unperturbed by a decrease in pH from pH 7.4 to 4.9 at all levels, secondary, tertiary and quarternary (Chapter 2). The ^{15}N-^{1}H HSQC of Bcl-$X_L\Delta$TM at pH 7.4 is shown in Figure 3.2. This spectrum is typical of an all

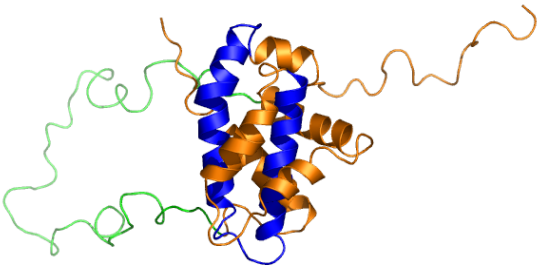

Figure 3.1 Solution structure of Bcl-$X_L\Delta$TM with the long, unstructured loop region highlighted in green.

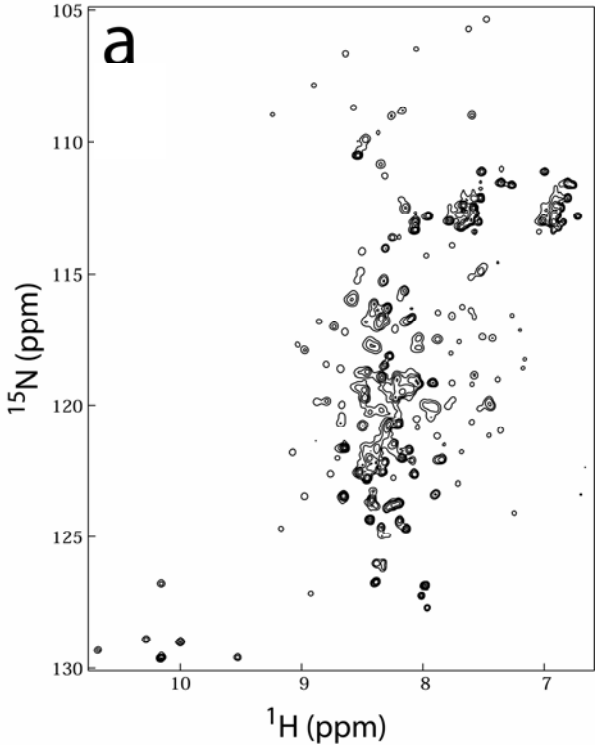

Figure 3.2 ^{15}N-^{1}H HSQC of Bcl-$X_L\Delta$TM in 20 mM sodium phosphate, pH 7.4 indicating a variation in peak intensities suggesting differences in dynamics.

α-helical protein with poor dispersion in the amide proton region. It is also important to note that some peaks, most of them in the middle part of the spectrum show increased intensity relative to the well dispersed ones on the outside. These intense peaks are presumably arising from the residues of the long, unstructured loop region (residues 26-83) of Bcl-X_LΔTM and are characterized by their increased intensity (highly mobile regions of the protein exhibit smaller line widths and sharper peaks) and collapsed spectrum (due to them being part of an unstructured, floppy part of the molecule). The variations in peak intensity are consistent with the notion of a wide variety of motions for the molecule in its native form in solution. These observations suggested that although there were no obvious structural changes in solution (Chapter 2), there might be changes in protein dynamics as a function of pH to mediate the insertion of the protein into the membrane.

In order to study the heterogeneities in the dynamics of Bcl-X_L in detail, we employed Carr-Purcell-Meiboom-Gill (CPMG) based NMR techniques that measure dynamics in the μs-ms timescale (Loria et al., 1999; Palmer et al., 2001; Wang et al., 2001). The reason for this is two fold: (i) A very significant advantage that NMR spectroscopy does provide is the residue-specific information that could be obtained with regards to protein structure, interactions or conformational change (Eisenmesser et al., 2002; Hill et al., 2000a; Mandel et al., 1996). High-field NMR and advances in protein dynamics have opened avenues for the study of protein folding at high resolution using NMR spectroscopy. (ii) The understanding of protein dynamics in the folding timescale, which is in the order of μs-ms for most globular proteins is possible using the relaxation compensated CPMG experiments that are uniquely positioned to measure dynamics in

this biologically relevant timescale. This would aid us in the exploring the importance of local motions and heterogeneities during the conformational change. These techniques could be powerful in providing a kinetic analysis of the protein in residue-specific detail with respect to biologically relevant processes like molecular recognition, conformational change, catalysis and protein folding (Eisenmesser et al., 2002; Hill et al., 2000a; Mandel et al., 1996).

Relaxation compensated CPMG experiments are well suited to measure protein motions involved in protein folding

NMR relaxation is the process by which a spin system perturbed from equilibrium regains it through interaction with the thermal molecular environment. Specifically, the transverse relaxation or spin-spin relaxation or T_2 relaxation rate constant, R_2 (calculated as T_2^{-1}) refers to the rate of decay of coherences in a spin system perturbed from equilibrium (Levitt, 2001). The Carr-Purcell-Meiboom-Gill experiments explicitly measure T_2*, the intrinsic transverse relaxation constant while removing contributions from magnetic field inhomogeneity (Carr and Purcell, 1954; Meiboom and Gill, 1958). However, this intrinsic T_2* includes the contribution from chemical exchange to the transverse relaxation rate. The novel relaxation compensated CPMG experiments can explicitly measure this contribution to transverse relaxation from chemical exchange (Loria et al., 1999). NMR chemical shift exchange, typically referred to as "chemical exchange" arises from the conformational exchange processes that result from NMR-sensitive nuclei exchanging between two distinct chemical shift environments. Conformational exchange in the chemical shift timescale (typically the μs-ms timescale)

results in a significant alteration of the intensity, line width, and chemical shift of the NMR signal which are reflected in the transverse relaxation rate constant (Loria et al., 1999). Thus, these novel relaxation compensated CPMG methods, which measure the chemical exchange contribution to R_2 enable quantification of conformational dynamics in the μs-ms timescale (Figure 3.3).

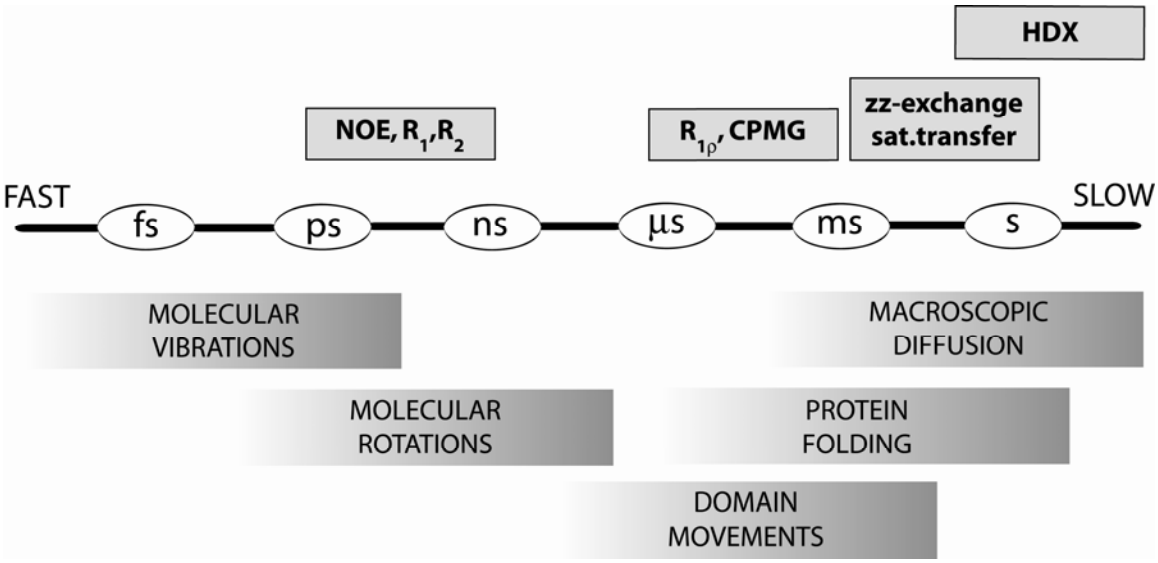

Figure 3.3 NMR spectroscopy is suited to measure dynamics in a wide range of timescales from "fast" ps motions to "slow" motions in the sec – hour timescales. The CPMG methods are uniquely positioned to measure biologically relevant motions involved in protein folding and conformational change.

In a relaxation compensated CPMG experiment, different values of the τ_{CP} delay are used resulting in a modulation of the exchange contribution to R_2 (Loria et al., 1999). The value of R_2 measured at various values of τ_{CP} generates a relaxation dispersion curve that could be fit to the chemical exchange equations resulting in an estimation of four parameters. For an exchange between two conformational states, A and B, these parameters are k_{ex}, the rate of exchange between states A and B, $R_{2,0}$ representing the intrinsic transverse relaxation rate, p_a representing the population of state A and $\Delta\omega$ referring to the chemical shift differences between the two states.

To systematically measure the μs-ms timescale motions in protein dynamics, we had proposed the following four steps (Thuduppathy and Hill, 2004b):

(i) Simulate the relaxation dispersion curves using data available from literature and/or using reasonable approximations. This step addresses the applicability of the relaxation compensated CPMG techniques to the dynamic process under investigation.

(ii) Measure ΔR_2 at two extreme values of τ_{CP}. Significant non-zero values of ΔR_2 clearly indicate the presence of chemical exchange processes that could be quantified using the relaxation compensated CPMG experiments.

(iii) Measure the scaling parameter, α, from the experiments at different static magnetic field strengths. α reflects the R_{ex} dependence of the static magnetic field strength and explicitly determines whether the conformational exchange is fast or slow on the chemical shift timescale (Millet et al., 2000).

(iv) Measure R_2 at 6 values of τ_{CP} to generate the relaxation dispersion curves and curve fit to estimate k_{ex}, $R_{2,0}$, p_a and $\Delta\omega$. This step explicitly determines the kinetic parameter for the conformational exchange, k_{ex}.

In this study, we present preliminary experiments with Bcl-$X_L\Delta$TM to measure μs-ms timescale dynamics using the CPMG methods to identify differences in the dynamics in Bcl-X_L as a function of pH. However, before we embarked on a detailed study of the conformational dynamics of interpretation of Bcl-$X_L\Delta$TM, it was essential to evaluate the accuracy and precision of the measurements obtained using these novel relaxation compensated CPMG methods. This was done by the application of the

relaxation compensated CPMG methods on a well characterized process, the folding of the immunoglobulin binding domain B1 of the streptococcal protein G.

GB1 provides a good model system for the study of protein folding

The immunoglobulin binding domain B1 of Streptococcal protein G, referred to as GB1 has been extensively studied as a small, globular protein model for protein folding studies. This 56-residue independently folding domain has many favorable features – no prolines, no disulfides, one tryptophan for fluorescence studies and a mixed α/β structure. The structure consists of a β-sheet formed by a pair of slightly twisted β-hairpins and an α-helix wrapped over one side of the β-sheet (Gronenborn et al., 1991). GB1 is thermally stable with a T_m of 87.5 °C at pH 5.4 and also stable in guanidine hydrochloride remaining folded up to 2 M at pH 2 (Alexander et al., 1992a; Alexander et al., 1992b). There has been evidence indicating deviation from two-state folding behavior during GB1 folding as observed by continuous-flow folding, time-resolved fluorescence and Hydrogen-Deuterium exchange experiments. Continuous flow kinetic studies monitored using fluorescence spectroscopy and quenched-flow hydrogen-deuterium exchange experiments indicate collapse to a semi-compact state followed by the formation of a native state in a fast step with a $t_{1/2}$ of 5.2 ms at 5 °C (Kuszewski et al., 1994; Park et al., 1999). Computational studies using all-atom simulations have also generated a similar atomic level picture of folding of GB1 (Sheinerman and Brooks, 1998). It has been postulated that there is an initial partial collapse of the polypeptide chain forming ~ 35% of the native structure, followed by the formation of non-local native contacts resulting in the final three-dimensional structure. The overwhelming

thermodynamic and kinetic data available on the folding of GB1 and the observations of heterogeneities in the folding landscape make this an ideal system for the application of CPMG-based techniques. Here, we present an initial characterization of the equilibrium folding of this protein in an attempt to generate equilibrium folding curves in residue specific detail. In addition, we want to measure dynamics in the μs-ms timescale using CPMG based methods to quantitate the dynamics of protein motions involved in folding.

Materials and Methods

Protein Expression and purification

(i) Purification of Bcl-X_LΔTM

Human Bcl-X_L(1-209) that lacks the C-terminal hydrophobic 24 amino acids was sub-cloned into pHis-GB vector and expressed using induction with IPTG as described in Chapter 2. To increase the yield of protein in the soluble fraction and for isotopic labeling purposes, *E.coli* Rosetta (Stratagene) cells containing the plasmid coding for Bcl-X_LΔTM were grown at 37 ˚C in 2 liters of LB media to a OD_{600} of ~0.7, collected by centrifugation, and gently resuspended in 0.5 L of M9 minimal media and continued to grow at 37 ˚C (Marley et al., 2001). After one hour, protein expression was induced by the addition of 0.5 mM IPTG. The cells were harvested by centrifugation after 5-6 hours at 37 ˚C and purified as detailed in Chapter 2. The protein samples were stored at 4 °C until used.

(ii) Purification of the B1 domain of protein G

Isotopically labeled (^{15}N and ^{13}C, ^{15}N labeled) GB1 was purified from *E.coli* containing the plasmid expressing GB1 (Dr. Martin Stone, Indiana Univ.) grown in minimal media containing $^{15}NH_4Cl$ and ^{13}C-glucose. *E.coli* cells containing a plasmid expressing GB1 were grown in LB medium containing 200 μg/ml Ampicillin until an OD_{600} of 0.7 was reached. Cells were spun down and resuspended in M9 minimal media containing the appropriate isotopically labeled nitrogen and carbon sources (Marley et al., 2001). The cells were incubated at 37 ˚C to recover for an hour and then protein expression induced by the addition of IPTG. After 4-5 hours, cells were harvested and

resuspended in lysis buffer containing 20 mM Tris, pH 8.0 and protease inhibitors (Complete protease inhibitor cocktail, Roche). Cell lysis was carried out using the French press (3 passes) and the supernatant was collected after centrifugation of the sample. The supernatant was loaded on to an anion exchange column (Q FF Sepharose, GE Healthcare). After washing extensively with 20 mM Tris, pH 8.0, the protein was eluted from the column with 20 mM Tris, pH 8.0 containing 1 M NaCl. The fractions containing protein were pooled, concentrated and dialyzed into 50 mM Tris, pH 8.0 containing 150 mM NaCl. The concentrated protein was loaded on a Sephacryl S-100 HR size exclusion column and fractions containing GB1 were isolated and pooled. This sample was then dialyzed into deionized water, lyophilized and stored at -20 ˚C.

NMR Sample Preparation

(i) Bcl-X_LΔTM sample

0.5 mM sample of ^{15}N Bcl-X_LΔTM in 20 mM sodium phosphate, pH 7.4 (containing 10% D_2O) was used for the relaxation compensated CPMG experiments as described in REF. For the experiments at pH 4.9, the protein sample was titrated from pH 7.4 to pH 4.9 using small amounts of 0.1 N hydrochloric acid.

(ii) GB1 samples

Aliquots of concentrated ^{15}N labeled GB1 were lyophilized in microcentrifuge tubes. Ten aliquots of ^{15}N labeled GB1 were prepared each containing 6.5 mg of protein. To each of these aliquots buffer solutions containing 45 mM sodium acetate, pH 5.4 and varying amounts of deionized urea were added. The final concentration of protein in the 350 μL sample was 3 mM. The urea concentrations in the different samples were

determined using refractometry and were: 0, 0.97, 1.90, 2.90, 3.81, 4.78, 5.71, 6.62, 7.60 and 8.25 M. For triple resonance NMR experiments, a 4.6mM ^{13}C,^{15}N labeled GB1 sample in 45 mM sodium acetate, pH 5.4 and 8 M urea was used.

NMR Spectroscopy

All the NMR experiments were carried out on Varian INOVA 500 MHz, Bruker AVANCE 600 MHz or Varian INOVA 800 MHz NMR spectrometers.

(i) Bcl-X_LΔTM dynamics experiments

Relaxation compensated CPMG experiments were carried out on a ^{15}N-labeled sample of Bcl-X_LΔTM at pH 7.4 and pH 4.9 as described (Wang et al., 2001). The parameters for these experiments were as follows: ^{1}H x ^{15}N – 1024 x 128 data points with sweep widths of 8000 x 1200 Hz on a Varian INOVA 500 MHz spectrometer. The ^{15}N carrier was placed at 118 ppm. The temperature was maintained at 25 ˚C for all the experiments. For these initial experiments, R_2 values were measured at the two extreme values of τ_{CP}, 1ms and 10ms. The R_2 experiment at pH 7.4 with τ_{CP} = 1ms was collected with the T_2 delays of 10, 40, 60, 80, 100 and 120 ms while the τ_{CP} = 10 ms experiment was collected with T_2 delays of 20, 40, 60, 80, 100 and 120 ms. The R_2 experiment at pH 4.9 with τ_{CP} = 1ms was collected with the T_2 delays of 10, 40, 60, 80, 100 and 120 ms while the τ_{CP} = 10 ms experiment was collected with T_2 delays of 20, 40, 60, 80, 100 and 120 ms. 20 representative peaks displaying analyzable T_2 decay curves were selected and the data was fit to estimate R_2 values. R_2 values were obtained by fitting the decay curves to a single exponential decay equation, with $I = I_0 \exp(-R_2 \bullet t)$. The difference

between the R_2 values measured at the two τ_{CP} values, $\Delta R_2 = R_2(10\ ms) - R_2(1\ ms)$ was calculated for each of the 20 residues.

(ii) Triple resonance experiments for assigning the native and denatured states in urea

HNCA, HN(CO)CA, HNCACB and HNCOCACB experiments were collected on the Varian INOVA 500 MHz spectrometer with the following parameters. 1792 points on ^{1}H, 128 and 52 increments were collected in the indirect detected ^{13}C and ^{15}N respectively. The sweep width was kept at 12800 Hz for ^{1}H, 5800 Hz for ^{13}C and 1864 Hz for ^{15}N. The ^{15}N carrier was centered at 117.5 ppm.

(iii) ^{15}N-^{1}H HSQC on samples with varying concentrations of urea

The HSQC spectra were collected at two different field strengths, on a Bruker Avance 600 MHz spectrometer and on a Varian INOVA 800 MHz spectrometer. The data was collected using the following parameters: at 600 MHz, 1118 x 128 complex points were collected and the sweep width was 8000 x 2000 Hz and at 800 MHz, 1512 x 128 complex points were collected with the sweep width at 10800 x 2500 Hz. The carrier was kept at 117.5 ppm for ^{15}N.

(iv) Thermal denaturation study in the presence of 8M urea

^{15}N-^{1}H HSQC spectra were collected on samples of ^{15}N labeled GB1 in 8 M urea at different temperatures ranging from 5 ˚C to 55 ˚C on the Bruker AVANCE 600 MHz spectrometer. At 55 ˚C and 8M urea, the protein was completely denatured. The experimental parameters for these experiments were: 1024 x 256 complex points with sweep widths of 8000 x 2000 Hz in the ^{1}H and the ^{15}N dimensions respectively. ^{15}N carrier was set at 117.5ppm for these experiments.

(v) Relaxation compensated CPMG experiments to measure chemical exchange during GB1 folding

Relaxation compensated CPMG experiments as described in REF were used for probing the timescales of dynamic motion during GB1 folding on a ^{15}N GB1 sample in ~8 M urea. The experiments were carried out at 25 ˚C. Relaxation compensated CPMG experiments were collected with T_2 delays of 400, 16, 100, 68, 32, 152, 284, 200, 16, 400 ms at τ_{CP} =1ms and 400, 40, 120, 80, 240, 160, 280, 320, 40, 400 ms at τ_{CP} =10ms. 832 x 128 complex points were collected with sweep widths of 6500 x 1800 Hz in ^{1}H and ^{15}N respectively and the ^{15}N carrier was set at 118 ppm.

The second set of experiments was carried out at an elevated temperature of 35°C on a sample of ^{15}N GB1 in 7.60 M urea. The pulse sequences used in these experiments are as described in (Wang et al., 2001). These experiments were collected with 1148 x 128 data points with a sweep width of 10000 x 1450 Hz in ^{1}H and ^{15}N dimensions respectively. The ^{15}N carrier was kept at 118.5 ppm. R_2 experiments were collected at τ_{CP} values of 1 ms and 10 ms with the following T_2 delays: 4, 12, 20, 32, 48, 72, 88, 120, 204, 248 and 300 ms at τ_{CP} = 1 ms and 21.6, 43.2, 64.8, 86.4, 108, 129.6, 172.8, 216 and 280.8 ms at τ_{CP} = 10.8 ms. The data was processed using NMRPipe and analyzed using the Rate analysis module in NMRView (Delaglio et al., 1995; Johnson, 2004; Johnson, 1994b). The T_2 decay curves were fit to a monoexponential decay curve with the $I = I_0 \exp(-R_2 \bullet t)$ description. R_2 values from the two different τ_{CP} experiments were used to calculate ΔR_2 as R_2(10ms) - R_2(1ms). ΔR_2 values for the different residues were then analyzed for presence of chemical exchange in the CPMG timescale.

Simulation of relaxation dispersion curves

All the simulations were carried out in Microcal Origin 5.0. The two-site chemical exchange process, i.e., exchange between two sites A and B distinguishable from each other by a difference in chemical shift Δω is represented by,

$$A \underset{k_{ex}}{\longleftrightarrow} B \tag{3.1}$$

The equation describing the R_2 dependence of chemical exchange under these conditions is as follows (Carver and Richards, 1972; Davis et al., 1994; Jen, 1974; Jen, 1978):

$$R_2(1/\tau_{cp}) = \frac{1}{2}\left(R_a + R_b + k_{ex} - \frac{1}{\tau_{cp}} \cosh^{-1}\left[D_+ \cosh(\eta_+) - D_- \cos(\eta_-) \right] \right) \tag{3.2}$$

where $D_\pm = \frac{1}{2}\left[\pm 1 + \frac{\psi + 2\Delta\omega^2}{\sqrt{\psi^2 + \zeta^2}} \right]$,

$$\eta_\pm = \frac{\tau_{cp}}{\sqrt{2}}\left[\pm\psi + \sqrt{\psi^2 + \zeta^2} \right]^{\frac{1}{2}},$$

$$\psi = \left(R_a - R_b - p_a k_{ex} + p_b k_{ex} \right)^2 - \Delta\omega^2 + 4 p_a p_b {k_{ex}}^2$$

and $\zeta = 2\Delta\omega\left(R_a - R_b - p_a k_{ex} + p_b k_{ex} \right)$

The simulations are carried out with a priori knowledge of the values of R_a, R_b, p_a, p_b, k_{ex} and Δω from the literature. The k_{ex} parameters are reasonably estimated from kinetics data available from Park et al. and McCallister et al. (McCallister et al., 2000; Park et al., 1999) The Δω is estimated from the difference in the folded and unfolded

state peaks of individual residues as seen in the HSQC. R_a and R_b are assumed to be equal and having values of 10 s^{-1} while reasonable approximations are also used for p_a and p_b. The simulations are shown in Figures 3.13 and 3.14.

Results

Interesting pH-dependent changes in protein dynamics observed in Bcl-$X_L\Delta TM$

In order to identify pH-dependent differences in the dynamic motions in the μs-ms timescale for Relaxation Compensated CPMG experiments were carried out at pH 7.4 and pH 4.9 as described in the Materials and Methods section of this chapter. 20 representative peaks were picked for analysis based on the decay curves that they exhibited. ΔR_2 values generated from the experiments at pH 7.4 and pH 4.9 indicated that while most of the peaks did not show pH-dependent changes in dynamics, few of them did (Figure 3.4). Using chemical shift assignments provided by Dr. Wagner's group (assignments from a ΔloopΔTM construct), we were able to identify three of these residues. We found that all three residues mapped to the loop at the C-terminal end of the molecule. This loop would presumably connect to the TM segment in the full length molecule. Relative to pH 7.4, the ΔR_2 values of these residues at pH 4.9 were smaller indicating decreased protein dynamics in the μs-ms timescale under acidic pH conditions.

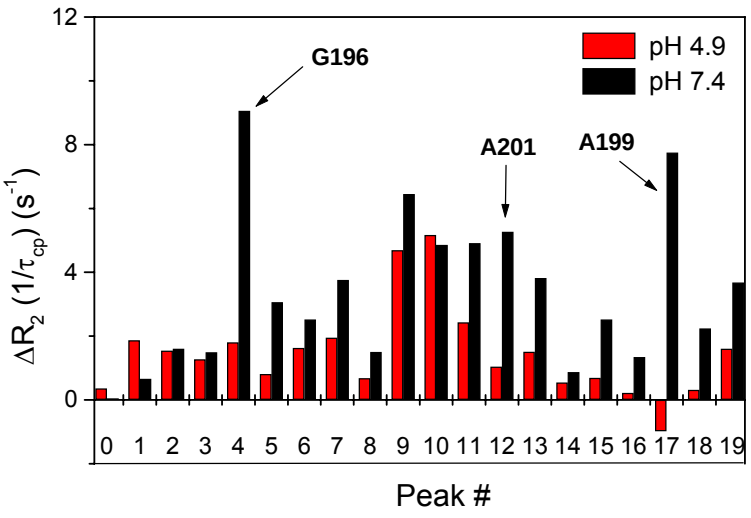

Figure 3.4
Differences were observed in the μs-ms timescale dynamics of Bcl-$X_L\Delta TM$ as a function of pH. Less contribution from chemical exchange was observed at pH 4.9 for residues, G196, A201 and A199. See Materials and Methods section for experimental details.

GB1 as a model system

Before investigating the pH-dependent dynamics of Bcl-$X_L\Delta$TM, we wanted to evaluate the accuracy and precision of the measurements of conformational dynamics obtained using the CPMG relaxation experiments. In order to determine the accuracy and precision of these novel methods, we decided to choose a simpler system that is interesting and has been well characterized. After considering various small, globular proteins like the headpiece of villin, p53 tetramerization domain and the WW domain, we decided upon the B1 domain of Streptococcal protein G due to the following reasons.

(i) A large amount of information about the structure, thermodynamics and kinetics of folding of GB1 is available in the literature (Figure 3.5).

(ii) A number of NMR experiments have been carried out on the GB1 system confirming its amenability to the NMR based dynamics experiments.

(iii) Earlier studies using fluorescence spectroscopy and quenched flow hydrogen exchange suggest possible intermediates during folding of GB1. This system would be ideal to demonstrate the advantages of residue specific detail provided by NMR based methods in resolving the controversy of whether the folding of GB1 is really two-state (McCallister et al., 2000; Park et al., 1999).

Both the folded and the unfolded resonances during urea unfolding of GB1 can be assigned

To characterize the folding equilibrium of GB1, we measured the denaturant dependence of the ^{1}H and the ^{15}N chemical shifts of GB1 under conditions of varying urea concentrations by NMR spectroscopy. Initial ^{15}N-^{1}H HSQC spectra of GB1 in 8 M urea

indicated the presence of at least two species, a folded state with well-dispersed peaks and an unfolded state with resonances collapsed in the ^{1}H and ^{15}N dimensions (Figure 3.6).

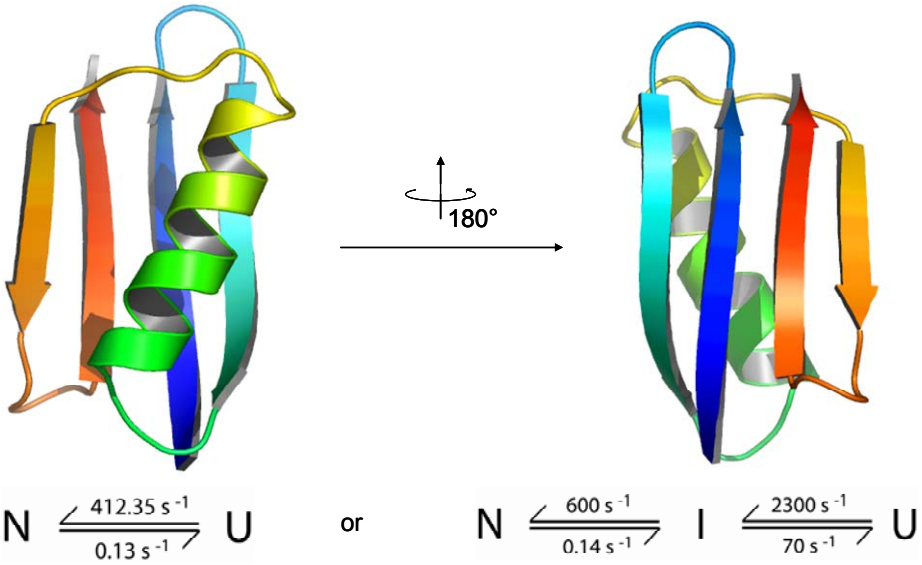

Based on kinetic data from McCallister et al., NSB 2000 and Park et al., NSB 1999

Figure 3.5 Structure of GB1 form 2GB1.pdb shows the mixed α/β structure of GB1 in two different orientations. Kinetic data from literature was extrapolated to 4 M GuHCl in order to mimic conditions similar to 8 M urea.

Unfolding was not complete even in the presence of 8 M urea at pH 5.4, with at least 20 % of the molecule still existing in the native conformation. This agrees well with the previous thermodynamic observations of GB1 unfolding with urea using other spectroscopic methods. Most of the residues appear to be in slow exchange on the chemical shift timescale and were observed as two peaks in the HSQC in 8 M urea, one corresponding to the native state with well dispersed peaks and another corresponding to the denatured state. The denatured state is represented by the peaks collapsed in the ^{15}N and ^{1}H dimensions, especially in the ^{1}H dimension where all the resonances appear between 8 and 8.5 ppm.

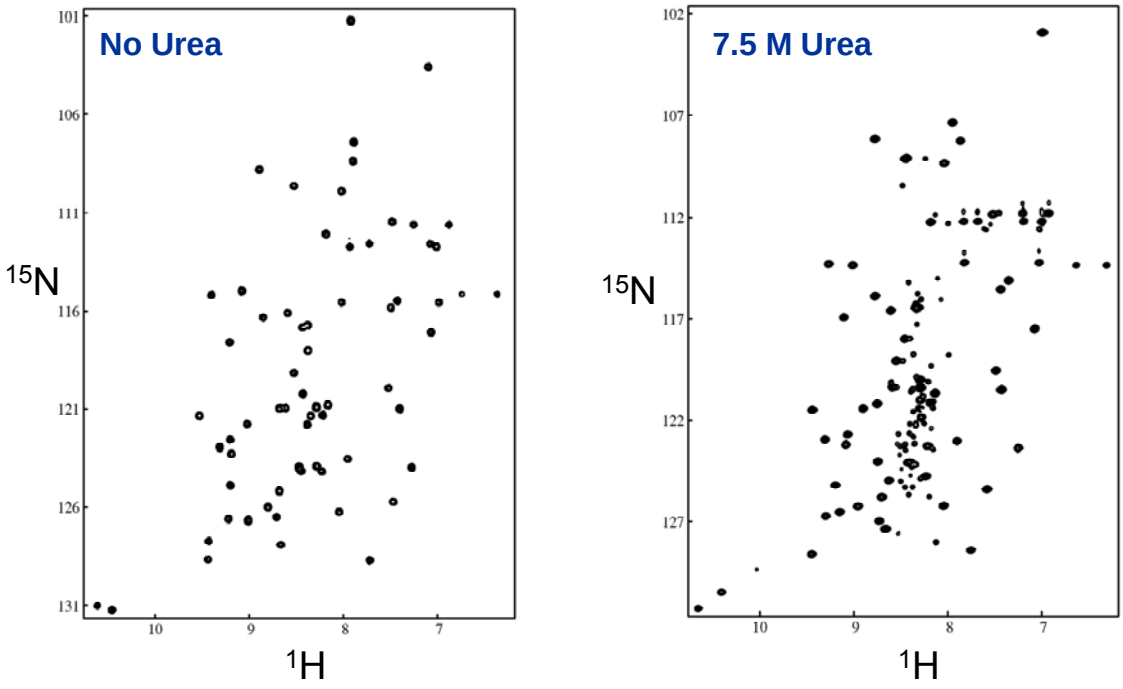

Figure 3.6 Well dispersed resonances are observed for GB1 under native conditions in 50 mM sodium acetate, pH 5.4(left panel). Slow dynamics of the unfolding of GB1 in the presence of 7.5 M urea at pH 5.4 was observed by the presence of two sets of peaks, one corresponding to the native state and the other representing the denatured form (collapsed in the ^{1}H dimension between 8 and 8.5 ppm).

Using standard triple resonance based experiments, I was able to generate the assignments of the folded state of GB1 in the presence of 8 M urea (Figure 3.7). There were changes in the chemical shift of resonances representing the native state in the spectra collected at 0 M urea and at 8.25 M urea. These changes were relatively small and we were able to assign the native state resonances at both urea concentrations. The assignment of the unfolded state of GB1 in 8 M urea was carried out by Ann Monahan, an undergraduate student in the lab using standard triple-resonance based methods (Figure 3.8). Salvador Casares, a post-doctoral fellow in the lab confirmed these assignments to generate the final peak lists for analysis.

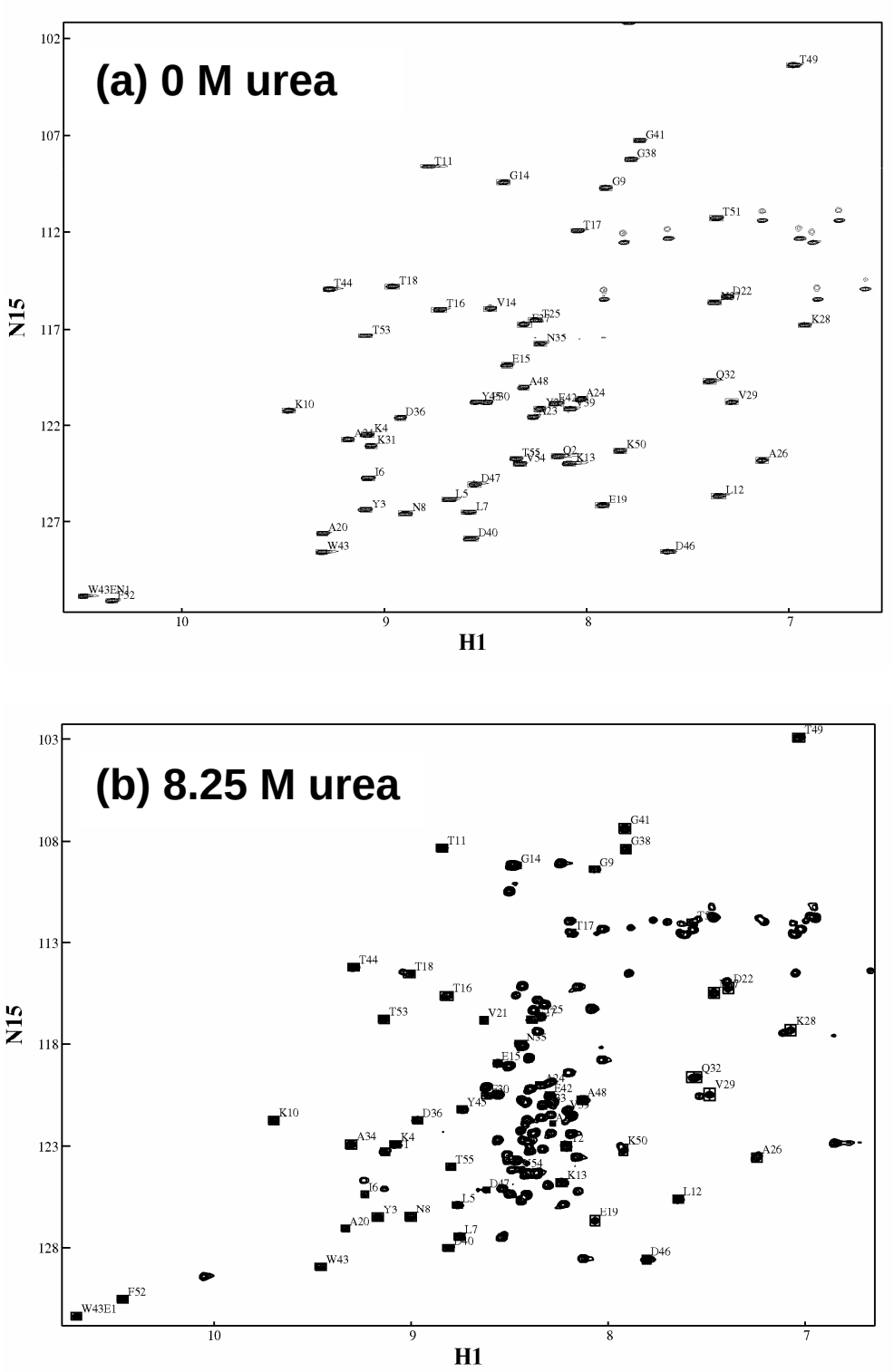

Figure 3.7 (a) ^{15}N-^{1}H HSQC of GB1 under native conditions in 0 M urea with assignments of the native state resonances. (b) ^{15}N-^{1}H HSQC of GB1 under denaturing conditions in ~ 8 M urea with assignments of resonances from the native state.

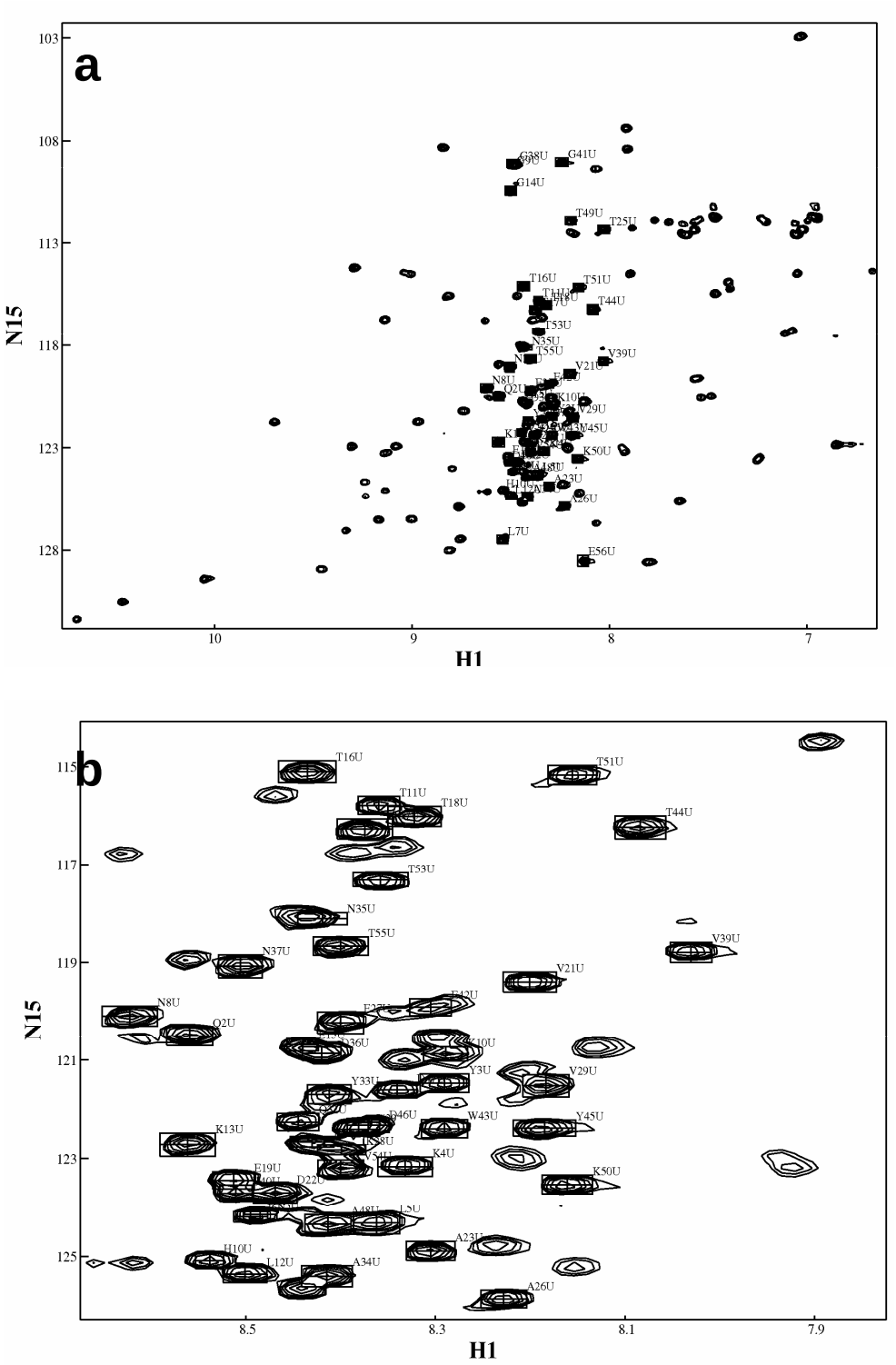

Figure 3.8 (a) ^{15}N-^{1}H HSQC of GB1 under denaturing conditions in 8.25 M urea with assignments of resonances from the denatured state. (b) A closer view of the denatured state with the assignments.

Monitoring the unfolding of individual residues during urea unfolding

In an attempt to further understand the equilibrium thermodynamic perspective of GB1 folding at a residue level, we collected ^{15}N-^{1}H HSQC spectra at ten different urea concentrations ranging from 0 to 8.25 M urea (Figure 3.9a-j). Using the assignments obtained for the folded and the unfolded states in 8 M urea and information from the literature, we were able to monitor the populations of the folded and unfolded states at different urea concentrations. The ^{15}N-^{1}H HSQC spectra from 0 M urea to 4.78 M urea did not display any significant peaks corresponding to the unfolded state (Figure 3.9a-f). However, the samples in 5.71 M urea, 6.62 M urea, 7.60 M urea and 8.25 M urea displayed the presence of peaks corresponding to the unfolded state with the relative intensity of the peaks of the peaks of the unfolded state increasing with urea concentration (Figure 3.9g-j).

Since the samples had varying concentrations of urea, there were observable but subtle differences in the chemical shifts of the peaks corresponding to the folded and the unfolded states. The individual spectra were analyzed and the chemical shift assignments were re-adjusted for the different spectra. Now that the intensity of the folded state and the unfolded state was known at every urea concentration tested, we were able to calculate the fraction of folded molecules in the population as the ratio of the intensity of the folded peak to the sum total of the intensity of the folded and unfolded peaks.

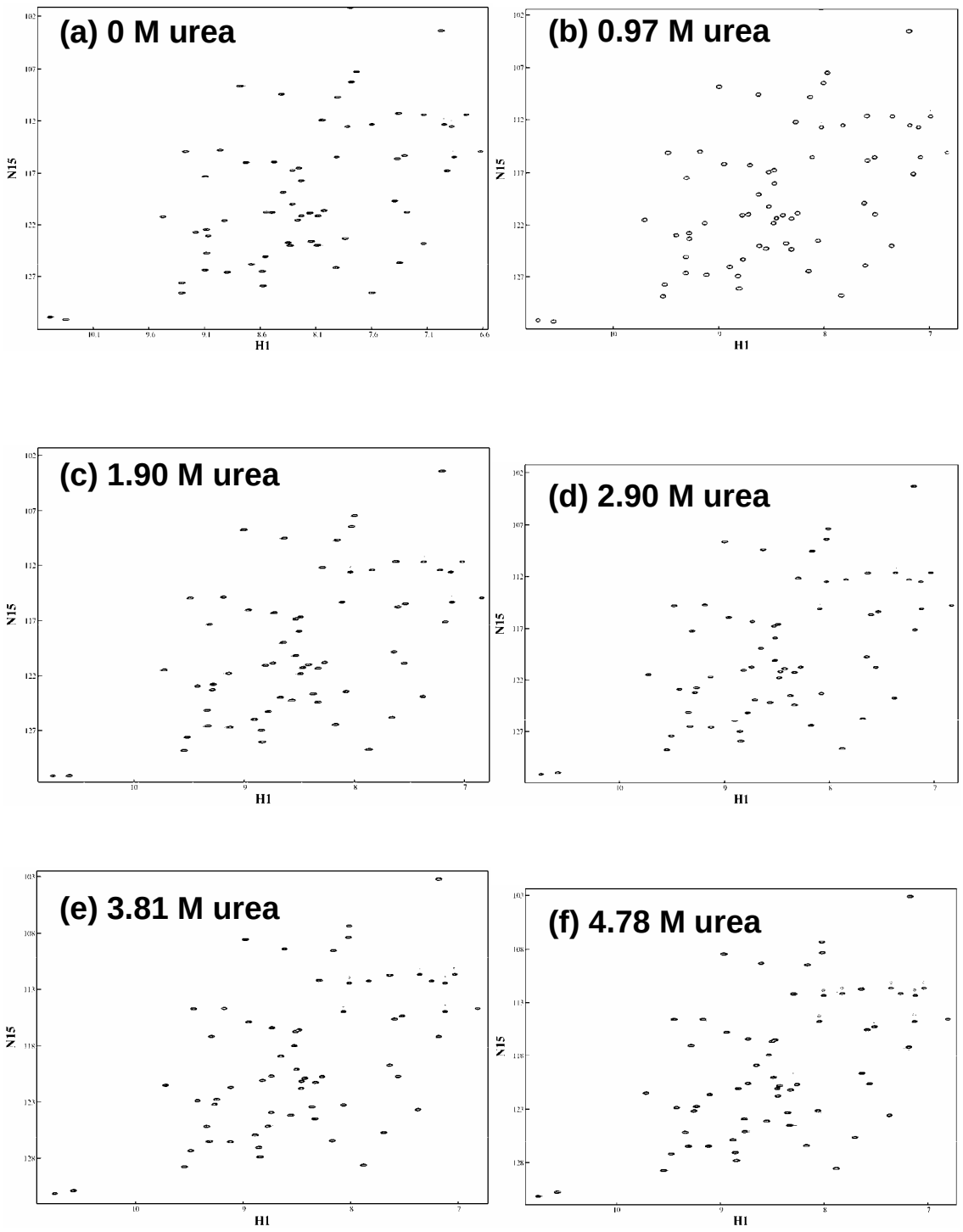

Figure 3.9 ^{15}N-^{1}H HSQC spectra of GB1 at varying concentrations of urea. The spectra were collected using a ~ 3 mM GB1 sample in the presence of (a) 0 M urea, (b) 0.97 M urea, (c) 1.90 M urea, (d) 2.90 M urea, (e) 3.81 M urea and (f) 4.78 M urea. There is no significant contribution from the unfolded state under these conditions.

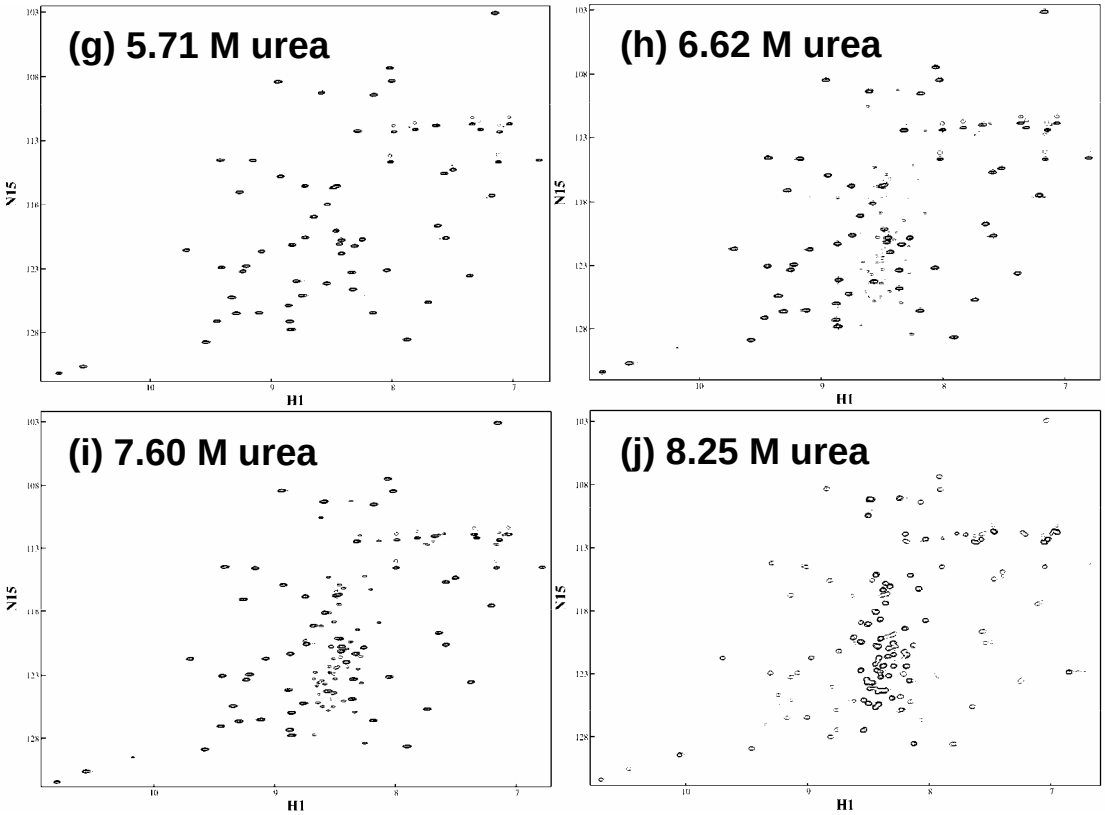

Figure 3.9 (continued) ^{15}N-^{1}H HSQC spectra of GB1 at varying concentrations of urea. The spectra were collected using a ~ 3 mM GB1 sample in the presence of (g) 5.71 M urea, (h) 6.62 M urea, (i) 7.60 M urea and (j) 8.25 M urea. There are two sets of resonances that are observable, one corresponding to the native state and the other corresponding to the denatured state.

Understanding the equilibrium folding of GB1 in the presence of urea

Using the intensity of the resonances for the individual peaks, we were able to calculate the fraction of population in the native state, F_N for each individual residue (the amide proton-nitrogen correlation corresponding to the backbone of each residue) as a function of urea concentration. The value of F_N typically ranges between 1 and 0 with 1 corresponding to all folded and 0 corresponding to all unfolded and the value decreases from 1 to 0 with increasing urea concentration.

The curve of F_N vs [urea] is similar to the folding curves generated using other spectroscopy based methods except with residue specific detail. The data generated for a handful of residues is shown in Figure 3.10. The scatter in the curves in the transition region suggests heterogeneities in folding although they might be within the experimental errors of estimating peak intensities. Even at the highest concentration of urea that was tested, 8.25 M, we weren't able to observe complete unfolding. At 8.25 M urea, the F_N was still around 0.25 on the average for most of the residues. In order to use the two-state folding equations, we assumed that GB1 was completely unfolded at urea concentrations of 9M and higher, a reasonable assumption based on available data. We added three data points with F_N of 0 at 9, 10 and 11 M urea. With this complete data set, we fit to the two-state folding equilibrium equation. The ΔG^0 that we obtained from a global fit of a few residues was approximately 24 kcal•mole^{-1}. This absurdly high value for ΔG^0 would also indicate that there might be heterogeneities that lead to a high ΔG^0 value due to two-state constraints. The assumption of a thermodynamic intermediate populated at slightly destabilizing conditions, for example, will generate a better description of the data indicating that the folding is not really two-state.

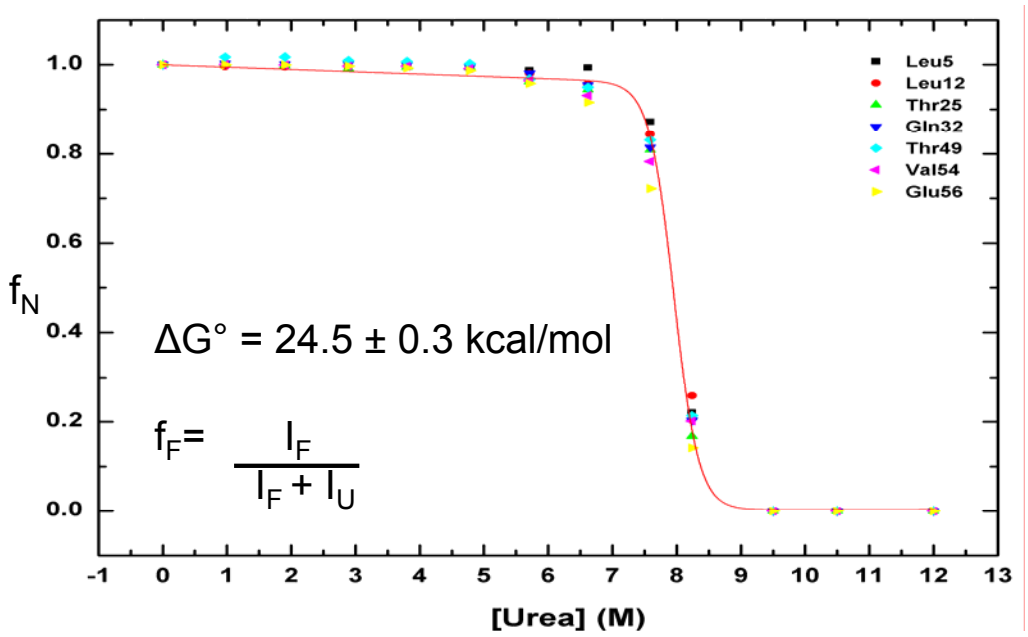

Figure 3.10 Globally fitting the unfolding data for a few of the residues resulted in an unreasonably high value for ΔG° indicating that the two-state assumption might not be valid and suggesting the presence of equilibrium intermediates.

Identification of the intermediate state

Our analysis of the HSQC spectra of GB1 in the presence of 6.62 M to 8.25 M urea indicated the existence of extra unassigned peaks (Figure 3.11a-c). Some of these peaks were less intense as compared to the folded and unfolded peaks in that sample. These peaks appeared and disappeared with increasing urea concentrations suggest that arise from an intermediate state.

In an attempt to characterize the structural features of the intermediate state, we recollected the triple resonance experiments and ^{15}N-NOESY-HSQC at a urea concentration of 7.60 M where we observed the most intense signal from the intermediate peaks. This data was used to identify the residues corresponding to the intermediate state by Salvador Casares, a post-doctoral fellow in the Hill Lab and has resulted in the identification of 3 of the 7 peaks as T11, A23 and D46.

These residues map to different regions of the protein far away from each other (Figure 3.11d). Our current interpretation of this result, based on previous observations, is that the surface exposed residues in the loops become unstructured first independent of the core of the molecule. Upon a further increase in urea concentration, the core melts in a cooperative manner. The thermodynamic intermediate could be the result of differences in the unfolding profiles of the surface residues and the residues from the hydrophobic core of the molecule. This difference could result in an intermediate where the surface is destabilized while the core still retains native-like interactions.

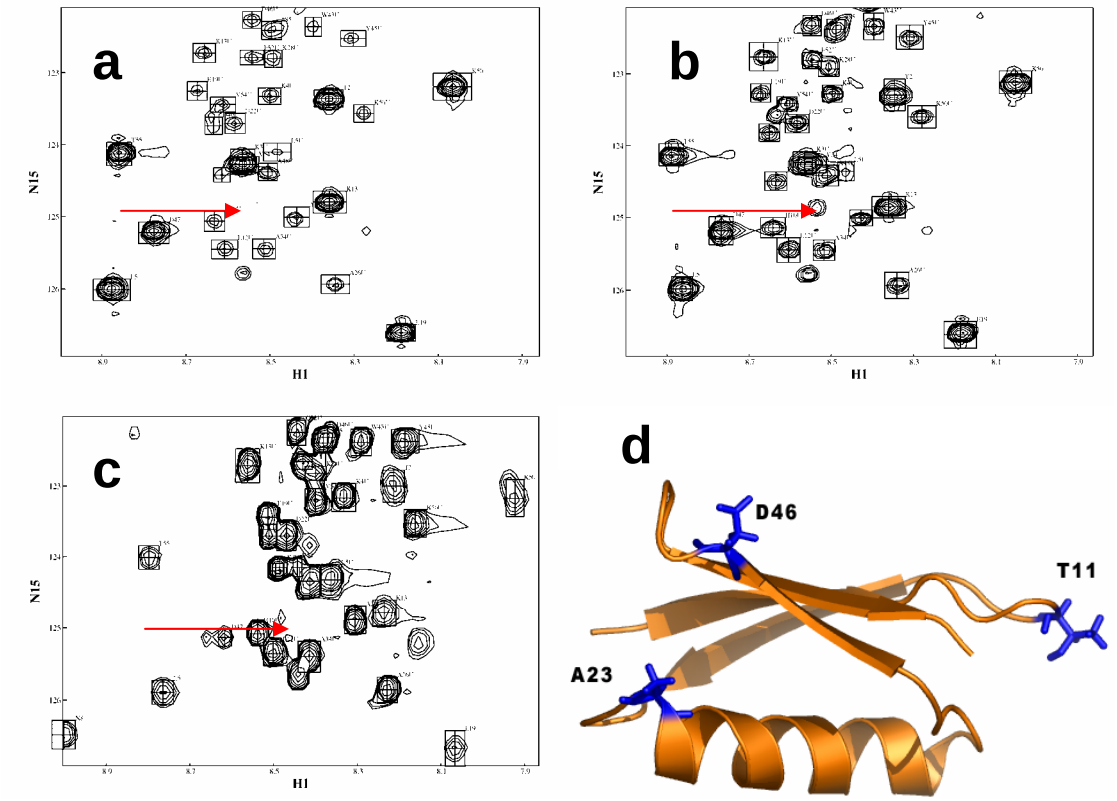

Figure 3.11 (a-c) Intermediates during equilibrium unfolding of GB1 identified as extra peaks (one of them indicated by the red arrow) that were seen during the initial stages of unfolding with urea. Spectra displayed were collected in the presence of (a) 6.62 M urea, (b) 7.60 M urea and (c) 8.25 M urea. (d) Three of the extra peaks were assigned to T11, A23 and D46 suggesting that these residues might exist in a different environment in the intermediate state relative to the native and denatured state.

Equilibrium folding of GB1 in urea under thermal denaturation conditions

To completely unfold GB1, we used two methods:

1. addition of guanidine hydrochloride as a stronger denaturant to unfold GB1.
2. increase temperature to 55 ˚C in the presence of 8 M urea to further unfold GB1 which is only partially unfolded at 8 M urea.

We observed that GB1 was completely unfolded in 6 M guanidine hydrochloride at pH 5.4. However, the disadvantages of using NMR on samples at high salt concentrations prevented us from investigating this option further. To investigate heterogeneities during equilibrium unfolding under highly destabilizing conditions, we observed the effects of increasing temperature on the ^{15}N-^{1}H HSQC spectra of GB1 in 8 M urea (Figure 3.12). In our studies of the thermal denaturation profile of GB1 in 8M urea, we observed heterogeneities in GB1 folding suggesting a different folding landscape for some of the residues in GB1. For example, residues Y45, K50, T51 and E56 show heterogeneities during thermal denaturation from 298 K to 328 K as shown in Figure 3.12.

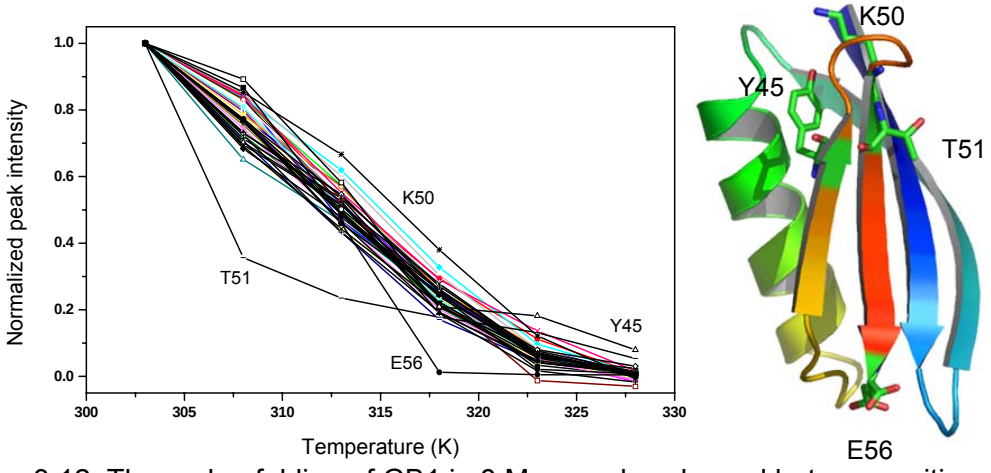

Figure 3.12 Thermal unfolding of GB1 in 8 M urea also showed heterogeneities suggesting presence of intermediate conformations (left). Although these residues were different from those identified from the urea unfolding studies (Figure 2.10), they were localized to similar, solvent exposed parts of the structure (right), consistent with the idea of an initial hydrophobic collapse and a second step where there is a re-arrangement of the surface.

Simulation of relaxation dispersion curves of folding dynamics

As described earlier, we have evidence for the presence of a thermodynamic intermediate and heterogeneities of the kinetics of GB1 folding at a residue specific level will help corroborate this finding. To estimate whether the CPMG based techniques would be able to measure the folding kinetics for each residue of GB1 folding, we simulated the relaxation dispersion curves using the thermodynamic data in the literature and reasonable approximations for some of the unknown parameters. Using data from the literature of either two-state or three-state folding of GB1, we simulated relaxation dispersion curves for the different scenarios of GB1 folding. The simulations indicated scenarios where we would be able to observe relaxation dispersion, i.e., non-zero R_{ex} values, which could be quantified to obtain kinetic folding parameters. The two state folding data simulated no CPMG detectable chemical exchange (Figure 3.13).

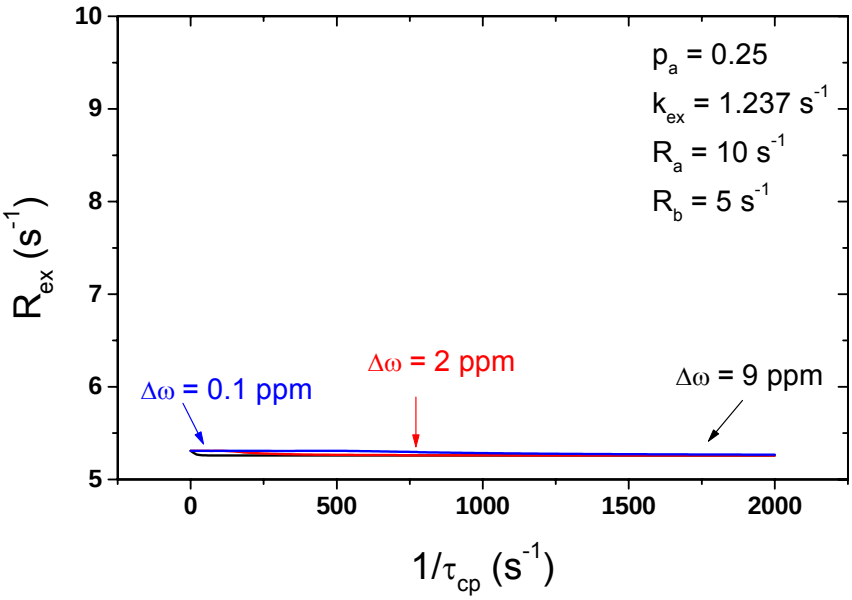

Figure 3.13 Simulation of the relaxation dispersion curves for GB1 folding dynamics using data from McCallister et al based on a two-state kinetic description and the equation described in the Materials and Methods section. Reasonable values were assumed for R_a and R_b, p_a was estimated based on our observations from the HSQC spectra and $\Delta\omega$ from the differences observed between the native and denatured state resonances of GB1 in the presence of 8M urea.

However, the three-state kinetic data suggested that there would be detectable chemical exchange in the CPMG timescale prompting us to further investigate the kinetics of GB1 folding using the relaxation compensated CPMG techniques (Figure 3.14). Evidence from equilibrium unfolding of GB1 suggests that this three-state description is the more plausible case although the rate constants could still be different.

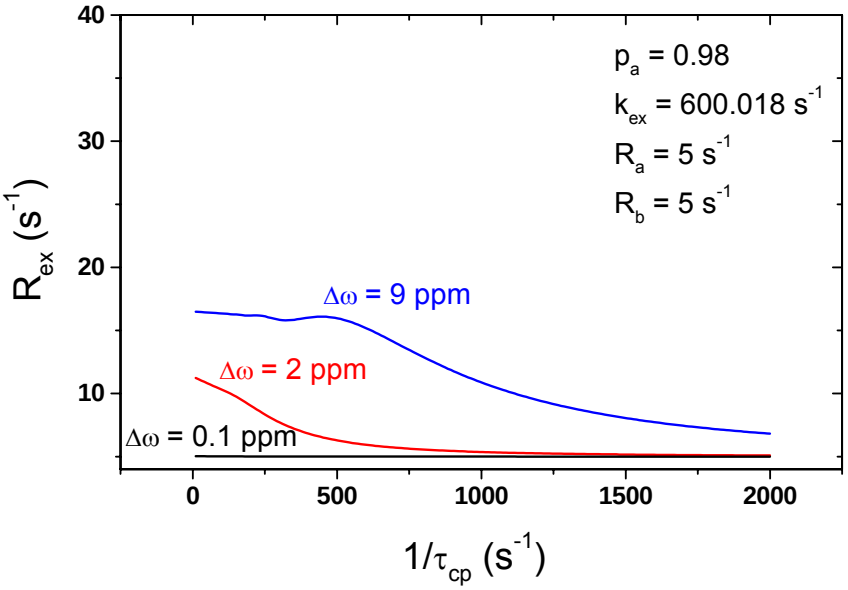

Figure 3.14 Simulation of the relaxation dispersion curves for GB1 folding dynamics using data from Park et al and equation 1 as described in the materials and methods section. The kinetic data was from a three-state kinetic description of GB1 folding obtained using continuous flow mixing monitored by fluorescence spectroscopy. Reasonable values were assumed for R_a and R_b, p_a was estimated based on our observations from the HSQC spectra and $\Delta\omega$ from the differences observed between the native and denatured state resonances of GB1 in the presence of 8 M urea.

Initial experiments at the two extreme value of the CPMG field strength did not indicate any chemical exchange in this timescale at 25 ˚C in 8 M urea (Figure 3.15). This suggested that GB1 under these conditions is likely out of the limits of detection of the CPMG timescale. To alter the dynamics and enable detection using these methods, we raised the temperature of the system to 35 ˚C. Even under these conditions, we did not observe any contribution from chemical exchange for R_2 (Figure 3.16).

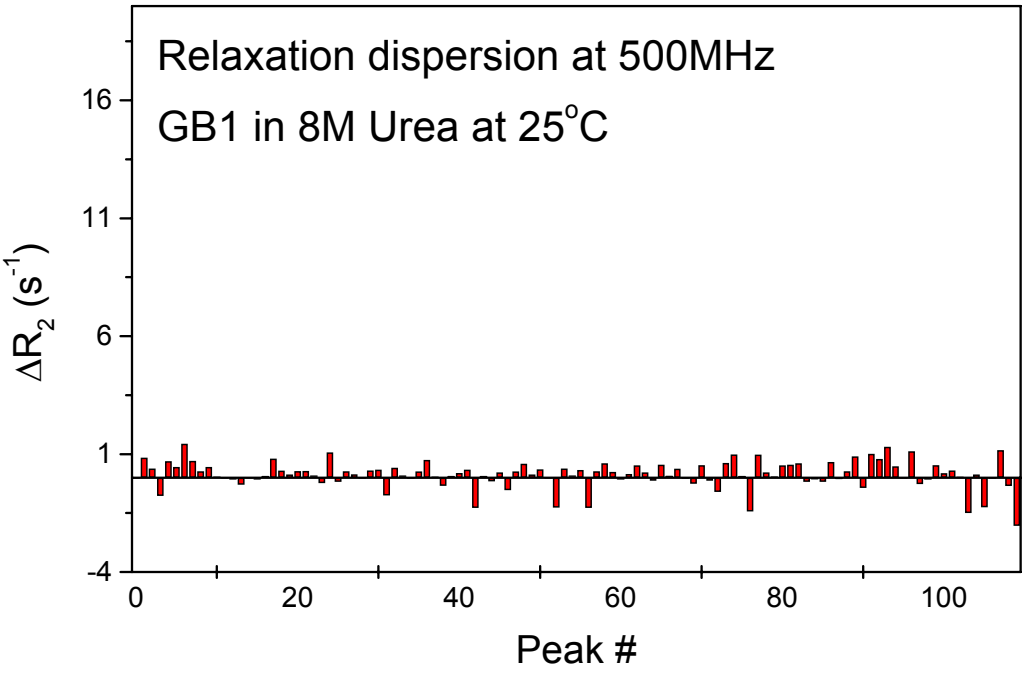

Figure 3.15 Relaxation compensated CPMG experiments at 500 MHz in the presence of ~ 8 M urea at 25 ˚C indicated no significant non-zero ΔR_2 values suggesting no CPMG detectable dynamics under these conditions. Both the native and denatured state peaks were analyzed for chemical exchange.

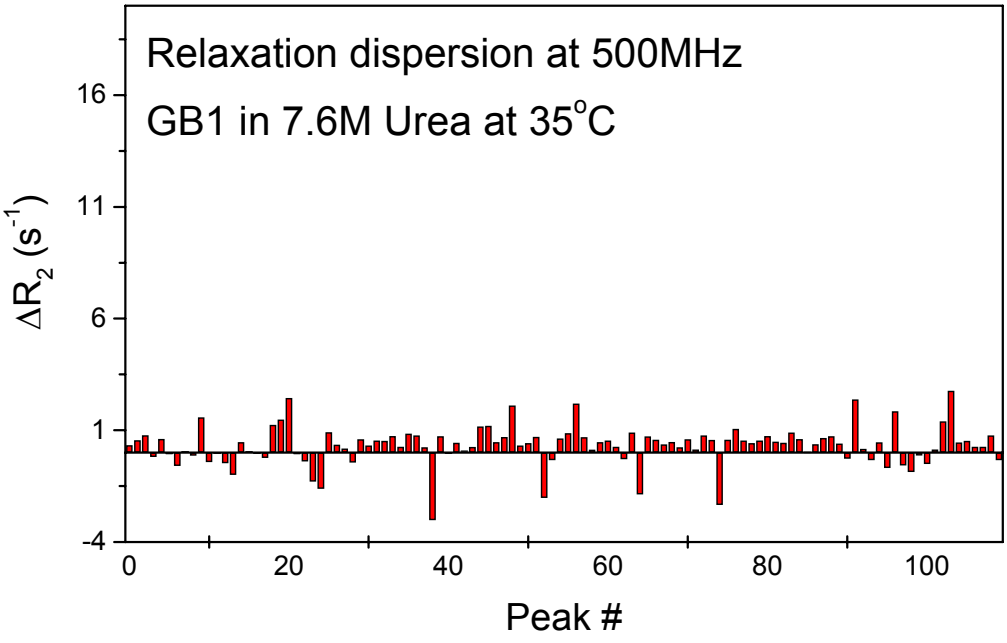

Figure 3.16 Relaxation compensated CPMG experiments at 500 MHz in the presence of 7.6 M urea at 35 ˚C indicated no significant differences from the previous conditions (Figure 2.12) suggesting that the increased temperature did not change the dynamics of the motions enough to bring it to the CPMG detectable timescales.

Discussion

We tested the role of protein dynamics in the pH dependent conformational change of Bcl-$X_L\Delta$TM using relaxation-compensated CPMG based NMR experiments at two different pH conditions, pH 7.4 and 4.9. These experiments identified interesting pH-dependent differences in μs-ms timescale protein dynamics of Bcl-$X_L\Delta$TM that were localized in the C-terminal end of the protein. The backbone of Bcl-X_L displays highly variable dynamics as seen by the variation in the intensity of peaks in the ^{15}N-^{1}H HSQC spectrum. This variation in the dynamics limited our analysis of the CPMG relaxation experiments to the highly mobile regions of the protein. As inferred from the crystal structure and the solution structure of Bcl-$X_L\Delta$TM, there is a large part of the protein that is well structured but there are also parts of the protein including the long, unstructured loop (residues 26-83) that are highly mobile (Muchmore et al., 1996). In our preliminary analysis, we found that the sharp, intense peaks from the mobile parts of the protein gave rise to decay curves that could be used to reliably estimate R_2 values. However, most of the protein peaks in the spectrum did not give rise to well-described decay curves under the experimental conditions that were used. For our preliminary analysis, we picked 20 peaks that gave rise to well-defined T_2 decay curves that could be described by a mono-exponential fit to the data. The preliminary observations indicate that the changes are localized to the more dynamic regions of the protein at the C-terminal end. The identification of these residues was possible due to the assignments that we had obtained from Dr. Gerhard Wagner at the Harvard Medical School. Although our analysis was limited to the highly dynamic regions of the protein, i.e., the residues that gave rise to the

sharp, highly intense peaks, it is interesting to note that changes were observed in the dynamics of the backbone of residues G196, A199 and A201 (Figure 3.17). Our preliminary results suggest that there is a decrease in the µs-ms timescale dynamics of the protein at pH 4.9 relative to pH 7.4. This was surprising because we had expected an increase in the dynamics of the protein under acidic pH conditions that would be representative of its ability to access both the solution and membrane conformations at pH 4.9 as opposed to only the solution conformation at pH 7.4. The preliminary observations, however, do suggest that the dynamics of the C-terminal TM segment present in the full length molecule could be modulated by pH changes. These results could be interpreted using information from the crystal structure of Bax.

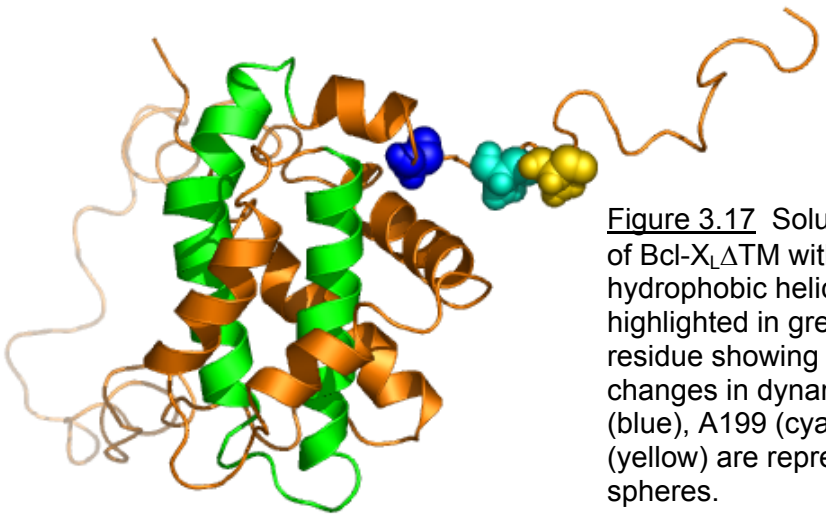

Figure 3.17 Solution structure of Bcl-X_LΔTM with the hydrophobic helical hairpin highlighted in green. The three residue showing pH-dependent changes in dynamics, G196 (blue), A199 (cyan) and A201 (yellow) are represented as spheres.

The structure of full length Bcl-X_L with the C-terminal TM segment is not known, but the structure of Bax (Figure 1.3), which shares the same overall fold, suggests that the C-terminal TM segment of Bcl-X_L could be bound into the hydrophobic cleft formed by the BH1, BH2 and BH3 regions in Bcl-X_L (Muchmore et al., 1996; Suzuki et al., 2000b). This binding could be dynamic with a two different populations of Bcl-X_L existing in equilibrium in solution; one with the C-terminal TM exposed and the other having it

bound into the hydrophobic cleft. Our results are consistent with the model that a decrease in pH perturbs the equilibrium by "freezing" the structure with the C-terminal TM segment exposed and helps anchor Bcl-X_L into the membrane. This anchoring would bring the entire molecule closer to the membrane surface and help mediate the solution to membrane conformational change. Before delving deep into a detailed interpretation of the pH-dependence of protein dynamics in Bcl-$X_L\Delta$TM, we explored the applications of the CPMG based techniques and high resolution NMR spectroscopy towards understanding conformational dynamics during protein folding using a model system.

GB1 provided a good model system for the application of high resolution NMR and CPMG techniques for two main reasons:

1. the simplicity of the system and the overwhelming amount of information available on the thermodynamics and kinetics of folding of this protein.
2. evidence for heterogeneities during GB1 folding that warrant further exploration and the ability of the experimental methods to resolve the controversy surrounding the nature of the folding pathway of GB1(Kuszewski et al., 1994; Park et al., 1997; Park et al., 1999).

Equilibrium folding studies were initially carried out by unfolding GB1 with urea. Even at the highest concentration of urea that was tested, GB1 was only 80% unfolded. Analysis of ^{15}N-^{1}H HSQC spectra revealed the presence of intermediates during the folding of GB1. The assignments of some of these resonances revealed that residues T11, A23 and D46, which are localized to the loops or to the extremities of the β-strands, could exist in conformations distinctly different from the native and denatured state

conformations. The data are consistent with a model where the native state unfolds to an intermediate state, which is characterized by a native-like hydrophobic core. In the following step, the intermediate state then unfolds completely to form the denatured ensemble. The intermediate state has a native-like hydrophobic core and displays a different surface relative to the native state. This is confirmed also by observations from thermal denaturation experiments, where there were heterogeneities observed in the folding of GB1 localized to residues on the surface at the ends of the hairpins. The results from thermal denaturation experiments were also consistent with a model where there is an initial collapse of the structure to form the hydrophobic core. The analysis of equilibrium unfolding of GB1 by urea and temperature are consistent with previous observations from quenched flow hydrogen-deuterium exchange experiments and predictions from all atom simulations of GB1 folding (Sheinerman and Brooks, 1998). In contrast to the predictions from the computational studies, our data indicates that more than 80 % of the molecule is folded in the first step and that the second step is just a minor rearrangement of the surface of the molecule (Sheinerman and Brooks, 1998).

Since the evidence from equilibrium folding studies suggests the existence of folding intermediates, we believed that a detailed description of the kinetics of conformational exchange during GB1 folding using the relaxation compensated CPMG techniques would corroborate that observation. Since the first step in the systematic application of relaxation compensated CPMG methods is the simulation of relaxation dispersion curves based on kinetic data, we carried out the simulations using kinetic data from McCallister et al., and Park et al (McCallister et al., 2000; Park et al., 1999). The simulations were carried out using the k_{ex} values extrapolated to 4 M guanidine

hydrochloride. This was done based on the assumption from available data that the destabilization of GB1 at 4 M guanidine hydrochloride would be similar to the destabilization in the presence of 8 M urea. The simulations based on the three state kinetics data of Park et al., suggested that under certain conditions, there were CPMG detectable motions in the folding process of GB1. However, the simulations using data from the two-state description of McCallister et al. suggested that there were no CPMG detectable motions during GB1 folding. Our data which showed no relaxation dispersion was consistent with the two-state kinetic description of GB1 folding. However, it is in contrast with the three-state thermodynamic description of GB1 folding that we observed during equilibrium folding experiments. To resolve the differences between the simulations (of three-state kinetics) and the results from the relaxation compensated CPMG experiments indicating no exchange, we analyzed each parameter that was used in the simulation. There are four parameters used for the simulation of relaxation dispersion curves:

1. p_A and p_B, the fractional populations of the native and intermediate state in the presence of 8 M urea. We assumed that the pA was 0.98 based on the relative intensities of peaks from the ^{15}N-^{1}H HSQC spectra and this was a reasonable assumption. Since the relaxation compensated CPMG experiments can detect even contributions from minor populations (~ 1% of total), we would be able to detect contributions from the intermediate state.
2. R_A and R_B, the intrinsic R_2 relaxation rates of the native and intermediate state. The intrinsic R_2 depends on the size of the molecule and for a small, globular protein the size of GB1, 5 s^{-1} is a reasonable estimation based on the Solomon

equations. Also, since we had observed that the intermediate state resembles the native state from the HSQC spectra, we assumed that the intrinsic R_2 was the same for both the forms of GB1.

3. $\Delta\omega$, the difference between the ^{15}N chemical shifts of the native and intermediate state. Since we did not have a complete assignment of the intermediate state, a rigorous treatment of this was not possible. Hence, we determined the range of $\Delta\omega$ observed for the native and denatured states and simulated curves at three different values of $\Delta\omega$, the two extremes ($\Delta\omega$ = 0.1 ppm and $\Delta\omega$ = 9 ppm) and an intermediate value ($\Delta\omega$ = 2 ppm). As shown in Figure 3.13, there are CPMG detectable motions under conditions were $\Delta\omega$ is at least 2 ppm.
4. k_{ex}, is the rate constant for conformational exchange between the native and intermediate states based on data from Park et al. This data was extrapolated to 4 M guanidine hydrochloride based on k_{NI}, k_{IN} and the m-values for the N-to- I and I-to-N transitions (Park et al., 1999). It is reasonable to assume that this data from 4 M guanidine hydrochloride will be similar to the conditions in the presence of 8 M urea.

Although we believe that the simulations are based on available data and reasonable assumptions, the discrepancies observed between the simulation and experimental data could be a result of (i) $\Delta\omega << 2$ ppm, which would result in the motions being non-observable using the relaxation compensated CPMG methods, and/or (ii) incomplete kinetic description due to the limitations of fluorescence spectroscopy used by Park et al. Although the data does not rule out the three-state kinetic model, there are no motions during the folding of GB1 that are detectable using relaxation compensated CPMG

experiments. The CPMG experiments accurately measure motions in the 100 s^{-1} – 3000 s^{-1} timescale (Thuduppathy and Hill, 2004b). It is possible that the dynamics of motions during GB1 folding are outside this time regime and the quantitation of this dynamics would require other NMR techniques like zz-relaxation (0.1 – 10 s^{-1}) or R1ρ (for faster motions ~ 25000 s^{-1}) relaxation spectroscopy (Farrow et al., 1994; Massi et al., 2005; Massi et al., 2004). The results from the GB1 folding experiments highlight the advantages of the residue-specific detail provided by high resolution NMR spectroscopy and potential advantages of CPMG based techniques in cases where there is exchange in the CPMG timescale. Although further exploration of the dynamics of the folding of GB1 and the conformational change of Bcl-X_L are beyond the scope of this thesis work, the pH-dependent dynamics of Bcl-X_L on a biologically relevant timescale (μs-ms) warrants further investigation to determine whether these motions are important in the pH-dependent solution-to-membrane conformational change that is critical for the regulation of Bcl-X_L and apoptosis.

References

Alexander, P., S. Fahnestock, T. Lee, J. Orban, and P. Bryan. 1992a. Thermodynamic Analysis of the Folding of the Streptococcal Protein-G Igg-Binding Domains B1 and B2 - Why Small Proteins Tend to Have High Denaturation Temperatures. *Biochemistry* 31(14):3597-3603.

Alexander, P., J. Orban, and P. Bryan. 1992b. Kinetic-Analysis of Folding and Unfolding the 56-Amino Acid Igg-Binding Domain of Streptococcal Protein-G. *Biochemistry* 31(32):7243-7248.

Carr, H.Y., and E.M. Purcell. 1954. Effects of Diffusion on Free Precession in Nuclear Magnetic Resonance Experiments. *Physical Review* 94(3):630-638.

Carver, J.P., and R.E. Richards. 1972. General 2-Site Solution for Chemical Exchange Produced Dependence of T2 Upon Carr-Purcell Pulse Separation. *Journal of Magnetic Resonance* 6(1):89-&.

Davis, D.G., M.E. Perlman, and R.E. London. 1994. Direct Measurements of the Dissociation-Rate Constant for Inhibitor-Enzyme Complexes Via the T-1-Rho and T-2 (Cpmg) Methods. *Journal of Magnetic Resonance Series B* 104(3):266-275.

Delaglio, F., S. Grzesiek, G.W. Vuister, G. Zhu, J. Pfeifer, and A. Bax. 1995. NMRPipe: a multidimensional spectral processing system based on UNIX pipes. *J Biomol NMR* 6(3):277-293.

Eisenmesser, E.Z., D.A. Bosco, M. Akke, and D. Kern. 2002. Enzyme dynamics during catalysis. *Science* 295(5559):1520-1523.

Farrow, N.A., O.W. Zhang, J.D. Formankay, and L.E. Kay. 1994. A Heteronuclear Correlation Experiment for Simultaneous Determination of N-15 Longitudinal Decay and Chemical-Exchange Rates of Systems in Slow Equilibrium. *Journal of Biomolecular Nmr* 4(5):727-734.

Gronenborn, A.M., D.R. Filpula, N.Z. Essig, A. Achari, M. Whitlow, P.T. Wingfield, and G.M. Clore. 1991. A Novel, Highly Stable Fold of the Immunoglobulin Binding Domain of Streptococcal Protein-G. *Science* 253(5020):657-661.

Hill, R.B., C. Bracken, W.F. DeGrado, and A.G. Palmer. 2000. Molecular motions and protein folding: Characterization of the backbone dynamics and folding equilibrium of alpha D-2 using C-13 NMR spin relaxation. *Journal of the American Chemical Society* 122(47):11610-11619.

Jen, J. 1974. Chemical Exchange and Nmr-T2 Relaxation. *Advances in Molecular Relaxation Processes* 6(2):171-183.

Jen, J. 1978. Chemical Exchange and Nmr T2 Relaxation - Multisite Case. *Journal of Magnetic Resonance* 30(1):111-128.

Johnson, B.A. 2004. Using NMRView to visualize and analyze the NMR spectra of macromolecules. *Methods Mol Biol* 278:313-352.

Johnson, B.A., and Blevins, R. A. 1994. NMRView: A computer program for the visualization and analysis of NMR data. *Journal of Biomolecular NMR* 4(603-615).

Kuszewski, J., G.M. Clore, and A.M. Gronenborn. 1994. Fast Folding of a Prototypic Polypeptide - the Immunoglobulin Binding Domain of Streptococcal Protein-G. *Protein Science* 3(11):1945-1952.

Levitt, M.H. 2001. Spin Dynamics: Basics of Nuclear Magnetic Resonance. John Wiley.

Loria, J.P., M. Rance, and A.G. Palmer. 1999. A relaxation-compensated Carr-Purcell-Meiboom-Gill sequence for characterizing chemical exchange by NMR spectroscopy. *Journal of the American Chemical Society* 121(10):2331-2332.

Mandel, A.M., M. Akke, and A.G. Palmer. 1996. Dynamics of ribonuclease H: Temperature dependence of motions on multiple time scales. *Biochemistry* 35(50):16009-16023.

Marley, J., M. Lu, and C. Bracken. 2001. A method for efficient isotopic labeling of recombinant proteins. *J Biomol NMR* 20(1):71-75.

Massi, F., M.J. Grey, and A.G. Palmer. 2005. Microsecond timescale backbone conformational dynamics in ubiquitin studied with NMR R-1p relaxation experiments. *Protein Science* 14(3):735-742.

Massi, F., E. Johnson, C.Y. Wang, M. Rance, and A.G. Palmer. 2004. NMR R-1 rho rotating-frame relaxation with weak radio frequency fields. *Journal of the American Chemical Society* 126(7):2247-2256.

McCallister, E.L., E. Alm, and D. Baker. 2000. Critical role of beta-hairpin formation in protein G folding. *Nature Structural Biology* 7(8):669-673.

Meiboom, S., and D. Gill. 1958. Modified Spin-Echo Method for Measuring Nuclear Relaxation Times. *Review of Scientific Instruments* 29(8):688-691.

Millet, O., J.P. Loria, C.D. Kroenke, M. Pons, and A.G. Palmer. 2000. The static magnetic field dependence of chemical exchange linebroadening defines the NMR chemical shift time scale. *Journal of the American Chemical Society* 122(12):2867-2877.

Muchmore, S.W., M. Sattler, H. Liang, R.P. Meadows, J.E. Harlan, H.S. Yoon, D. Nettesheim, B.S. Chang, C.B. Thompson, S.L. Wong, S.L. Ng, and S.W. Fesik. 1996. X-ray and NMR structure of human Bcl-xL, an inhibitor of programmed cell death. *Nature* 381(6580):335-341.

Palmer, A.G. 2001. NMR probes of molecular dynamics: Overview and comparison with other techniques. *Annual Review of Biophysics and Biomolecular Structure* 30:129-155.

Palmer, A.G., M.J. Grey, and C.Y. Wang. 2005. Solution NMR spin relaxation methods for characterizing chemical exchange in high-molecular-weight systems. *Nuclear Magnetic Resonance of Biological Macromolecules, Part C* 394:430-465.

Palmer, A.G., C.D. Kroenke, and J.P. Loria. 2001. Nuclear magnetic resonance methods for quantifying microsecond-to-millisecond motions in biological macromolecules. *Nuclear Magnetic Resonance of Biological Macromolecules, Pt B* 339:204-238.

Park, S.H., K.T. ONeil, and H. Roder. 1997. An early intermediate in the folding reaction of the B1 domain of protein G contains a native-like core. *Biochemistry* 36(47):14277-14283.

Park, S.H., M.C.R. Shastry, and H. Roder. 1999. Folding dynamics of the B1 domain of protein C explored by ultrarapid mixing. *Nature Structural Biology* 6(10):943-947.

Sheinerman, F.B., and C.L. Brooks. 1998. Molecular picture of folding of a small alpha/beta protein. *Proceedings of the National Academy of Sciences of the United States of America* 95(4):1562-1567.

Suzuki, M., R.J. Youle, and N. Tjandra. 2000. Structure of Bax: Coregulation of dimer formation and intracellular localization. *Cell* 103(4):645-654.

Thuduppathy, G.R., and R.B. Hill. 2004. Applications of NMR spin relaxation methods for measuring biological motions. *Numerical Computer Methods, Pt E* 384:243-264.

Wang, C.Y., M.J. Grey, and A.G. Palmer. 2001. CPMG sequences with enhanced sensitivity to chemical exchange. *Journal of Biomolecular Nmr* 21(4):361-366.

Chapter 4

Electrostatics plays a key role in the solution to membrane conformational change of Bcl-X_L

Summary

Signals from a number of stress sensing pathways are integrated at the mitochondria to decide the commitment of a cell towards apoptosis. The regulation of cytochrome c release from inside the mitochondrion into the cytosol signals commitment to apoptosis, and is regulated by the pro-apoptotic and pro-survival Bcl-2 proteins. In their soluble cytosolic form, or anchored on the mitochondrial outer membrane, the pro-survival proteins (Bcl-2/Bcl-X_L) can heterodimerize and neutralize the activity of the pro-apoptotic proteins like Bax and Bak. The anti-apoptotic protein Bcl-X_L elicits its biological function not only via the solution conformation in the cytosol but also in the membrane inserted conformation, in the outer mitochondrial membrane. *In vitro*, it has been observed that a variant of Bcl-X_L, lacking the C-terminal hydrophobic segment, is able to insert into membrane bilayers containing anionic lipids in a pH-dependent manner. We had shown earlier that this conformational change is not aided by the destabilization of the native protein structure in solution upon acidification (Chapter 2). Here, we show that the presence of the lipid bilayer is essential in driving this conformational change and that electrostatics might play a key role in this interaction. This conformational change is coupled with an increase in helicity and insertion of parts of the protein into the membrane bilayer including one or more of the tryptophan residues. We have characterized this pH-dependent conformational change and show that the deprotonation of histidine side chains or the presence of divalent cations like calcium do not play a significant role in mediating this interaction.

Introduction

Apoptosis is a fundamental process that is essential for the development and survival of a multicellular organism (Rathmell and Thompson, 2002). A number of stress signals that have been shown to initiate apoptosis, integrate at the mitochondria to cause the downstream effects of cell death. The Bcl-2 family of proteins plays a critical role in the regulation of the mitochondrial pathway of apoptosis (Adams and Cory, 1998; Green and Reed, 1998; Hengartner, 2000; Kuwana and Newmeyer, 2003). The delicate balance of this process regulated by the Bcl-2 proteins is very important to the survival of the organism as a whole. Dysregulation of this balance leads to the development of a number of diseased states, too much cell-death causes neurodegenerative disorders like Alzheimer's and Parkinson's while too little results in tumor formation and cancer.

Stress signals activate upstream effectors of apoptosis that cause mitochondrial membrane permeabilization and the release of cytochrome c and other apoptosis inducing factors (AIF, Smac/DIABLO etc.) from the intermitochondrial membrane space into the cytosol (Hengartner, 2000; Kuwana and Newmeyer, 2003). The release of cytochrome c into the cytosol results in the formation of a functional apoptosome through the interaction of cytochrome c with Apaf-1 and procaspase-9 (Li et al., 1997). The formation of the apoptosome activates procaspase-9, leading to an amplification of the caspase cascade and ultimately resulting in cell death. In mammals, this critical step of cytochrome c release is controlled by the Bcl-2 family: a host of pro-apoptotic proteins like Bax and Bak and pro-survival proteins like Bcl-2 and Bcl-X_L that maintain the balance by acting in opposition with each other (Adams and Cory, 1998; Green and Reed,

1998; Gross, 2001; Hengartner, 2000; Kelekar and Thompson, 1998; Kuwana and Newmeyer, 2003; Reed, 1997b). Bax and Bak facilitate the loss of mitochondrial membrane potential and cause permeabilization of the mitochondrial outer membrane (Chipuk et al., 2004; Kluck et al., 1999; Scorrano and Korsmeyer, 2003). Bcl-X_L and Bcl-2 functionally rescue cells from apoptosis by preventing the release of cytochrome c and could play a direct role in preventing mitochondrial membrane permeabilization (Kuwana and Newmeyer, 2003; Lucken-Ardjomande and Martinou, 2005). A great deal of structural, functional and physiological information is available on the Bcl-2 proteins but the mechanism of their action at the mitochondrial membrane is still under debate.

The pro-survival proteins (Bcl-2/ Bcl-X_L) and the pro-apoptotic proteins (Bax/Bak) act by heterodimerizing with each other and neutralizing their activities. Bcl-2/ Bcl-X_L could heterodimerize with Bax/Bak either in the cytosol or when anchored into the outer mitochondrial membrane through their C-terminal transmembrane segment. Evidence also exists for Bcl-2 and Bcl-X_L acting directly at the outer mitochondrial membrane to prevent mitochondrial membrane permeabilization (Shimizu et al., 2000; Vander Heiden et al., 1997; Vander Heiden et al., 2001). These proteins also insert into lipid vesicles and planar bilayers *in vitro* and form ion channels with cation selective properties and moderate ion conductances (Minn et al., 1997; Schendel et al., 1998; Schendel et al., 1997). Additionally, Bcl-X_L also modulates the activity of the Voltage Dependent Anion Channel (VDAC), a component of the mitochondrial permeability transition pore (PTP) (Vander Heiden et al., 2001). In an interesting study to investigate the functional relevance of the membrane inserted form of Bcl-X_L in apoptosis, Minn et al. showed that the heterodimerization activity and the membrane activity of the protein

are both required for rescuing cells from apoptosis (Minn et al., 1999). These observations suggest that Bcl-2 proteins like Bcl-X_L have a dynamic role in apoptosis with their ability to elicit biological activity in both solution and membrane conformations. It should also be noted that both the cytosolic and membrane associated forms of Bcl-X_L have anti-apoptotic functions and a change in their intracellular localization occurs during apoptosis. Evidence points to the redistribution of Bcl-X_L from being partly cytosolic to being all membrane-bound when apoptosis is induced (Hsu et al., 1997). This change in intracellular localization is associated with a dramatic solution to membrane conformational change.

Understanding the conformational change from solution to the membrane would

1. unravel the role of the Bcl-2 proteins in apoptosis.
2. reveal essential aspects of the plasticity of an amino acid sequence in specifying multiple conformations.
3. identify intermediate conformations in the solution to membrane conformational change that would be attractive targets for therapeutic intervention.

Initial insights into the structural duality of Bcl-X_L arose from the structural similarity shared with bacterial pore-forming toxins like diphtheria toxin and colicins. The central hydrophobic helical hairpin (HHH) that is common between Bcl-X_L and the pore-forming toxins is thought to mediate their insertion into membranes (Lacy and Stevens, 1998; Lakey et al., 1992; Lesieur et al., 1997; Muchmore et al., 1996). It has been proposed that some colicins and diphtheria toxin use a "cloak and dagger" strategy for insertion with the hydrophobic helical hairpin forming the dagger for insertion. Bcl-X_L like the bacterial toxins inserts into membranes in a pH-dependent manner forming

ion-channels with moderate conductance properties (Minn et al., 1997). In this study, we characterize the dramatic conformational change that is associated with the insertion of Bcl-X_L into lipid vesicles at low pH. It has also been observed that electrostatic interactions play important roles in the insertion of colicins into membranes (Heymann et al., 1996). Here, we test the role of electrostatics in the solution to membrane conformational change of Bcl-$X_L\Delta$TM.

Materials and Methods

Protein Expression and Purification

The gene sequence for human Bcl-X_LΔTM (1-209) lacking the C-terminal 24 amino acids was subcloned into the pGB1 fusion construct using standard procedures (Sambrook, 2001). This construct produces Bcl-X_LΔTM as a fusion protein with 6x His-tagged Streptococcal protein G B1 domain on the N-terminus. The presence of GB1 domain in the fusion construct increases expression in bacterial cells as well as the amount of desired protein in the soluble fraction. A TEV protease recognition site is present between the GB1 domain and the Bcl-X_LΔTM sequence enabling isolation of Bcl-X_LΔTM away from GB1 following cleavage with TEV protease. Cleavage with TEV protease leaves Bcl-X_LΔTM with the amino acid sequence GEF at the N-terminus as a cloning artifact. *E.coli* cells (Tuner DE3) containing this plasmid construct were grown at 37 ˚C in LB media containing Carbenicillin (50 μg/ml) to a OD_{600} of ~0.7. Protein expression was induced by the addition of 0.3 mM IPTG and the cells were allowed to grow at 25˚C for 10-12 hours. At this time, chloramphenicol was added to a final concentration of 200 μg/ml to increase the amount of protein expressed in the soluble fraction and cells were maintained at 25°C for an additional 6-8 hours after which the cells were harvested by centrifugation (Carrio and Villaverde, 2001; Carrio and Villaverde, 2002). The cell pellet was resuspended in Buffer A (20 mM Tris, 0.5 M NaCl, pH 8.0) containing protease inhibitors and 1 mg/ml lysozyme, incubated at 4˚C for 2 hours and lysed by three passes using a French press. The protein present in the soluble fraction was then purified by affinity purification on a Ni^{2+} chelating column (Ni^{2+}

chelating sepharose, GE Healthcare), followed by dialysis into TEV protease cleavage buffer (50 mM Tris, 50 mM NaCl, 1 mM DTT, pH 8.0). The fusion protein was then cleaved for at least 4 hours at 4 °C with a His-tagged recombinant TEV protease (1:100 w/w ratio) to generate Bcl-$X_L\Delta$TM. The reaction mixture was loaded onto the Ni^{2+} chelating column again and the flow-through containing Bcl-$X_L\Delta$TM was collected, concentrated, dialyzed and loaded onto a Superdex 75 gel filtration column equilibrated with 20mM Tris, pH 8.0 containing 150 mM NaCl, 1mM DTT and 1mM EDTA. The fractions containing Bcl-$X_L\Delta$TM were collected and quantitated using UV-absorbance (ε_{280} = 41820 $M^{-1}cm^{-1}$ in 6 M GdnHCl). The yield of pure protein was approximately 15-20 mg/L. The purity was greater than 95% as judged by Coomassie-stained SDS-PAGE gel electrophoresis. ^{15}N labeled samples were prepared in a similar manner in the presence of $^{15}NH_4Cl$ in M9 minimal medium (Marley et al., 2001). All the proteins were stored at 4 °C until used.

Preparation of Large Unilamellar Vesicles (LUV)

1,2-distearoyl-9,10-dibromo-*SN*-glycero-3-phosphocholine (TBPC), dioleoyl phosphatidyl glycerol (DOPG), lissamine rhodamine B labeled dioleoyl phosphatidyl ethanolamine (Rh-DOPE), 1-palmitoyl-2-stearoyl-(6,7-dibromo)-*SN*-glycerophosphocholine and 1-palmitoyl-2-stearoyl-(11,12-dibromo)-*SN*-glycerophosphocholine were purchased from Avanti Polar Lipids. The lipids were mixed in the appropriate ratio and the chloroform from the lipid mixture was evaporated. Water was added to the lipids to reach a final concentration of lipids around 20 mM. The lipid suspension in aqueous solution was subjected to freeze-thaw cycles three times. The

suspension was then extruded through a 100 nm polycarbonate filter 11 times to make large unilamellar vesicles (LUV) with an average size around 100 nm (MacDonald et al., 1991). The homogeneity of these lipid vesicles was confirmed by size exclusion chromatography. The lipid vesicles were stored at 4 °C until further use.

Differential Scanning Calorimetry

All the differential scanning calorimetry experiments were carried out on a N-DSC nano differential scanning calorimeter (Calorimetry Sciences Corp.; Applied Thermodynamics). All samples were scanned from 10 °C to 90 °C using a scan rate of 1 °C / minute. For protein alone samples, the protein concentration was 40 μM. For the samples containing protein in the presence of lipid vesicles, the vesicles (DOPC : DOPG – 60:40) were added to a final concentration such that the Protein : Lipid (P:L) ratio was kept at 1:200. Samples containing protein with and without lipid vesicles were prepared at pH 7.4 and pH 4.9 using 20 mM sodium phosphate and 20 mM sodium acetate buffers respectively. The thermal unfolding transitions of the protein were found to be irreversible under all conditions.

Circular Dichroism spectropolarimetry

For the far-UV experiments, 1 μM samples of Bcl-$X_L\Delta$TM were prepared in buffer (20 mM sodium phosphate, pH 7.4 or 20 mM sodium acetate, pH 4.9) and in buffer containing lipid vesicles composed of DOPC and DOPG in the ratio 60:40. The lipid concentration in the samples containing lipid vesicles was 200 μM resulting in a protein: lipid (P:L) ratio of 1:200. Blank spectra were collected with buffer and with

buffer containing lipid vesicles. Spectra were collected using a 1cm path length cell scanning from 200 nm to 260 nm. Scan speed was 20 nm/min and response time was 2 seconds. 5 spectra were collected for each sample and averaged. For the near-UV CD experiments, protein concentration was 7.5 μM and lipid concentration in the vesicles was 1.5 mM for a P:L ratio of 1:200. Spectra were collected with wavelengths ranging between 320 nm and 250 nm in a 1 cm path length cell. Scan speed was 20 nm/min, response time was 2 seconds and 30 accumulations were averaged for each sample. The temperature was maintained at 25 °C during all experiments.

Steady state fluorescence spectroscopy

The association of protein and lipid vesicles was monitored real-time using a fluorescence assay on a PTI Model A1010 fluorimeter (Photon Technology International, Canada). Four different types of lipid vesicles were prepared as described above and used in the experiments: (i) DOPC and DOPG in a 60:40 ratio (ii) 1-palmitoyl-2-stearoyl (6,7-dibromo)-*SN*-glycerophosphocholine and DOPG in a 60:40 ratio (iii) 1-palmitoyl-2-stearoyl (11,12-dibromo)-*SN*-glycerophosphocholine and DOPG in a 60:40 ratio (iv) 1,2-distearoyl (9,10-dibromo)-*SN*-glycerophosphocholine and DOPG in a 60:40 ratio doped with Rh-DOPE. The excitation wavelength was 295 nm and emission was observed between 305 and 450 nm. The slit widths for excitation and emission were kept at 1 nm and 5 nm respectively with the experiment conducted at room temperature. The concentration of protein and lipid vesicles used for the fluorescence experiments were the same as used for the far-UV CD experiments, 1 μM in protein and 200 μM in lipids with a P:L ratio of 1:200. The buffers used for the studies were 20 mM sodium acetate at pH

4.9, 20 mM sodium phosphate at pH 7.4 and potassium acetate buffer at pH 5.0 with an ionic strength, I = 0.05(Perrin, 1963).

Sedimentation assay to measure protein binding to lipid vesicles

This assay was adapted from the procedure developed by Wimley et al. and a schematic representation of this assay is shown in Figure 4.1 (Wimley et al., 1998). It makes use of the higher density of brominated lipids to be able to sediment in a microcentrifuge at lower speeds compared to the ultracentrifugation based sedimentation methods. This method avoids the non ideality that is introduced at higher sedimentation forces (Wimley et al., 1998). Sedimentation was done in three steps with progressively increasing speeds which was shown by Wimley et al. to be necessary to remove a centrifugation speed dependence of partition coefficients measured (Wimley et al., 1998). The assay was optimized to identify conditions where there was complete sedimentation of the lipids in order to remove errors in the determination of protein concentration in the supernatant due to contamination from the lipid fraction. TBPC and DOPG were mixed in a molar ratio of 60:40 and doped with 0.25% Rh-DOPE to enable visualization of the lipid fraction. Bcl-$X_L\Delta$TM (10 μM) and lipid vesicles (200 μM) were incubated in the presence of an acetate buffer with an ionic strength, I=0.05 and varying concentrations of added salt, NaCl. Water was added to bring the total volume of the reaction up to 100 μL. The mixture was incubated overnight at 25 °C. It was then subject to centrifugation at increasing speeds (4000, 9000, 18000 x g) for 30 minutes each. At the end of the centrifugation, the supernatant was removed from the tube and assayed for total protein concentration by the Bradford method.

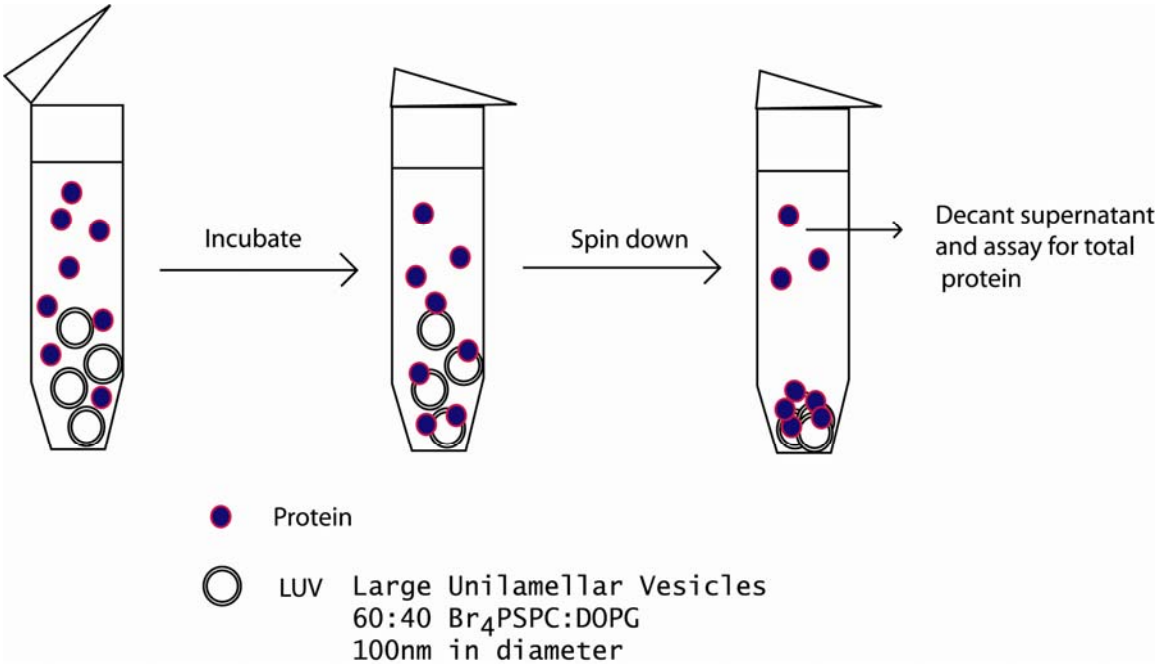

Figure 4.1 A schematic representation of the sedimentation assay used to measure the binding of Bcl-$X_L\Delta TM$ to lipid vesicles.

The standard curve for the Bradford assay was generated using standard concentrations of Bcl-$X_L\Delta TM$, which were determined using the absorbance at 280 nm. The amount of Bcl-$X_L\Delta TM$ bound to the vesicles was estimated using the difference between the amount of protein used in the reaction and the amount of protein remaining in the supernatant. The percentage of protein bound to the vesicles was calculated as follows:

$$\%\,\text{protein bound} = 100\left(1 - \frac{[\text{Protein in Supernatant}]}{[\text{Total Protein in reaction}]}\right) \qquad (1)$$

To determine the effects of Ca^{2+} on Bcl-$X_L\Delta TM$ binding to lipid vesicles, protein samples were incubated with vesicles at pH 5.0 acetate buffer (I=0.05) (Perrin, 1963)with 150 mM NaCl and varying amounts of $CaCl_2$ ranging between 0 mM and 10 mM. Following overnight incubation and centrifugation of the samples, the supernatant was isolated and

then assayed for total protein using Bradford Assay and the percentage of protein bound to lipid vesicles was calculated as shown above in equation (1).

Histidine pKa titration by NMR

The long-range HMQC experiments for monitoring histidine side chain protonation states were implemented using pulse sequences described elsewhere and were interpreted accordingly (Bachovchin, 1986; Bendall et al., 1983; Van Dijk et al., 1992). ^{15}N labeled NMR samples of Bcl-$X_L\Delta$TM (0.5 mM) were prepared in 20 mM sodium phosphate buffer containing 10% D_2O at pH 7.4. 420 × 30 complex points with acquisition times of 64 and 7.4 ms in ^{1}H and ^{15}N respectively were collected with the ^{15}N carrier placed at 205 ppm. Long range HMQC spectra were collected at pH 7.4, 7.0, 6.55, 6.25, 6.0, 5.75, 5.4, 5.2 and 4.8 by the addition of small amounts of hydrochloric acid to the sample. An identical sample was also titrated up to a pH of 8.55 by the addition of small amounts of NaOH and experiments collected at pH 7.45, 8.0 and 8.55. The NMR experiments were performed at 25 °C on a Varian INOVA 500 MHz spectrometer equipped with a triple resonance probe. The data were processed with nmrPipe (Delaglio et al., 1995) and displayed using NMRView (Johnson, 2004; Johnson, 1994b). Using the long range spectra collected from the H113A mutant, we were able to assign one of the 3 histidines that were detectable in the long range HMQC experiment to be H113. The other histidine residue in the globular part of Bcl-$X_L\Delta$TM, H177 was not assigned.

Results

pH-dependent stabilization of Bcl-$X_L\Delta$TM in the presence of LUVs

To study the thermodynamic stability of Bcl-$X_L\Delta$TM at different pH conditions in the presence of lipid vesicles, we monitored the changes in the thermal unfolding profile of the protein in the absence and presence of lipid vesicles (DOPC:DOPG – 60:40). At pH 7.4, the thermal unfolding profile of the protein is unchanged (within experimental uncertainty) in the absence and presence of the lipid vesicles (Figure 4.2a). However, at insertable pH conditions, pH 4.9, the thermal unfolding transition disappears from the thermogram only in the sample containing lipid vesicles (Figure 4.2b). The peak corresponding to the thermal unfolding of the protein is present at pH 4.9 in the absence of lipid vesicles.

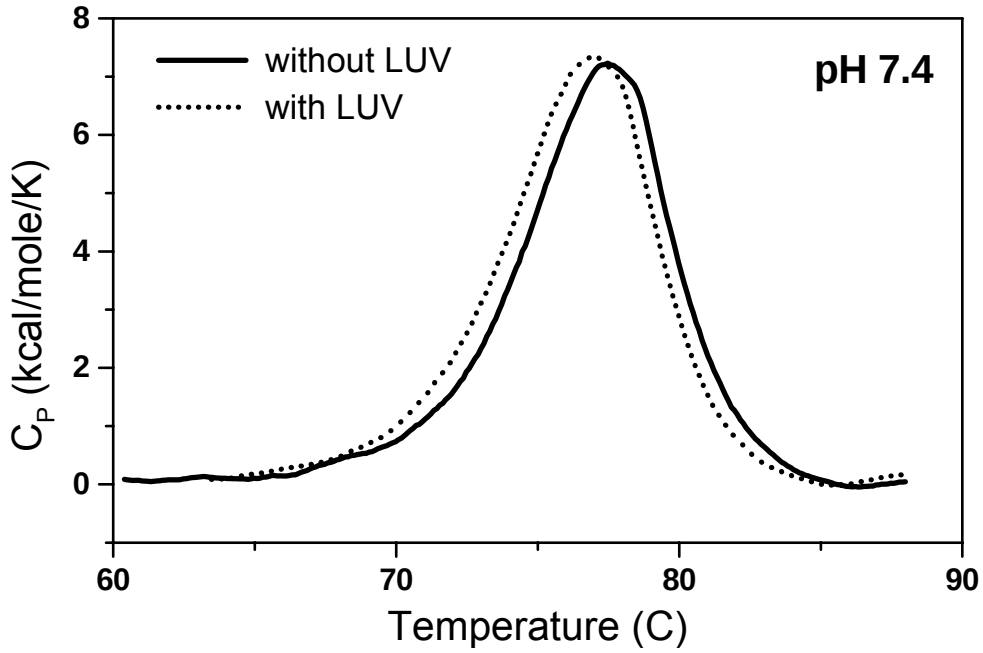

Figure 4.2a At pH 7.4, there is no interaction between Bcl-$X_L\Delta$TM and lipid vesicles.

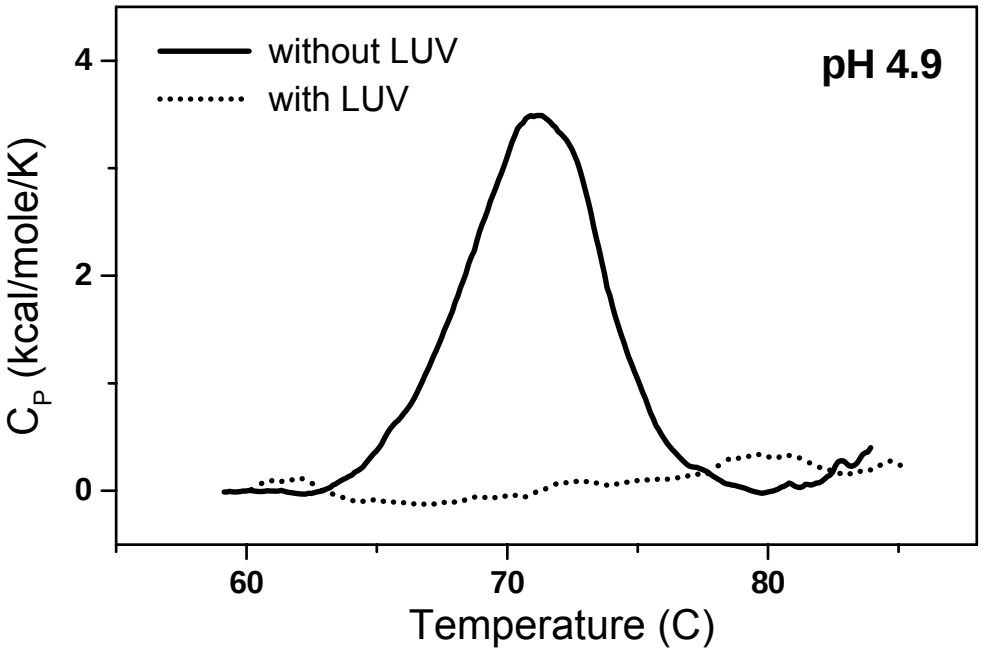

Figure 4.2b At pH 4.9, Bcl-$X_L\Delta$TM associates with lipid vesicles indicated by the disappearance of the thermal unfolding transition of the protein from the thermogram.

The disappearance of the protein unfolding peak from the thermogram in the presence of lipid vesicles at low pH suggests one of two possibilities: (i) the protein is completely unfolded in the presence of the lipid vesicles at low pH even at low temperatures such that no transition is visible upon increasing the temperature (ii) the protein is completely stabilized by the lipid vesicles in the temperature range under study such that there is no transition that is observed in the temperature range of the calorimetry experiment. The former possibility is ruled out since the far-UV CD spectrum in the presence of vesicles at low pH indicates the presence of secondary structural elements at 25 °C (Figure 4.3). Thus, the stabilization of the protein by the membrane is the only possible explanation for the observation in Figure 4.2, indicating a strong interaction between the protein and the lipids in the membrane. Dramatic changes in thermodynamic

stability are usually coupled with large conformational changes which were further investigated using spectroscopic methods.

Association of Bcl-X_LΔTM into lipid vesicles at low pH is coupled with secondary and tertiary structural changes

To determine the nature of the conformational change upon association with lipid vesicles, we measured the change in secondary structure using CD spectropolarimetry. At neutral pH, where there is no association between Bcl-X_LΔTM and lipid vesicles, we observe no significant changes between the far-UV CD spectra of the protein collected in the absence and presence of the vesicles. However, at pH 4.9, the far-UV CD spectrum of Bcl-X_LΔTM in the presence of lipid vesicles is different in the absence and presence of vesicles, indicating changes in secondary structure (Figure 4.3a). The increase in ellipticity at 222 nm at pH 4.9 upon the addition of lipid vesicles translates to an increase in helicity by about 25%.

The near-UV CD spectra at pH 7.4 of Bcl-X_LΔTM in the presence of lipid vesicles is similar to that in solution while at pH 4.9 in the presence of vesicles, the near-UV CD signal is significantly decreased (Figure 4.3b). This suggests a dramatic tertiary structural change and averaging of the rotameric states of the side chains of aromatic amino acids when the protein associates with lipid vesicles.

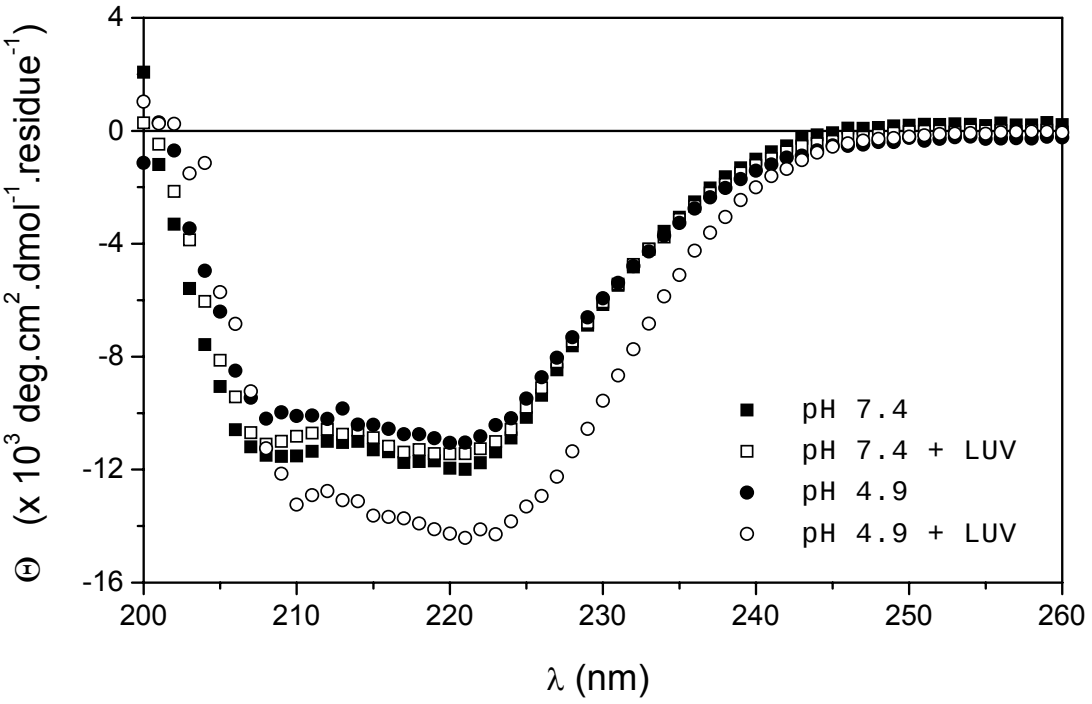

Figure 4.3a Secondary structural changes in Bcl-$X_L\Delta$TM are revealed by changes in the far-UV CD signal in the presence of lipid vesicles at low pH.

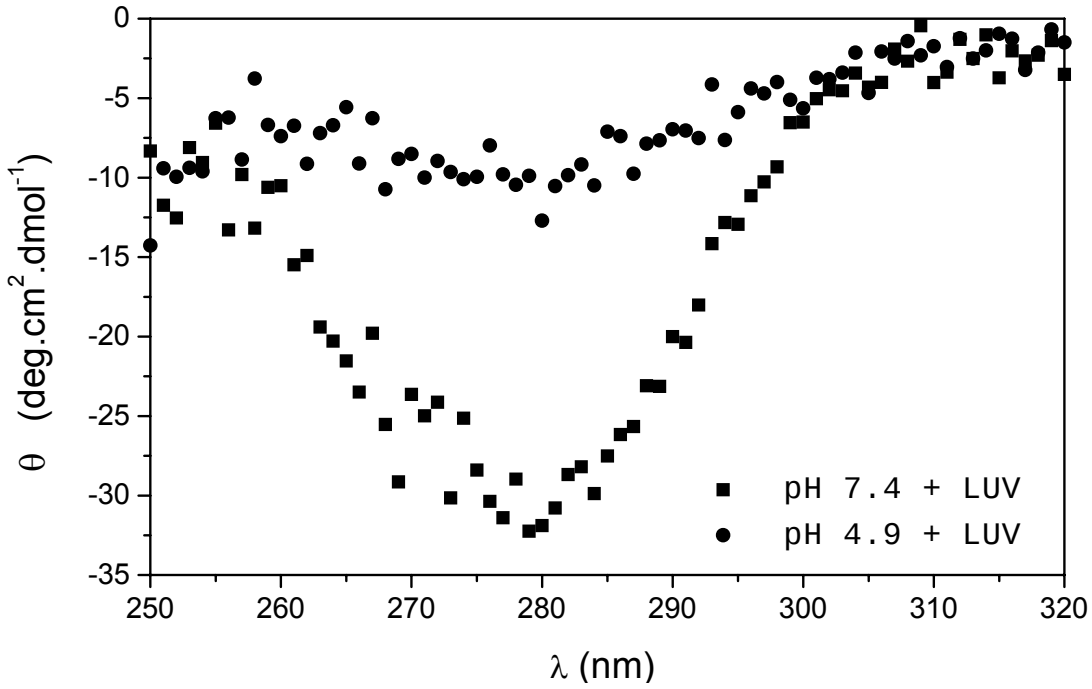

Figure 4.3b The changes in the near-UV CD signal suggest tertiary structural changes in Bcl-$X_L\Delta$TM upon association with lipid vesicles at acidic pH conditions.

To confirm the observations from near UV CD spectropolarimetry, we measured the change in the fluorescence emission spectrum of the protein upon association with lipid vesicles at pH 7.4 and pH 4.9. At pH 7.4, the addition of lipid vesicles does not cause significant changes in the fluorescence spectrum. However, upon the addition of lipid vesicles at pH 4.9, there is a big increase in the fluorescence intensity coupled with a blue shift in the λ_{max} of the emission spectrum (Figure 4.4). The native structure of Bcl-$X_L\Delta TM$ in solution (Figure 4.5) indicates the presence of tryptophans in both polar and non-polar environments in the protein. The blue shift in the λ_{max} suggests a net shift of the tryptophan residues towards a more non-polar environment upon the addition of lipid vesicles. This observation is consistent with the insertion of tryptophan residues into the non-polar hydrophobic core of the membrane bilayer. The observations from CD and fluorescence taken together indicate a dramatic conformational change in Bcl-$X_L\Delta TM$ going from solution to the membrane at pH 4.9.

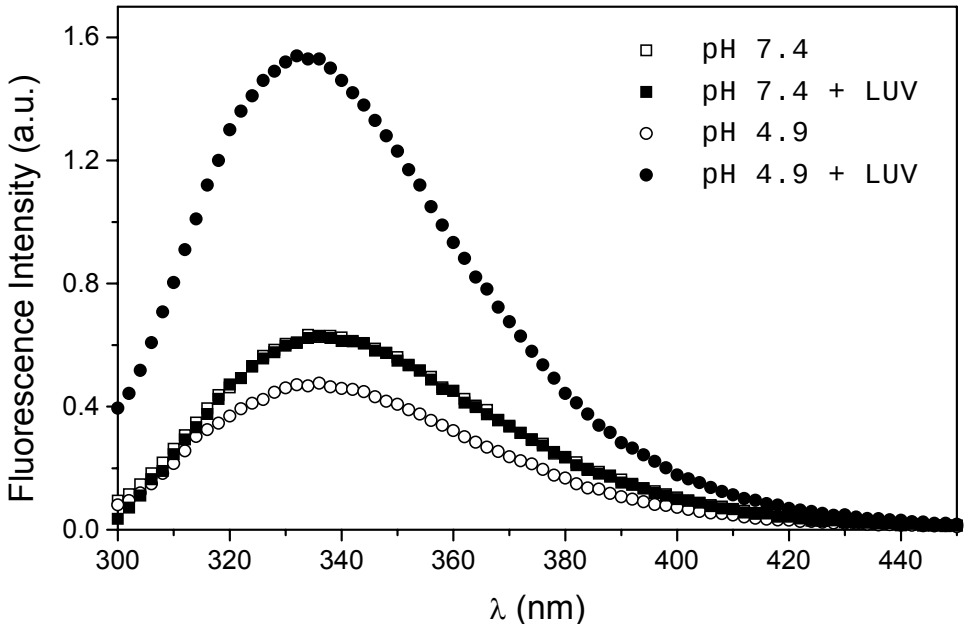

Figure 4.4 Fluorescence emission spectral changes in Bcl-$X_L\Delta TM$ indicate major structural changes upon association with lipid vesicles at low pH.

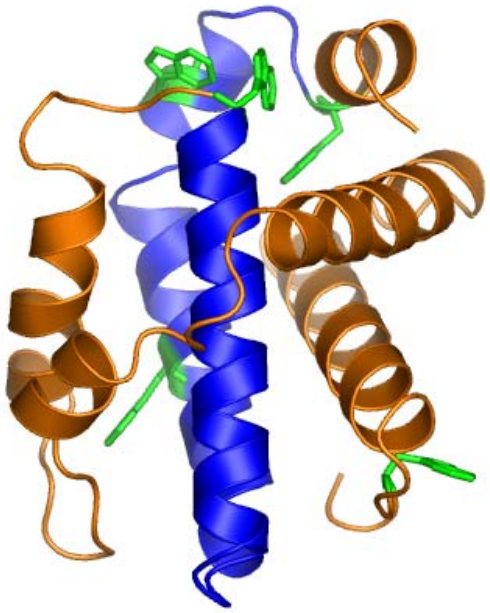

Figure 4.5 Crystal structure of Bcl-$X_L\Delta$TM with the hydrophobic helical hairpin highlighted in blue and tryptophan residues in green.

Tryptophan residue(s) insert deep into the bilayer of the vesicles

To ascertain the depth of insertion of Bcl-$X_L\Delta$TM into the lipid bilayer, we used the quenching of the intrinsic tryptophan fluorescence of the protein by the phospholipids brominated at different positions along the acyl chain. Distance dependent collisional quenching between the Trp fluorophore and brominated phospholipids leads to a decrease in the fluorescence signal that could be observed using steady-state fluorescence (Gonzalez-Manas et al., 1992). Under insertable conditions at pH 5.0, in the presence of non-brominated lipid vesicles, the fluorescence intensity is dramatically increased (Figure 4.6a). However, in the presence of vesicles composed of brominated lipids, the fluorescence intensity is quenched relative to that in vesicles composed of non-brominated lipids. Normalizing the intensity of fluorescence emission at 340 nm from Bcl-$X_L\Delta$TM in solution at pH 5.0 to be 100%, we observe an increase in intensity to almost 300% in the presence of vesicles composed of non-brominated lipids (Figure

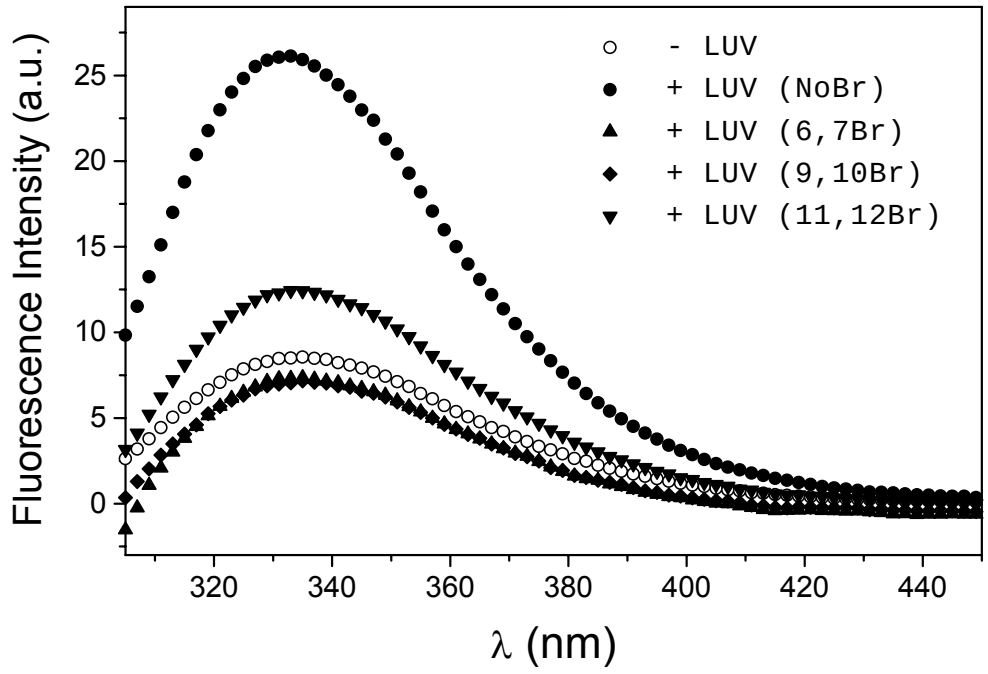

Figure 4.6a Quenching of intrinsic tryptophan fluorescence by brominated phospholipids suggests insertion of Bcl-$X_L\Delta$TM deep into the membrane bilayer at pH 5.0.

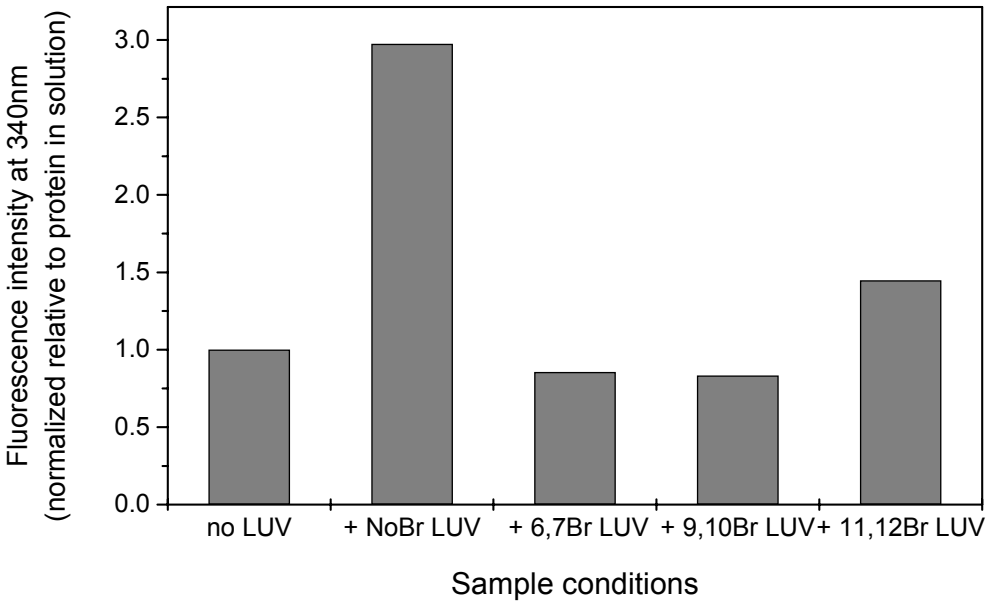

Figure 4.6b Comparison of the quenching of intrinsic tryptophan fluorescence by phospholipids brominated at different positions along the acyl chain indicates insertion deep into the bilayer.

4.6b). However, in the presence of brominated lipids, we observe an increase in intensity to only 150% in the presence of vesicles composed of 1-palmitoyl-2-stearoyl (11,12-dibromo)-*SN*-glycerophosphocholine indicating quenching of the intrinsic Trp fluorescence (Figure 4.6b). We also observed that in the presence of vesicles composed of 1,2-distearoyl-9,10-dibromo-*SN*-glycero-3-phosphocholine or 1-palmitoyl-2-stearoyl (6,7-dibromo)-*SN*-glycerophosphocholine, there was an even greater decrease in the fluorescence intensity to 90% of that of Bcl-$X_L\Delta$TM in solution at the same pH (Figure 4.6b). These observations suggest insertion of one or more tryptophan residues in Bcl-$X_L\Delta$TM into the membrane bilayer reaching to the middle of the acyl chains of the phospholipids. The fluorescence quenching in the presence of brominated lipids was also used to estimate the kinetics of insertion. The decrease in fluorescence intensity was monoexponential with a time constant of ~ 170 ms suggesting that the insertion process is fast (Figure 4.7).

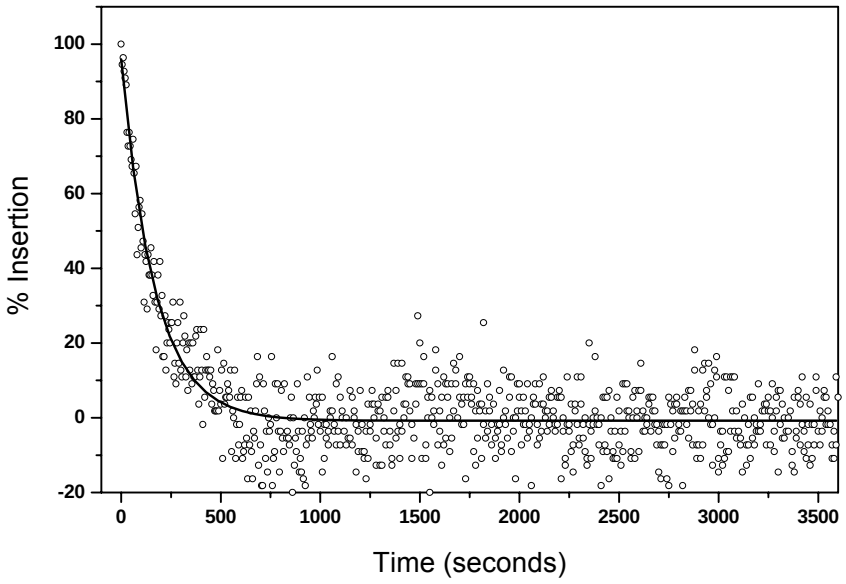

Figure 4.7 Kinetics of the quenching of intrinsic tryptophan fluorescence upon association with lipid vesicles fit to a mono-exponential decay suggests a time constant of 167 ± 7 seconds.

The results from Trp fluorescence quenching experiments were corroborated by the observations from our collaborator, Dr. Gorka Basanez at the University of Bilbao, Spain. Using a surface pressure change assay, he measured the ability of Bcl-$X_L\Delta TM$ to insert into a lipid monolayer. In this assay, the insertion of protein into a lipid monolayer was measured as an increase in the surface pressure on the monolayer surface. At pH 7.4, there was no insertion while at pH 4.9, the surface pressure increased to 40 mN/m indicating insertion of the protein into the bilayer.

Salt dependence of lipid binding suggests a role for electrostatic interactions in the insertion of Bcl-$X_L\Delta TM$ with lipid vesicles

The requirement for lipid vesicles composed of anionic lipids for insertion of Bcl-$X_L\Delta TM$ under acidic pH conditions suggested that electrostatic interactions might mediate the pH-dependent insertion. To confirm this requirement for anionic lipids for the solution to membrane conformational change of Bcl-$X_L\Delta TM$, we observed the thermal unfolding of the protein in the presence of vesicles using differential scanning calorimetry. In the presence of lipid vesicles containing DOPC and DOPG (in a 60:40 ratio), no thermal unfolding transition of the protein were observed. However, in the presence of all-neutral lipid containing vesicles (100% DOPC) at pH 4.9, the thermal unfolding transition of the protein was observed in the thermogram indicating that the presence of anionic lipids and low pH were both necessary for the association of Bcl-$X_L\Delta TM$ with lipid vesicles as witnessed by the abrogation of the thermal unfolding transition of the protein (Figure 4.8).

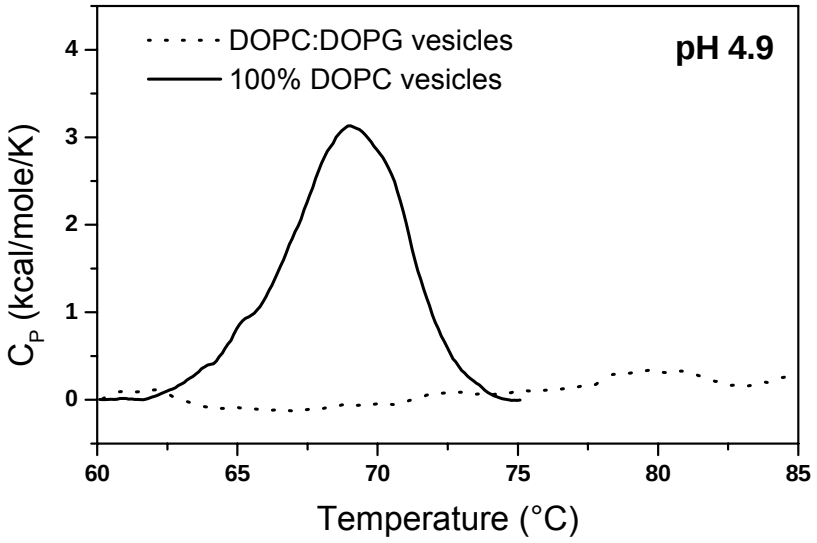

Figure 4.8 Requirement for anionic lipids on the membrane surface for the association of Bcl-$X_L\Delta TM$ suggests a role for electrostatics in this interaction.

To confirm the role of electrostatics in mediating the interaction between Bcl-$X_L\Delta TM$ and the lipid vesicles, we tested the ability of added salt (NaCl) to screen electrostatic interactions that could mediate this process. Increasing concentrations of NaCl reduced the binding of protein to the lipid vesicles as shown in Figure 4.9. This result indicates that electrostatics does play a role in mediating the pH-dependent insertion of Bcl-$X_L\Delta TM$ into lipid vesicles.

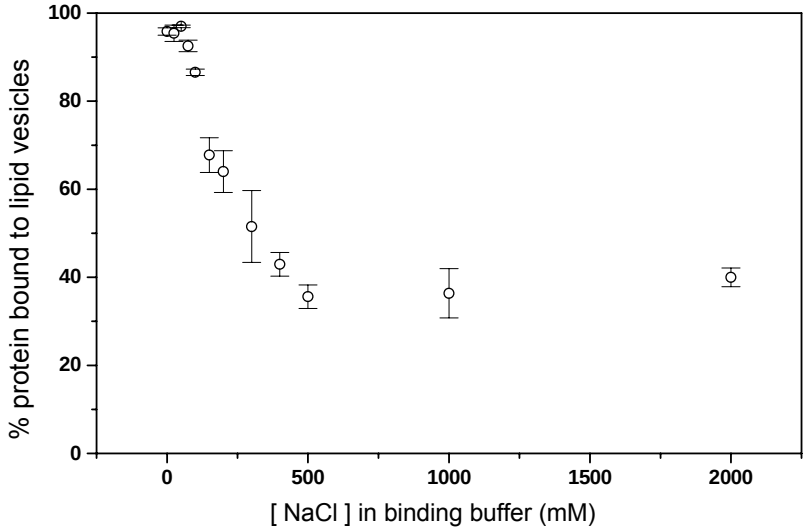

Figure 4.9 Salt dependence of Bcl-$X_L\Delta TM$ binding to lipid vesicles confirms the presence of electrostatic interactions.

This observation was also confirmed using steady state fluorescence experiments where the increase in intensity observed upon lipid binding at pH 5.0 was significantly decreased upon the addition of NaCl to 150 mM (data not shown).

Calcium does not appear to be mediating the interaction between the negatively charged protein surface and the negatively charged membrane surface

The surface of Bcl-X_LΔTM is highly negatively charged. Divalent cations like Ca^{2+} have been known to be able to mediate interactions between a negatively charged protein surface and a negatively charged membrane surface(Verdaguer et al., 1999). To test if this was a possible mechanism of interaction between Bcl-X_LΔTM and lipid vesicles, we investigated the effects of Ca^{2+} on the association of Bcl-X_LΔTM with lipid vesicles at pH 5.0. Addition of Ca^{2+} in the form of $CaCl_2$ was observed to cause no significant changes in the association between protein and lipid vesicles (Figure 4.10). The pH dependent binding profile of the binding of Bcl-X_LΔTM to lipid vesicles remained unaffected at Ca^{2+} concentrations up to 200 μM. Addition of Ca^{2+} at concentrations greater than 200 μM did cause a decrease in the binding but this could be attributed to a nonspecific salt screening effect on the binding of Bcl-X_LΔTM to lipid vesicles. Addition of EDTA up to 1 mM did not affect the binding of Bcl-X_LΔTM to lipid vesicles confirming that Ca^{2+} does not mediate protein-lipid interactions.

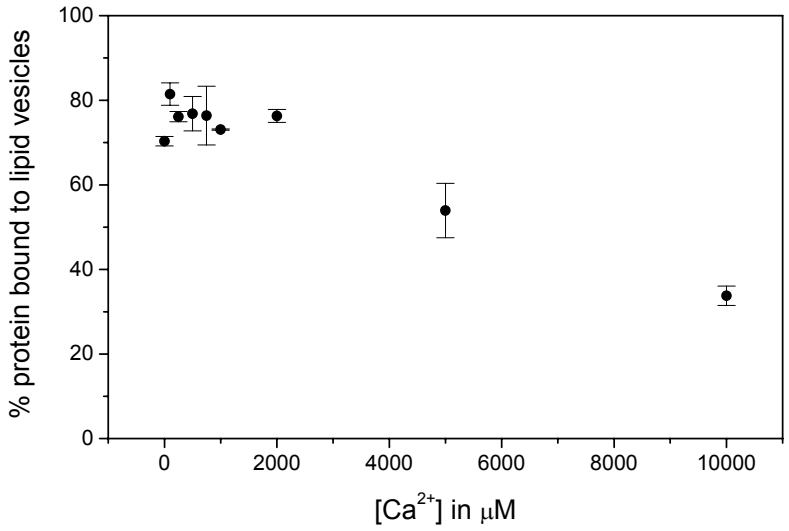

Figure 4.10 Ca^{2+} does not significantly alter the interaction between Bcl-$X_L\Delta$TM and negatively charged lipid vesicles at pH 5.0.

Histidines do not appear to play any significant role in the pH-dependent insertion of Bcl-$X_L\Delta$TM with lipid vesicles

The pH dependence profile of the insertion of Bcl-$X_L\Delta$TM into lipid vesicles suggests that the protonation / deprotonation equilibria of ionizable groups that titrate in the pH range between pH 5 and 7, such as histidines might play a role in mediating membrane insertion. To test the role of histidines in the soluble to the membrane conformational change, we used the long range HMQC titration experiments to explicitly monitor the pH titration profile of the histidine sidechains. We were able to follow the titration profiles of three of the four histidine residues in the protein (Figure 4.11) and all three of these titrated with midpoints of titration around pH 7.0 (Figure 4.12). Since the midpoint of histidine titration is at least 1.5-2.0 pH units away from the midpoint of the pH-dependent insertion into lipid vesicles, this observation indicates that the histidines do not play a role in the pH-dependent insertion into lipid vesicles.

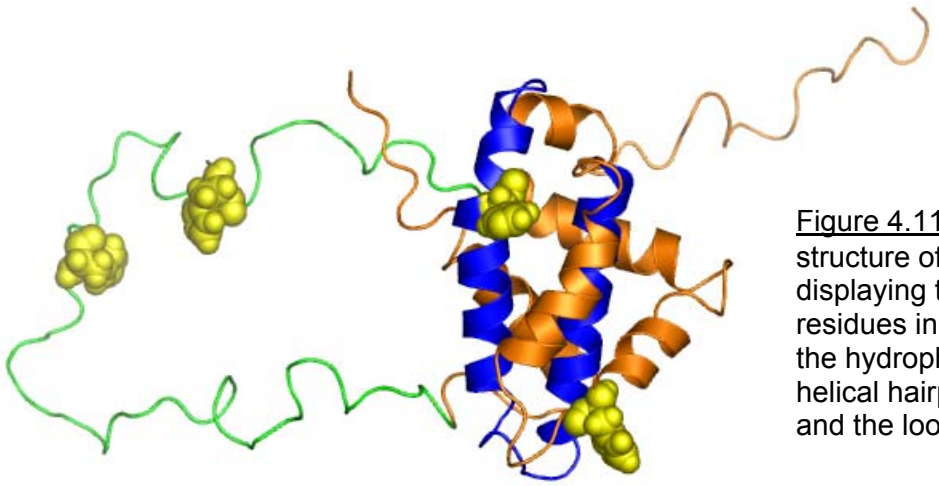

Figure 4.11 Solution structure of Bcl-$X_L\Delta$TM displaying the histidine residues in yellow an, the hydrophobic helical hairpin in blue and the loop in green.

The midpoints of histidine titration in Bcl-$X_L\Delta$TM appear to be much higher than that of free histidine in solution. This is expected because the electrostatic surface potential of Bcl-$X_L\Delta$TM is highly negative, which would be expected to elevate the pKa values of the histidines.

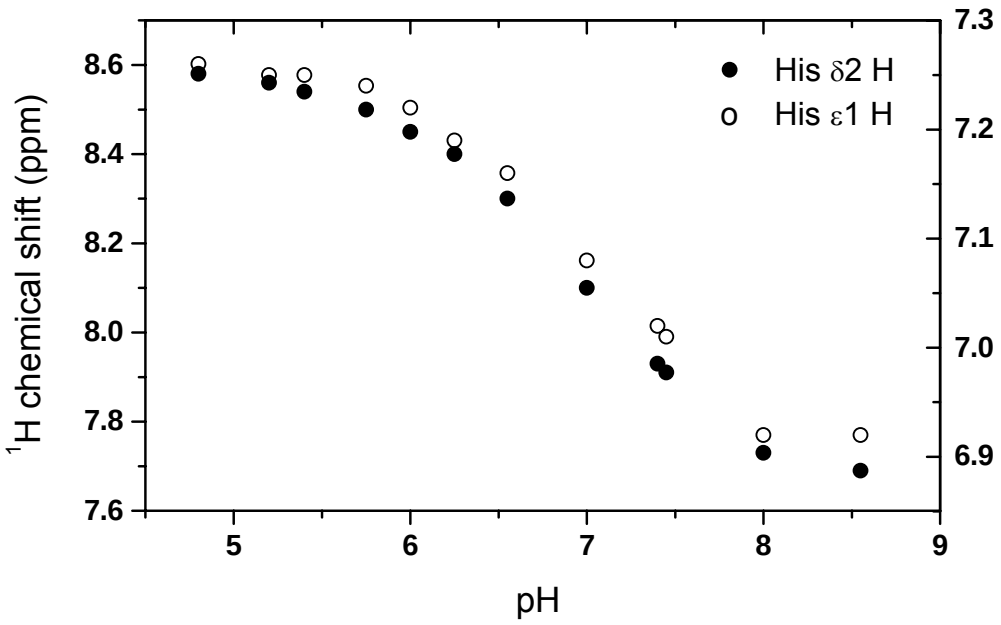

Figure 4.12 Histidines titrate in a pH range different from that of the conformational transition that is pH-dependent. A representative titration of one of the His residues in Bcl-$X_L\Delta$TM is shown below. Three of the four histidine residues were detectable by NMR and all three of them showed similar titration profiles.

Solution monomer and dimer of Bcl-$X_L\Delta TM$ have similar pH profiles for vesicle binding

Upon the inclusion of a size exclusion step in purification to further purify Bcl-$X_L\Delta TM$, we surprisingly observed that there were two peaks in the elution profile. Analysis of the peaks by SDS-PAGE indicated that both the peaks corresponded to Bcl-$X_L\Delta TM$. Fractions corresponding to either of the peaks was isolated and pooled to form two different samples. Analytical ultracentrifugation studies on these samples identified them as being composed primarily of monomer and dimer respectively. The monomer and dimer appeared to be stable and in slow equilibrium lasting over days as observed using native gel electrophoresis (data not shown). In order to test if dimerization provided an impetus for membrane insertion, we tested both the monomer and dimer Bcl-$X_L\Delta TM$ to the vesicle binding assay. The observation that both the fractions displayed identical pH profiles of binding to vesicles indicated that the monomer-dimer equilibrium does not have a role to play in mediating the solution to membrane conformational change (Figure 4.13). Previous studies (Chapter 2) had indicated the absence of any dimer both at pH 7.4 and at pH 4.9. However, these studies were carried out at much lower protein concentrations, 10-50 μM as compared to the current studies (both size exclusion and analytical ultracentrifugation) where the protein concentration was maintained > 1 mM. Even at these high concentrations, the fraction of dimer was less than 20 % of the total protein.

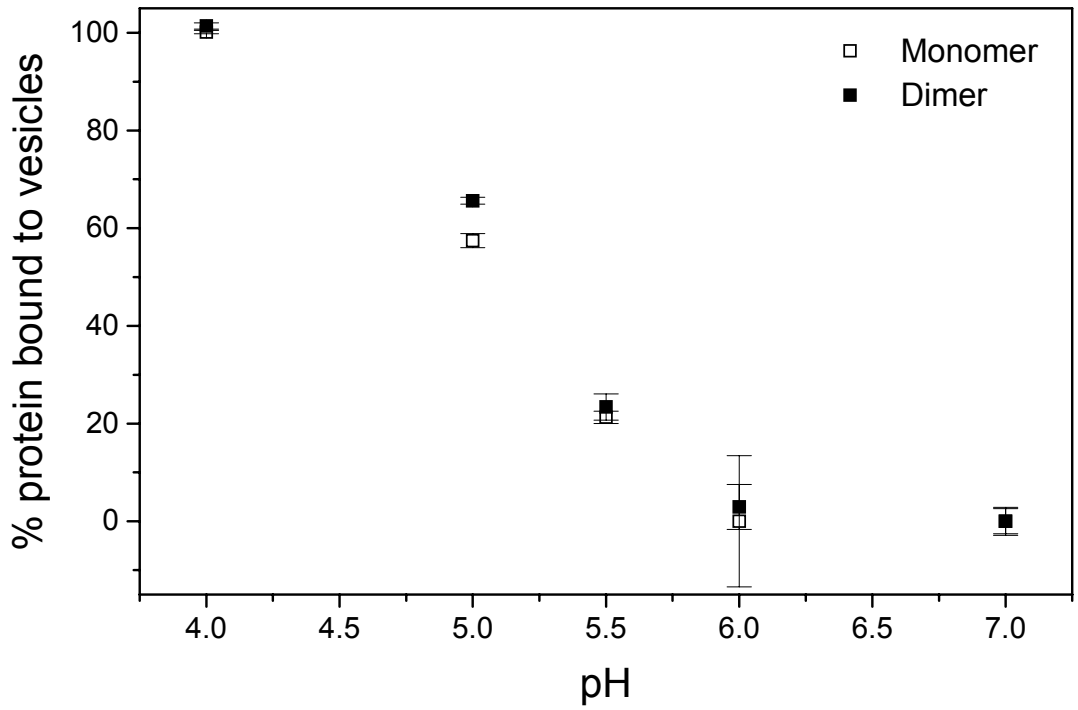

Figure 4.13 The monomer and dimer forms of Bcl-$X_L\Delta$TM did not display any differences in their pH titration profiles of binding to lipid vesicles.

Discussion

Bcl-X_LΔTM carries at net negative charge at physiological pH conditions and its pI is estimated to be 4.65. The protein surface is covered with a number of charged residues, many more of Glu and Asp residues as compared to Arg and Lys residues. So, what role do electrostatic interactions play in mediating the solution to membrane conformational change of Bcl-X_LΔTM? In attempting to answer this question, we started with a characterization of the conformational change of Bcl-X_LΔTM that occurs upon association with lipid vesicles at acidic pH conditions. Further experiments showed that electrostatics does play a key role in mediating this conformational change. In addition, we observed that the protonation of histidine sidechains or the presence of divalent calcium do not have a significant role to play in mediating the electrostatic interactions between Bcl-X_LΔTM and the negatively charged membrane surface.

We had shown previously in Chapter 1 that there were no significant pH-dependent changes in the secondary, tertiary and quarternary structure of Bcl-X_LΔTM in solution. This was surprisingly different from that of structurally similar diphtheria toxin and colicin A which undergo an acid-induced destabilization of the solution conformation to mediate the solution to membrane conformational change. We did, however, observe dramatic conformational changes as a function of pH in the presence of lipid vesicles. Far-UV CD spectropolarimetry indicated increase in helicity upon association with lipid vesicles at low pH. This increase in helicity observed is in accordance with previous observations of Bcl-X_LΔTM in DPC micelles, where an increase in helicity from 34% to 47% was observed upon the addition of DPC micelles (Losonczi et al., 2000). Near-UV

CD and steady state fluorescence spectroscopy results were consistent with a dramatic change in the environment of aromatic residues in the protein suggesting a dramatic change in the tertiary structure in the presence of lipid vesicles at low pH. NMR studies of Bcl-$X_L\Delta$TM in micelles had previously suggested a change in the chemical shift of the tryptophan side chains indicating a change in the environment around them supporting our observation (Losonczi et al., 2000).

Using lipid vesicles composed of brominated lipids, labeled with Br at different positions along the acyl chain (6,7 Br, 9,10 Br or 11,12 Br), we were able to ascertain the depth of insertion of Trp residues in the bilayer when Bcl-$X_L\Delta$TM is inserted into the membrane. The intrinsic Trp fluorescence is quenched by collisional quenching with the Br groups (Gonzalez-Manas et al., 1992) and since the quenching is very local, our data (Figure 6) suggests that one or more of the Trp residues is inserted deep into the bilayer presumably, somewhere up to the middle of the acyl chain of the outer layer of the bilayered membrane vesicle. Previous studies of Bcl-$X_L\Delta$loopΔTM in DPC micelles revealed the presence of protein-detergent NOEs that suggested helices 1 and 5 being inserted into the micelles (Losonczi et al., 2000). Using a glycosylation mapping experiment, peptides corresponding to the C-terminal TM helix and helix 6 in Bcl-$X_L\Delta$TM were found to be competent to insert into membrane bilayers (Garcia-Saez et al., 2004). It was also observed that α5 could insert synergistically in the presence of α6 strongly supporting the model of hydrophobic helical hairpin mediated insertion. These findings suggest that the insertion of the hydrophobic helical hairpin, the C-terminal TM segment and potentially, helix 1 deep into the bilayer forms the membrane-inserted conformation of Bcl-X_L. Insertion of Bcl-$X_L\Delta$TM into the membrane only under acidic

pH conditions, not at neutral pH, was also confirmed by an increase in the surface pressure in a monolayer insertion assay.

The requirement for acidic pH conditions and the observation that, *in vitro*, insertion is absolutely contingent upon the presence of anionic lipids in the membrane (as observed using differential scanning calorimetry) suggested an electrostatic component to this process. It has been suggested that a negative membrane surface potential could result in a reduced bulk pH according to the Gouy-Chapman theory (van der Goot et al., 1991). This further decrease in pH at the membrane surface is postulated to cause a structural destabilization of the protein leading to the formation of a structural intermediate that mediates insertion into the membrane (van der Goot et al., 1991). Although monovalent and divalent cations have been observed to be concentrated near the surface of a negatively charged membrane (McLaughlin, 1989), the interpretation that there is an increased proton concentration resulting in a decreased pH near the membrane surface is flawed. This is because protons in an aqueous solution are present as hydronium ions, H_3O^+ and tunnel through water molecules to move around. However, the pKa's of ionizable groups on the protein surface are altered when they approach closer to the negatively charged membrane surface due to contributions from dehydration and coulombic effects near the surface of the membrane. These altered pKa's could change the electrostatic profile of the protein enhancing electrostatic interactions resulting in the conformational change.

The addition of NaCl decreased the binding of Bcl-X_LΔTM to lipid vesicles, indicating a screening of interacting charges by the Na^+ and Cl^- ions. This observation confirms a role for electrostatics in the interaction between Bcl-X_LΔTM and the lipid

vesicles. The addition of salt did not appear to destabilize the protein at 150 mM NaCl concentration as observed using steady-state fluorescence spectroscopy. It was interesting to note that at salt concentrations upwards of 0.5 M, there was no additional decrease in the binding of Bcl-$X_L\Delta TM$ to lipid vesicles (the percentage bound was around 30%) indicating that there is a non-electrostatic component to this interaction. Additionally the pH on the membrane surface could also be influenced by the addition of salt and the change in pH might affect the electrostatic interaction between Bcl-$X_L\Delta TM$ and the LUVs. These observations strongly suggest an electrostatic component to the interaction between Bcl-$X_L\Delta TM$ and the membrane surface. Electrostatics mediated insertion has been observed to be an important mechanism for some of the pore-forming toxins like colicin E1. Electrostatic interactions have been shown to play important roles in the insertion of colicin E1 into the membrane and the membrane surface potential has been observed to present a tunable mechanism for toxin import (Heymann et al., 1996; Zakharov et al., 2002).

Since the protein is predominantly negatively charged and since there is a requirement for anionic lipids in the membrane, we also wanted to explore the possibility of divalent calcium playing a role by acting to bridge the two negative surfaces together and promote the interaction between them (Verdaguer et al., 1999). At pH 5.0, where we see around 70-80% protein bound to lipid vesicles, we wanted to test the effect of divalent calcium on binding. In the range we tested, divalent calcium ions did not seem to affect the interaction between the protein and the lipid vesicles indicating no role for Ca^{2+} ions in mediating the insertion of protein into the membrane milieu. Although there are no significant positively charged patches on the surface of Bcl-X_L to interact

electrostatically with the membrane surface (as seen from an electrostatic protein surface of Bcl-X_L), there might be specific titratable anionic groups on the surface which upon neutralization can give rise to significant positively charged patches on the surface. Since the interaction of Bcl-$X_L\Delta$TM with lipid vesicles is pH-dependent in the range between pH 5 and 7, we explored the possibility of specific ionizable residues, like histidines mediating the interaction. Bcl-$X_L\Delta$TM has four histidines, two in the globular part of the molecule (H113 and H177) and two in the unstructured loop region connecting helix 1 and helix 2 (Figure 4.11). Long-range HMQC NMR experiments indicated that at least 3 of the 4 histidines that were observed had a midpoint of titration above pH 7.0 indicating that the pKa's of histidines are well above the range required for them to play a role in the conformational transition from a soluble form to a lipid associated form. It is also interesting to note that although we observed the presence of a significant population of the dimer of Bcl-$X_L\Delta$TM formed in solution (up to 20%) at high protein concentrations, the dimerization was found not to be relevant to the membrane insertion process as both the monomer and dimer exhibited identical pH profiles for binding lipid vesicles.

Our results indicate that Bcl-X_L is able to adopt two structurally distinct and thermodynamically stable conformations in two different environments, one in solution and another inserted into the membrane. Electrostatics appears to be mediating a critical step in this transition. We have excluded the possible roles that the presence of Ca^{2+}, protonation of histidine sidechains or dimerization in solution could play in mediating the electrostatic interaction between Bcl-$X_L\Delta$TM and the lipid vesicles. A careful study of the molecular features of the electrostatic interactions would reveal insights into the soluble to membrane conformational change of Bcl-$X_L\Delta$TM.

References

Adams, J.M., and S. Cory. 1998. The Bcl-2 protein family: arbiters of cell survival. *Science* 281(5381):1322-1326.

Bachovchin, W.W. 1986. 15N NMR spectroscopy of hydrogen-bonding interactions in the active site of serine proteases: evidence for a moving histidine mechanism. *Biochemistry* 25(23):7751-7759.

Bendall, M.R., D.T. Pegg, and D.M. Doddrell. 1983. Pulse Sequences Utilizing the Correlated Motion of Coupled Heteronuclei in the Transverse Plane of the Doubly Rotating Frame. *Journal of Magnetic Resonance* 52(1):81-117.

Carrio, M.M., and A. Villaverde. 2001. Protein aggregation as bacterial inclusion bodies is reversible. *FEBS Lett* 489(1):29-33.

Carrio, M.M., and A. Villaverde. 2002. Construction and deconstruction of bacterial inclusion bodies. *J Biotechnol* 96(1):3-12.

Chipuk, J.E., T. Kuwana, L. Bouchier-Hayes, N.M. Droin, D.D. Newmeyer, M. Schuler, and D.R. Green. 2004. Direct activation of Bax by p53 mediates mitochondrial membrane permeabilization and apoptosis. *Science* 303(5660):1010-1014.

Delaglio, F., S. Grzesiek, G.W. Vuister, G. Zhu, J. Pfeifer, and A. Bax. 1995. NMRPipe: a multidimensional spectral processing system based on UNIX pipes. *J Biomol NMR* 6(3):277-293.

Garcia-Saez, A.J., I. Mingarro, E. Perez-Paya, and J. Salgado. 2004. Membrane-insertion fragments of Bcl-xL, Bax, and Bid. *Biochemistry* 43(34):10930-10943.

Gonzalez-Manas, J.M., J.H. Lakey, and F. Pattus. 1992. Brominated phospholipids as a tool for monitoring the membrane insertion of colicin A. *Biochemistry* 31(32):7294-7300.

Green, D.R., and J.C. Reed. 1998. Mitochondria and apoptosis. *Science* 281(5381):1309-1312.

Gross, A. 2001. BCL-2 proteins: regulators of the mitochondrial apoptotic program. *IUBMB Life* 52(3-5):231-236.

Hengartner, M.O. 2000. The biochemistry of apoptosis. *Nature* 407(6805):770-776.

Heymann, J.B., S.D. Zakharov, Y.L. Zhang, and W.A. Cramer. 1996. Characterization of electrostatic and nonelectrostatic components of protein--membrane binding interactions. *Biochemistry* 35(8):2717-2725.

Hsu, Y.T., K.G. Wolter, and R.J. Youle. 1997. Cytosol-to-membrane redistribution of Bax and Bcl-X(L) during apoptosis. *Proc Natl Acad Sci U S A* 94(8):3668-3672.

Johnson, B.A. 2004. Using NMRView to visualize and analyze the NMR spectra of macromolecules. *Methods Mol Biol* 278:313-352.

Johnson, B.A., and Blevins, R. A. 1994. NMRView: A computer program for the visualization and analysis of NMR data. *Journal of Biomolecular NMR* 4(603-615).

Kelekar, A., and C.B. Thompson. 1998. Bcl-2-family proteins: the role of the BH3 domain in apoptosis. *Trends Cell Biol* 8(8):324-330.

Kluck, R.M., M.D. Esposti, G. Perkins, C. Renken, T. Kuwana, E. Bossy-Wetzel, M. Goldberg, T. Allen, M.J. Barber, D.R. Green, and D.D. Newmeyer. 1999. The

pro-apoptotic proteins, Bid and Bax, cause a limited permeabilization of the mitochondrial outer membrane that is enhanced by cytosol. *J Cell Biol* 147(4):809-822.

Kuwana, T., and D.D. Newmeyer. 2003. Bcl-2-family proteins and the role of mitochondria in apoptosis. *Curr Opin Cell Biol* 15(6):691-699.

Lacy, D.B., and R.C. Stevens. 1998. Unraveling the structures and modes of action of bacterial toxins. *Curr Opin Struct Biol* 8(6):778-784.

Lakey, J.H., J.M. Gonzalez-Manas, F.G. van der Goot, and F. Pattus. 1992. The membrane insertion of colicins. *FEBS Lett* 307(1):26-29.

Lesieur, C., B. Vecsey-Semjen, L. Abrami, M. Fivaz, and F. Gisou van der Goot. 1997. Membrane insertion: The strategies of toxins (review). *Mol Membr Biol* 14(2):45-64.

Li, P., D. Nijhawan, I. Budihardjo, S.M. Srinivasula, M. Ahmad, E.S. Alnemri, and X. Wang. 1997. Cytochrome c and dATP-dependent formation of Apaf-1/caspase-9 complex initiates an apoptotic protease cascade. *Cell* 91(4):479-489.

Losonczi, J.A., E.T. Olejniczak, S.F. Betz, J.E. Harlan, J. Mack, and S.W. Fesik. 2000. NMR studies of the anti-apoptotic protein Bcl-xL in micelles. *Biochemistry* 39(36):11024-11033.

Lucken-Ardjomande, S., and J.C. Martinou. 2005. Regulation of Bcl-2 proteins and of the permeability of the outer mitochondrial membrane. *C R Biol* 328(7):616-631.

MacDonald, R.C., R.I. MacDonald, B.P. Menco, K. Takeshita, N.K. Subbarao, and L.R. Hu. 1991. Small-volume extrusion apparatus for preparation of large, unilamellar vesicles. *Biochim Biophys Acta* 1061(2):297-303.

Marley, J., M. Lu, and C. Bracken. 2001. A method for efficient isotopic labeling of recombinant proteins. *J Biomol NMR* 20(1):71-75.

McLaughlin, S. 1989. The electrostatic properties of membranes. *Annu Rev Biophys Biophys Chem* 18:113-136.

Minn, A.J., C.S. Kettlun, H. Liang, A. Kelekar, M.G. Vander Heiden, B.S. Chang, S.W. Fesik, M. Fill, and C.B. Thompson. 1999. Bcl-xL regulates apoptosis by heterodimerization-dependent and -independent mechanisms. *Embo J* 18(3):632-643.

Minn, A.J., P. Velez, S.L. Schendel, H. Liang, S.W. Muchmore, S.W. Fesik, M. Fill, and C.B. Thompson. 1997. Bcl-x(L) forms an ion channel in synthetic lipid membranes. *Nature* 385(6614):353-357.

Muchmore, S.W., M. Sattler, H. Liang, R.P. Meadows, J.E. Harlan, H.S. Yoon, D. Nettesheim, B.S. Chang, C.B. Thompson, S.L. Wong, S.L. Ng, and S.W. Fesik. 1996. X-ray and NMR structure of human Bcl-xL, an inhibitor of programmed cell death. *Nature* 381(6580):335-341.

Perrin, D.D. 1963. Buffers of Low Ionic Strength for Spectrophotometric Pk Determinations. *Australian Journal of Chemistry* 16(4):572-&.

Rathmell, J.C., and C.B. Thompson. 2002. Pathways of apoptosis in lymphocyte development, homeostasis, and disease. *Cell* 109 Suppl:S97-107.

Reed, J.C. 1997. Double identity for proteins of the Bcl-2 family. *Nature* 387(6635):773-776.

Sambrook, J., and Russell, D.W. 2001. Molecular Cloning: A Laboratory Manual. Cold Spring Harbor Laboratory Press.

Schendel, S.L., M. Montal, and J.C. Reed. 1998. Bcl-2 family proteins as ion-channels. *Cell Death Differ* 5(5):372-380.

Schendel, S.L., Z. Xie, M.O. Montal, S. Matsuyama, M. Montal, and J.C. Reed. 1997. Channel formation by antiapoptotic protein Bcl-2. *Proc Natl Acad Sci U S A* 94(10):5113-5118.

Scorrano, L., and S.J. Korsmeyer. 2003. Mechanisms of cytochrome c release by proapoptotic BCL-2 family members. *Biochem Biophys Res Commun* 304(3):437-444.

Shimizu, S., A. Konishi, T. Kodama, and Y. Tsujimoto. 2000. BH4 domain of antiapoptotic Bcl-2 family members closes voltage-dependent anion channel and inhibits apoptotic mitochondrial changes and cell death. *Proc Natl Acad Sci U S A* 97(7):3100-3105.

van der Goot, F.G., J.M. Gonzalez-Manas, J.H. Lakey, and F. Pattus. 1991. A 'molten-globule' membrane-insertion intermediate of the pore-forming domain of colicin A. *Nature* 354(6352):408-410.

Van Dijk, A.A., R.M. Scheek, K. Dijkstra, G.K. Wolters, and G.T. Robillard. 1992. Characterization of the protonation and hydrogen bonding state of the histidine residues in IIAmtl, a domain of the phosphoenolpyruvate-dependent mannitol-specific transport protein. *Biochemistry* 31(37):9063-9072.

Vander Heiden, M.G., N.S. Chandel, E.K. Williamson, P.T. Schumacker, and C.B. Thompson. 1997. Bcl-xL regulates the membrane potential and volume homeostasis of mitochondria. *Cell* 91(5):627-637.

Vander Heiden, M.G., X.X. Li, E. Gottleib, R.B. Hill, C.B. Thompson, and M. Colombini. 2001. Bcl-xL promotes the open configuration of the voltage-dependent anion channel and metabolite passage through the outer mitochondrial membrane. *J Biol Chem* 276(22):19414-19419.

Verdaguer, N., S. Corbalan-Garcia, W.F. Ochoa, I. Fita, and J.C. Gomez-Fernandez. 1999. Ca(2+) bridges the C2 membrane-binding domain of protein kinase Calpha directly to phosphatidylserine. *Embo J* 18(22):6329-6338.

Wimley, W.C., K. Hristova, A.S. Ladokhin, L. Silvestro, P.H. Axelsen, and S.H. White. 1998. Folding of beta-sheet membrane proteins: a hydrophobic hexapeptide model. *J Mol Biol* 277(5):1091-1110.

Zakharov, S.D., T.I. Rokitskaya, V.L. Shapovalov, Y.N. Antonenko, and W.A. Cramer. 2002. Tuning the membrane surface potential for efficient toxin import. *Proc Natl Acad Sci U S A* 99(13):8654-8659.

Chapter 5

Tuning the pH-dependence of the solution-to-membrane conformational change of Bcl-X_LΔTM using electrostatic mutants

Summary

Bcl-X_L undergoes a dramatic conformational change from the solution form to the membrane inserted form. This conformational change is not mediated through an acid-induced destabilization of the solution form. Rather, it is aided by electrostatic interactions between the protein and the membrane surface (Chapter 2, 4). However, we lack a complete understanding of the details of the electrostatic interactions and how these drive the insertion into the membrane. To test our current hypothesis that electrostatic interactions provide the initial thrust for the insertion of the hydrophobic helical hairpin into the membrane, we designed mutants of Bcl-X_L with altered electrostatic surface profiles and tested the pH-dependence of their binding to lipid vesicles. One mutant, PM (E153Q/D156N), bound to lipid vesicles with a significantly different pH profile relative to the wild-type protein. This result was also corroborated by the alteration in the membrane insertion properties, as measured using the monolayer insertion assay. The ability of PM to be able to inhibit dextran release induced by Bax by 200% relative to wildtype Bcl-X_L, suggests that the alteration in membrane activity would be translated into potential biological activity in vivo. All these results confirm the importance of electrostatic interactions between the protein and the membrane and its role in the solution-to-membrane conformational change. Using these data, we have formulated a thermodynamic model to estimate the thermodynamic parameters that illuminate the thermodynamic mechanism of the solution-to-membrane conformational change. We also found that the alteration in membrane insertion properties translated into an enhanced inhibition of Bax induced dextran release from lipid vesicles. These

findings strongly support the relevance of the membrane form in the biological function of Bcl-X_L in cells.

Introduction

The solution to membrane conformational change

The change in the localization of Bcl-X_L during apoptosis suggests that the solution to membrane conformational change is essential for the regulation of its biological activity. In previous chapters, we demonstrated that this conformational change requires anionic lipids and acidic conditions (Chapter 4), yet the acidic conditions did not affect the thermodynamic stability or the structure of Bcl-X_L in solution (Chapter 2). In this chapter, we investigate in detail the electrostatic nature of this conformational change.

For Bcl-X_L, the absolute requirement *in vitro* for negatively charged lipids for vesicle binding and *in vivo*, the targeting to the negatively charged mitochondrial outer membrane, suggested that the membrane surface charge plays a key role in mediating this interaction between Bcl-X_L and the mitochondrial outer membrane. In our *in vitro* system, we mimic the mitochondrial membrane with lipid vesicles composed of 60% DOPC, a zwitterionic phospholipid and 40% DOPG, an anionic phospholipid. Upon a reduction in pH, protonation of ionizable groups on the protein as well as on the membrane surface is possible depending on the pKa values of the various titratable groups on the surface of Bcl-X_L as well as that on the membrane. Excellent work on the electrostatics of the membrane surfaces aids in the prediction of the altered pKa values of ionizable groups at the membrane surface, especially in cases where the membrane is composed of anionic lipids giving rise to a net negative charge on the membrane surface (Cevc and Marsh, 1987). The following sections discuss the electrostatics of the

membrane and protein surfaces to provide a basis for understanding of the electrostatic interactions between Bcl-$X_L\Delta$TM and the membrane.

Electrostatics of the membrane surface

The electrostatic nature of biological membrane surfaces have been exploited by proteins which insert into membranes using electrostatic interactions. The attraction of charged species in the solution towards the charged membranes is predicted very well by "smeared charge" theories like the Gouy-Chapman theory, which assume that the membrane surface is a diffuse double layer (Chapman, 1913; Gouy, 1910; McLaughlin, 1989). The "smeared-charge" theories as opposed to "discrete-charge" theories quantify surface potential not in terms of discrete charged groups, but as a potential that is smeared on the membrane surface. The Gouy-Chapman theory predicts the surface potential and attraction of monovalent ions and some divalent ions to a charged membrane surface. However, the theory breaks down when applied to multivalent charged species like proteins and peptides and it cannot give accurate predictions for electrostatic attractions between protein and membrane. The Gouy-Chapman theory assumes the charge on the membrane surface as smeared uniformly over a plane, the bulk aqueous phase as of uniform dielectric constant, the charges in the aqueous phase as point charges and describes the membrane electrostatic potential as,

$$\psi(0) = \sigma / \varepsilon_a \varepsilon_0 \kappa \tag{5.1}$$

where σ is the average surface charge density, ε_a is the dielectric constant of the aqueous phase, ε_0 is the permittivity of free space and κ^{-1} is the Debye length, which defines the scale over which a charge carrier can screen out electric fields.

This potential falls off with the distance *x* from the membrane in a mono-exponential fashion and is given by, $\psi(x) = \psi(0) \bullet e^{-\kappa x}$

The electrostatic potential attracts counter ions from the bulk aqueous phase and the concentration c(0) of the ions near the surface of the membrane is described by the following equation,

$$c(0) = c \bullet e^{(-ze\psi(0)/kT)} \cong A^2\sigma^2 \tag{5.2}$$

where c is the bulk ion concentration, z is the valence, e is the magnitude of the electronic charge and A is $\frac{1}{\sqrt{8\varepsilon_a\varepsilon_0 kT}}$. This equation states that the concentration of ions near a charged membrane surface is determined by the Poisson description of the electrostatic attraction of ions to a charged surface and the Boltzmann description of the statistical tendency of the ions to move away from the region of high ion concentration (McLaughlin, 1989). This equation accurately predicts the concentration of monovalent ions like Li^+, Na^+, K^+, Cs^+ etc. and even some divalent ions like Mg^{2+} and Ca^{2+} near the membrane surface (Eisenberg et al., 1979; Mclaughlin, 1983; McLaughlin, 1989; Mclaughlin and Eisenberg, 1979).

Since the association of Bcl-X_L with lipid vesicles has been observed to require pH ~5.0 and anionic lipids *in vitro* and since the cytosol never reaches a pH ~ 5.0, it has been argued that the negative charges on the membrane surface reduce the pH near the membrane surface to ~ pH 5.0, mediating the solution-to-membrane conformational change. The reduced pH near the membrane surface has been explained as the trigger for conformational change in pH-dependent solution-to-membrane conformational change of

colicin A (van der Goot et al., 1991). Although it has been argued that the increase in cation concentration near a negatively charged membrane surface as predicted using the Gouy-Chapman theory applies as well to protons resulting in a decrease in pH (up to 2.7 pH units near a 100% DOPG membrane as predicted by Gouy-Chapman theory), this has been countered by the observation that the proton mobility in aqueous solutions is through the hydrogen bonded structure of water (Agmon, 1995a; Agmon, 1995b). This eliminates the concentration of protons near the membrane surface in response to the electrostatic membrane surface potential and thereby the decrease in pH. Studies monitoring TNS binding to membrane surfaces with varying charge densities estimate a decrease in pH near the membrane surface up to 1.6 pH units near a 100% DOPG membrane. However, the binding of the dye and hence, the increase in the fluorescence signal that is monitored are dependent upon membrane surface potential and not pH (Eisenberg et al., 1979). The alteration in TNS and binding should only be interpreted as a change in the membrane surface potential and not pH.

Although there is no decrease in pH near a negatively charged membrane surface, the pKa values of ionizable groups are altered due to dehydration and electrostatics near the membrane surface. The pKa of an ionizable group near the membrane surface can be described using the following equation (Cevc and Marsh, 1987):

$$\begin{aligned} p\mathrm{K}_\mathrm{a} &= p\mathrm{K}_\mathrm{a}^0 + \Delta p\mathrm{K}_\mathrm{h} + \Delta p\mathrm{K}_\mathrm{el} \\ &= p\mathrm{K}_\mathrm{a}^0 + \Delta p\mathrm{K}_\mathrm{h} + \frac{e\psi}{2.3kT} \end{aligned} \tag{5.3}$$

where pK_a^0 is the intrinsic pKa of the ionizable group, ΔpK_h is the alteration due to dehydration near the membrane surface and ΔpK_{el} is the alteration in the pKa due to the

electrostatic surface potential of the membrane surface. The pKa values of the lipid headgroups determined using equation (3) are 2.6 for phosphatidyl serine (PS) and 2.9 for phosphatidyl glycerol (PG) as estimated in a 0.1M monovalent electrolyte solution (Cevc and Marsh, 1987). Thus at physiological salt concentrations, around 0.15M monovalent salts, the above values might be the actual pKa values suggesting that either with PS or with PG, there might not be a significant protonation in the pH range in which the binding of Bcl-$X_L\Delta$TM to the membrane is modulated (i.e., pH 4.0 – 7.0). Thus the two main conclusions from the electrostatics of membrane surfaces are:

(i) the pH near the membrane surface is not decreased due to the negative surface electrostatic potential on the membrane.

(ii) the lipid headgroups do not undergo a protonation/deprotonation equilibrium in the range where the binding of Bcl-$X_L\Delta$TM to lipid vesicles is modulated.

Electrostatics of the protein surface

The lipid headgroups do not undergo protonation on the surface of the membrane at pH 5.0 suggesting that the electrostatic attraction between Bcl-$X_L\Delta$TM and the membrane is solely modulated by changes in the electrostatic profile of the protein surface. Bcl-$X_L\Delta$TM has 31 acidic residues (Glu and Asp) and 20 basic residues (Arg and Lys). Of these, the unstructured loop has 11 acidic residues and 2 basic residues while the residues 84-209 which form the central part of the molecule (minus helix 1) contain 18 acidic residues as opposed to 12 basic residues. Most of the acidic residues are evenly distributed across the surface of the molecule creating an overwhelmingly negatively charged surface at neutral pH (Figure 5.1).

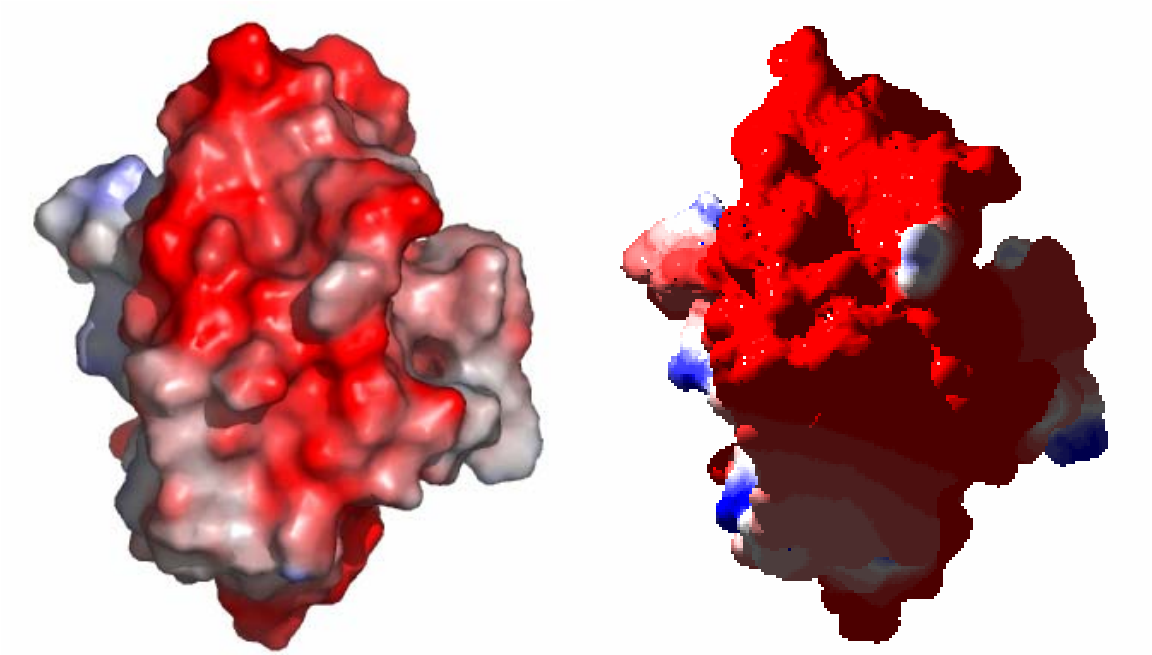

Figure 5.1 (left) Structure of Bcl-$X_L\Delta$TM with an electrostatic surface generated using PyMol. The surface is calculated based on the charges on the protein surface in vacuum. (right) Structure of Bcl-$X_L\Delta$TM with an electrostatic surface at pH 7.0 in solution calculated using a coulombic potential using Swiss-PDB viewer.

The pKa values of exposed Asp and Glu side chains in proteins are estimated to be 3.9 and 4.3 respectively. However, when they are near the surface of a charged membrane, these values are altered due to two factors. First, the proximity to a highly charged membrane surface would alter the pKa value. Secondly, the dehydrated environment close to the membrane surface disfavors ionization thereby altering the pKa value. These altered pKa values could result in the protonation of the Glu and Asp residues at higher pH values changing the electrostatic surface of the protein to interact with the membrane. Such elevated pKa values could profoundly affect the overall surface electrostatic profile on Bcl-$X_L\Delta$TM between pH 7.4 and pH 5.0 where we observe a modulation of the vesicle binding ability. Therefore to test the hypothesis that the altered pKa values of ionizable groups on the surface of Bcl-$X_L\Delta$TM are important for binding to lipid vesicles, we designed mutants of Bcl-$X_L\Delta$TM that have altered electrostatic surface profiles.

To design these mutants, we first hypothesized that the initial point of contact of the protein with the membrane surface would involve the tip of helical hairpin (α5, α6). This hypothesis arises from two important observations: (i) in the structurally similar colicins and the T-domain of diphtheria toxin, insertion is thought to be mediated by the initial insertion of the commonly conserved hydrophobic helical hairpin motif into the membrane (Lakey et al., 1992; Lesieur et al., 1997; Zakharov and Cramer, 2002b) and (ii) it was noted that helix 5 and helix 6 were inserted into the membrane in NMR studies of Bcl-$X_L\Delta$TM in micelles (Losonczi et al., 2000). We therefore assumed that the partitioning of the hairpin into the membrane might be a critical step of this solution-to-membrane conformational change. In this scenario, the electrostatic interaction between the tip of the hairpin and the membrane surface would likely be the first productive interaction and therefore might be essential in driving the interaction between the protein and the membrane.

To understand the contributions of various electrostatic residues to this pH-dependent insertion process, we designed mutants of Bcl-$X_L\Delta$TM and evaluated the pH-dependence of their binding to lipid vesicles using the vesicle sedimentation assay.

Materials and Methods

Mutagenesis, protein expression and purification

Site directed mutagenesis was carried out on the wild-type sequence of Bcl-$X_L\Delta TM$ using the Quikchange mutagenesis kit (Stratagene). The mutant and the wildtype plasmid were transformed into E.coli Tuner DE3 cells which contain plasmids expressing rare tRNAs to help with overexpression of mammalian genes in recombinant E.coli. The constructs, the wild-type Bcl-$X_L\Delta TM$ sequence and the mutants all lack the C-terminal hydrophobic segment (residues 210-233). All these proteins were expressed and purified as described previously in Chapter 3. The purity was evaluated using Coomassie stained SDS-PAGE gel electrophoresis. The proteins were stored at 4 °C in the TEND buffer (20 mM Tris, pH 8.0 containing 1 mM EDTA, 500 mM NaCl and 1 mM DTT) until further use.

MPEx analysis

MPEx analysis (Steve White, UCIrvine) was used to predict the regions of Bcl-$X_L\Delta TM$ that would partition favorably into the membrane under various conditions (Jaysinghe et al., 2000). This program predicts the ability of protein sequences to partition into lipid bilayers or the interfacial region using parameters extracted from octanol-water partitioning studies of peptide substrates. The details of this parameterization are explained elsewhere (White and Wimley, 1999; Wimley et al., 1996; Wimley and White, 1996).

Assuming that the length of the helix that transverses a lipid bilayer is 19 to 22 residues, we set the window length in MPEx at the extremes, 19 and 22. We then compared the ability of the wild-type sequence and various mutants (generated *in silico*) to favorably partition into membranes (using the octanol-water partitioning data). The results of this analysis are shown in Table 5.1 and 5.2.

Lipid vesicle sedimentation assay

The details of the lipid vesicle binding assay have been discussed earlier in Chapter 4. The protein concentration used was 10 μM and the lipid concentration was kept at 2.5 mM. Constant ionic strength buffers were used (I = 0.05) and NaCl was added to a final [NaCl] of 150 mM (Perrin, 1963). The lipid composition was kept at a 60:40 ratio of DOPC : DOPG with 0.25% lissamine rhodamine B labeled DOPE added to visualize the lipid fraction. The concentration of the protein in the supernatant after centrifugation was determined using Bradford Assay in a microplate format. The standard curves were generated during each experiment in triplicate using the respective proteins, i.e., the wild-type standard for wildtype data and the K157A standard for K157A binding data. The standard curves were analyzed for linearity and only the linear regions of the curve were used. This ensures an accurate description of the binding profile.

To test for reversibility, Bcl-X_LΔTM was incubated with lipid vesicles at pH 4.0 overnight. The sample was then split into two equal parts, one that was maintained at pH 4.0 while the other was titrated up to pH 7.0 with the addition of small amounts of 0.1 N

sodium hydroxide. Both the samples were then subjected to centrifugation after which the supernatant was removed and assayed for total protein using the Bradford assay.

Thermodynamic model

As an initial step towards a thorough understanding of the solution to membrane conformational change, a simple thermodynamic model was developed coupling the protonation of certain charged residues to a partitioning of the protein into the membrane. A thermodynamic cycle is assumed wherein the two steps of protonation in the membrane and partitioning of the deprotonated form into the membrane are assumed to be highly unfavorable energetically and hence do not contribute to the overall reaction (Figure 5.2).

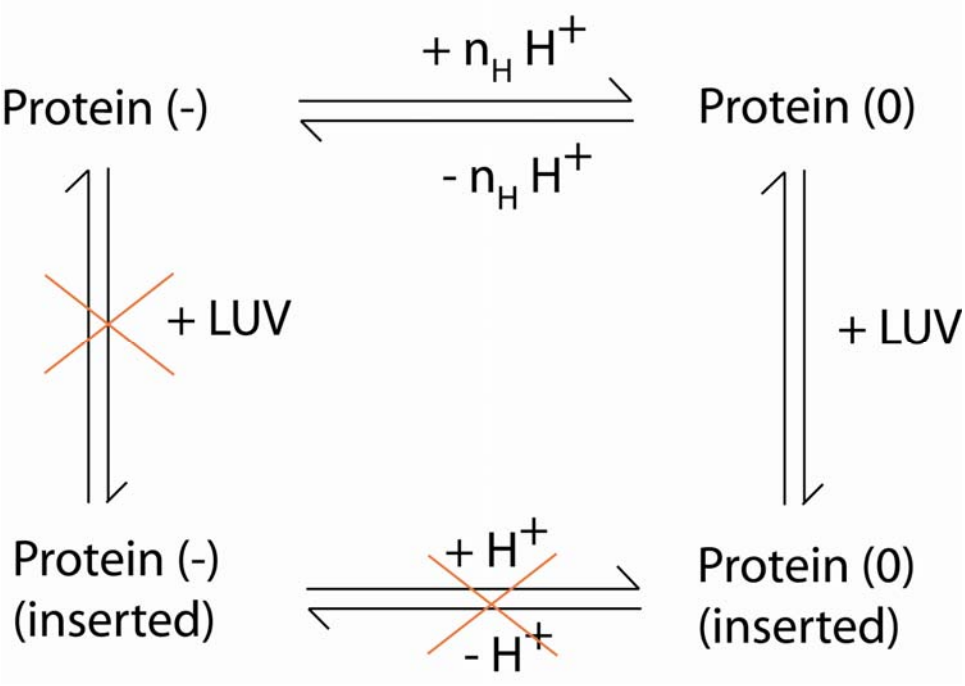

Figure 5.2 A simple thermodynamic cycle for the conformational change of Bcl-$X_L\Delta$TM from solution to the membrane.

This leads to the development of the coupled equilibrium from which the percentage of protein associating with the lipid vesicles could be calculated as described below. The different populations of Bcl-$X_L\Delta TM$, the protein in this system are represented as follows:

(i) P_{deprot} – is the protein that is completely deprotonated in the critical residues, the protonation of which defines the pH-profile of insertion.

(ii) P_{prot} – is the completely protonated version of the protein.

(iii) P_{bound} – corresponds to the population of the protein that is bound to the lipid vesicles.

The other components of the system include L and W which refer to the lipids and water (aqueous environment) respectively. The parameters that are estimated by the fitting process are n_H, pKa and Kx. n_H is the number of protonation sites on the protein the protonation of which defines the pH profile. pKa is a measure of the protonation / deprotonation equilibrium at those sites and Kx is the partition coefficient for the protonated Bcl-$X_L\Delta TM$ to partition into the lipid vesicles.

The key assumptions that are being made are:

(i) that the protonation process is cooperative and there is no significant contribution from the partially protonated species to the thermodynamic cycle.

(ii) There is no deprotonation of the protein once it is bound to the lipid vesicles.

(iii) The deprotonated form does not bind to the lipid vesicles.

(iv) The only form that can bind the lipid vesicles is the completely protonated form.

(v) The protonation sites are equal and independent.

(vi) There is no significant contribution from the protonation/deprotonation equilibria of the ionizable lipid headgroups in this pH range (pH 3-8).

These considerations gave rise to the following description:

We know,

$$pH = pK_a + \log \frac{[P_{deprot}]}{[P_{prot}]} \qquad (5.4)$$

$$[P_{total}] = [P_{deprot}] + [P_{prot}] + [P_{bound}] \qquad (5.5)$$

$$K_X = \frac{[P_{bound}] / [L]}{[P_{prot}] / [W]} \qquad (5.6)$$

For n_H sites of protonation,

$$\log \frac{[P_{deprot}]}{[P_{prot}]} = n_H \bullet (pH - pK_a)$$

$$\frac{[P_{deprot}]}{[P_{prot}]} = 10^{n_H \bullet \Delta} \text{ where } \Delta = (pH - pK_a) \qquad (5.7)$$

Rearranging, we have

$$F_{bound} = \frac{[P_{bound}]}{[P_{total}]} = \frac{1}{1 + \frac{[W]\, g\, (1 + 10^{n_H g \Delta})}{K_X\, g\, [L]}} \qquad (5.8)$$

The fraction bound as indicated by the ratio of protein bound to lipid vesicles to the total protein as a function of pH is simulated in the following figures (Figure 5.3). For a n_H of 1, the pKa was assumed to be 4.5 which is reasonable for an ionizable group like a Glu side chain. The Kx is assumed to be 10^6 and the fraction bound is simulated as a function of pH. The midpoint of the titration profile was around pH 6.0 (Figure 5.3a). Increasing Kx 10-fold to 10^7 (Figure 5.3b) or increasing the pKa by one unit to 5.5 (Figure 5.3c) resulted in identical profiles and midpoints of the titration profile shifted up to 7.0. These simulations demonstrate that the parameters pKa and Kx are interconnected and a variation of Kx by ten fold corresponds to an increase in pKa by 1

as illustrated (Figure 5.3). Since the partition coefficient Kx and the data from the vesicle sedimentation assay both describe the population of protein that is bound as well as inserted into the lipid vesicles, the data obtained from the vesicle sedimentation assay is fit to this equation in order to estimate reasonable values for Kx, pKa and n_H.

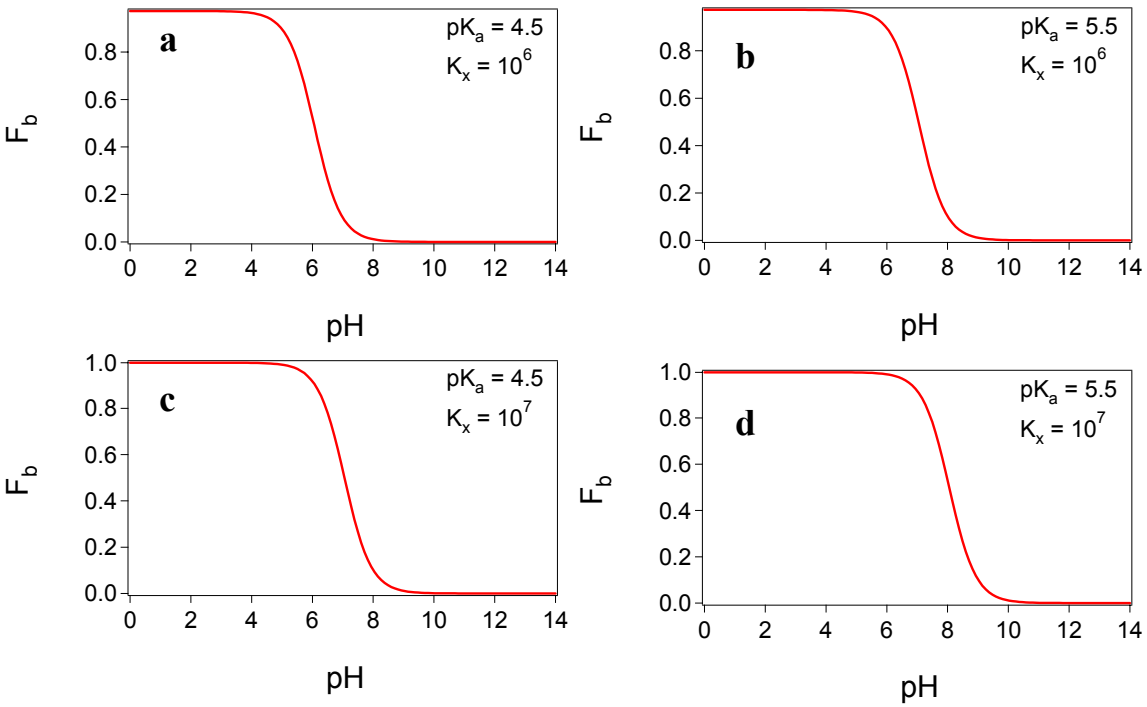

Figure 5.3 Simulations using arbitrary values of Kx and pKa and varying them indicate the relationship between the two parameters Kx and pKa, i.e., varying pKa by 1 (a to b) is equal to increasing Kx by 10-fold (a to c).

Since we obtained a value around 2 for n_H, we refined this model further by assuming two unequal but independent protonation sites (Figure 5.4). The development of this model is shown below with pK_1 and pK_2 representing the pKa values of the two ionizable groups and Kx representing the partition coefficient of the protein into the membrane.

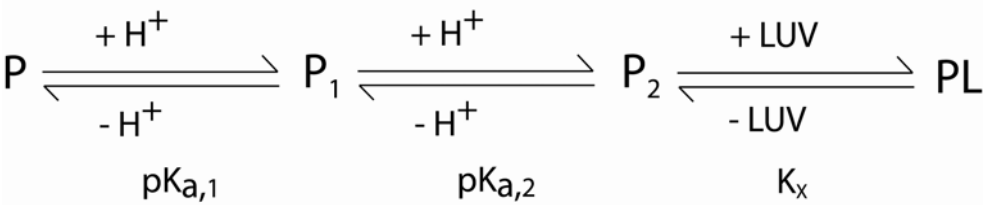

Figure 5.4 Thermodynamic model for the solution to membrane conformational change refined to include two unequal protonation sites.

This model improves upon the previous one by assuming unequal protonation sites and is based on fixing the n_H as 2. As shown in Figure 5.4, this model assumes four different populations of Bcl-X_LΔTM, P (deprotonated), P1 (protonated at 1 site), P2 (protonated at 2 sites) and PL (bound to lipids). The further assumptions that this model makes are:

(i) the protonation is sequential in linear order and

(ii) only P2 is competent to partition into membranes to any significant extent. This model still assumes a partitioning based equilibrium of insertion into the membrane which does not account for explicit electrostatic interactions between Bcl-X_LΔTM and the membrane surface. The development of this model is as detailed in the following section.

$$K_1 = \frac{[P]\bullet[H^+]}{[P_1]}; K_2 = \frac{[P1]\bullet[H^+]}{[P_2]}; K_X = \frac{[PL]\bullet[W]}{[P_2]\bullet[L]}$$

$$[P_{total}] = [P] + [P_1] + [P_2] + [PL]$$

$$[P_{total}] = [P] + \frac{[P]\bullet[H^+]}{K_1} + \frac{[P1]\bullet[H^+]}{K_2} + \frac{[P_2]\bullet K_X \bullet[L]}{[W]}$$

$$[P_{total}] = [P] + \frac{[P]\bullet[H^+]}{K_1} + \frac{[P]\bullet[H^+]^2}{K_1K_2} + \frac{K_X \bullet[L]}{[W]}\bullet\frac{[P]\bullet[H^+]^2}{K_1K_2}$$

The fraction bound, F_b is calculated to be

$$F_b = \frac{[PL]}{[P_{total}]} = \frac{\frac{K_X \bullet[L]}{[W]}\bullet\frac{[P]\bullet[H^+]^2}{K_1K_2}}{[P] + \frac{[P]\bullet[H^+]}{K_1} + \frac{[P]\bullet[H^+]^2}{K_1K_2} + \frac{K_X \bullet[L]}{[W]}\bullet\frac{[P]\bullet[H^+]^2}{K_1K_2}}$$

$$F_b = \frac{\frac{K_X \bullet[L]}{[W]}\bullet 10^{(pK_1+pK_2-2pH)}}{[1+10^{(pK_1-pH)} + 10^{(pK_1+pK_2-2pH)} + \frac{K_X \bullet[L]}{[W]}\bullet 10^{(pK_1+pK_2-2pH)}]}$$

Fitting the data sets of the fraction of protein bound to lipid vesicles, F_b vs. pH to the equation above helps estimate the parameters pK_1, pK_2 and Kx. These parameters are inter-related and therefore to obtain an accurate description of the system, a priori knowledge of at least one parameter is required. We believe that our collaboration with Dr. Diana Murray's group at the Cornell University medical center will help us obtain a reasonable estimation of the pK_1 and pK_2 by the application of non-linear Poisson Boltzmann methods thereby aiding a precise estimation of Kx.

NMR spectroscopy

^{15}N labeled Bcl-$X_L\Delta$TM was prepared as described in Chapter 4. 60 μM of the protein in 20 mM sodium phosphate at pH 7.25 was incubated with lipid vesicles (DOPC:DOPG – 60:40) overnight at room temperature. The lipid concentration was 12 mM resulting in a protein : lipid (P : L) ratio of 1:200. ^{15}N-^{1}H HSQC experiments were

carried out on a Bruker AVANCE 600 MHz spectrometer equipped with a cryoprobe. 1278 x 200 points were collected with sweep widths of 10000 Hz and 1520 Hz in ^{1}H and ^{15}N respectively. 16 transients were averaged for each data point with the ^{15}N carrier frequency at 119.5 ppm. The sample was titrated down to pH 4.65 by the addition of small amounts of 0.1 N hydrochloric acid. A HSQC spectrum was collected at this pH and then the sample was titrated back up to pH 7.4 by the addition of small amounts of 0.1 N sodium hydroxide. Another HSQC spectrum was collected at this pH and the three spectra were compared.

Results

Structural information in conjunction with *in silico* experiments suggest mutations

To evaluate the role of electrostatics in the pH dependent conformational change of Bcl-$X_L\Delta$TM, we designed mutants that would alter the electrostatic surface potential of Bcl-$X_L\Delta$TM without affecting its ability to partition into the membrane. By removing the contribution towards partitioning, we would explicitly test the roles of charged residues in mediating the electrostatic interaction between Bcl-$X_L\Delta$TM and the membrane. The choice of charged residues to mutate was based on the results of the Membrane Protein Explorer (MPEx) software program (Jaysinghe et al., 2000). This program can predict the partitioning of the different parts of a protein into the membrane bilayer based on amino acid sequence considerations. This software program is based on octanol/water partition coefficient data obtained using model peptides.

According to MPEx, the wild-type protein is able to partition helix 5 (forms the hydrophobic helical hairpin along with helix 6) and the C-terminal TM segment into the membrane. Biochemical and structural studies have suggested that in the membrane inserted form, helices 1, 5, 6 and the C-terminal TM helix are inserted into the membrane (Garcia-Saez et al., 2004; Losonczi et al., 2000). These observations, in conjunction with the bacterial toxin-derived concept of a hydrophobic helical hairpin that mediates insertion, prompted us to investigate the potential electrostatic interactions between the tip of the hairpin and the membrane surface (Lakey et al., 1992; Lesieur et al., 1997; Zakharov and Cramer, 2002b). The MPEx analysis was carried out using window lengths of 19 and 22 residues, with 19 and 22 residues representing the short and long

extremes of helix lengths spanning the membrane bilayer. The results from the MPEx analysis are shown in Tables 5.1 and 5.2. It shows a list of mutations that might / might not affect the ability of different regions of the protein to insert into the membrane.

Table 5.1 MPEx analysis on Bcl-X_L using a window length of 19 residues and predicting insertion based on the octanol-water partition coefficients.

Bcl-X_L mutant	Does α5 insert into the membrane?	Does α6 insert into the membrane?
Wild-type	**Yes**	**No**
D133N	Yes	No
E153Q	Yes	No
D156N	Yes	No
K157A	**Yes**	**No**
E158Q	Yes	No
D176N	Yes	Yes
E179Q	Yes	No
E184Q	Yes	No
E153Q/D156N	**Yes**	**No**
E153Q/D156N/E158Q	Yes	No
E153Q/D156N/K157A	Yes	No
E158Q/K157A	Yes	Yes
E153Q/D156N/E158Q/K157A	Yes	Yes

Table 5.2 MPEx analysis on Bcl-X_L using a window length of 22 residues and predicting insertion based on the octanol-water partition coefficients.

Bcl-X_L mutant	Does α5 insert into the membrane?	Does α6 insert into the membrane?
Wild-type	**No**	**No**
D133N	Yes	No
E153Q	Yes	No
D156N	No	No
K157A	**No**	**No**
E158Q	No	No
D176N	No	Yes
E179Q	No	Yes
E184Q	No	Yes
E153Q/D156N	**Yes**	**No**
E153Q/D156N/E158Q	Yes	No
E153Q/D156N/K157A	Yes	No
E158Q/K157A	No	Yes
E153Q/D156N/E158Q/K157A	Yes	Yes

Helix 5 partitions into membranes favorably as demonstrated by the NMR studies of Bcl-X_L in micelles and peptide insertion studies using a glycosylation mapping assay (Garcia-Saez et al., 2004; Losonczi et al., 2000). In order to explicitly test for the role of electrostatic interactions we decided to focus only on changes that did not affect the membrane partitioning character of the other part of the hydrophobic helical hairpin (helix 6) into the membrane. According to our working model, the insertion of helix 6 could provide the electrostatic switch for regulating the solution-to-membrane conformational change of Bcl-$X_L\Delta$TM. This electrostatic switch could be described as an electrostatic attraction between the net positively charged tip of the hairpin and the net negatively charged membrane surface at pH 5 or lower. The pH-dependence arises from the protonation of the Asp and Glu residues leaving a net positive charge on the protein from K157. The tip of the hairpin contains four charged residues, three negatively charged residues, E153, D156, E158 and the positively charged residue, K157. Mutation of E158 appears to alter the ability of helix 6 to partition into the membrane (Table 5.2). Hence, we focused on the other residues in the hydrophobic helical hairpin, E153, D156 and K157. From the tables above, we observe that K157A and E153Q/D156N mutations do not alter the ability of helix 6 to partition into the bilayer (predicted), giving us a system where partitioning of helix 6 is not affected while the charge properties are affected to perturb electrostatics of interaction between protein and lipids.

To test the hypothesis of an electrostatically driven solution-to-membrane conformational change of Bcl-$X_L\Delta$TM, we specifically created two mutants, (i) a positive mutant PM (net charge positive relative to wild-type) replacing the negative charged residues with isosteric uncharged ones, E153Q/D156N, which is expected to be

able to bind the membrane at higher pH values relative to the wild-type and (ii) a negative mutant NM (net charge negative relative to wild-type), replacing the positively charged lysine with the non-polar alanine, K157A, which is expected to display lesser binding to lipid vesicles relative to wild-type Bcl-X_LΔTM. The structure of Bcl-X_LΔTM with these residues highlighted is shown in Figures 5.5.

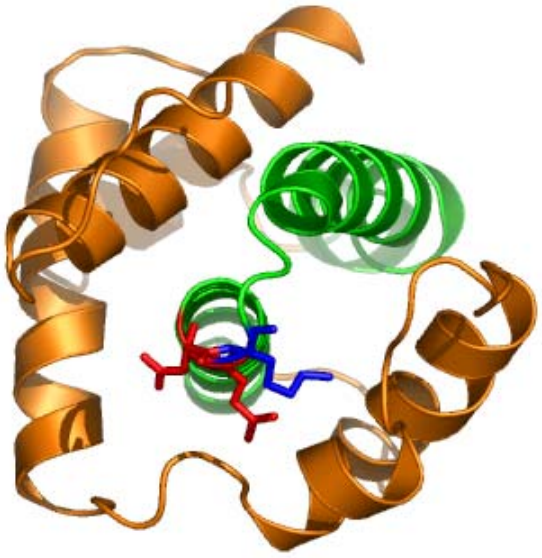

Figure 5.5 Crystal structure of Bcl-X_LΔTM looking at the tip of the hydrophobic helical hairpin highlighted in green. The residues E153 and D156 are shown in red. The residue K157 is highlighted in blue.

Mutants suggest electrostatic interactions playing a key role in insertion

Wild-type and mutant proteins were tested for their pH-dependent binding to lipid vesicles using a vesicle sedimentation assay. Contrary to our expectations, NM displayed an increase in binding to lipid vesicles relative to wild-type Bcl-X_LΔTM at pH < 6. However, the other mutant, PM bound better to lipid vesicles even at higher pH's relative to the wild-type as expected, although the differences were small. We also observed that PM bound to lipid vesicles significantly even at neutral pH conditions (Figure 5.6).

The alteration in the pH dependence of lipid vesicle binding of PM due to a change in the electrostatic profile of Bcl-X_LΔTM suggests the presence of electrostatic interactions between the tip of the hairpin and the membrane. However, the slope of the

pH-dependence is similar for both wild-type and the PM as observed from Figure 5.6. This suggests that the protonation of E153 and D156 do not play a direct role in regulating the pH-dependent solution-to-membrane conformational change. These observations are in support of a model describing electrostatic attraction between the tip of the hairpin and the membrane surface with the electrostatic character of the protein modulated by the changes in bulk pH. In an effort to better understand the system, we proceeded to develop a thermodynamic model that would better describe the data and help with a physical description of the process.

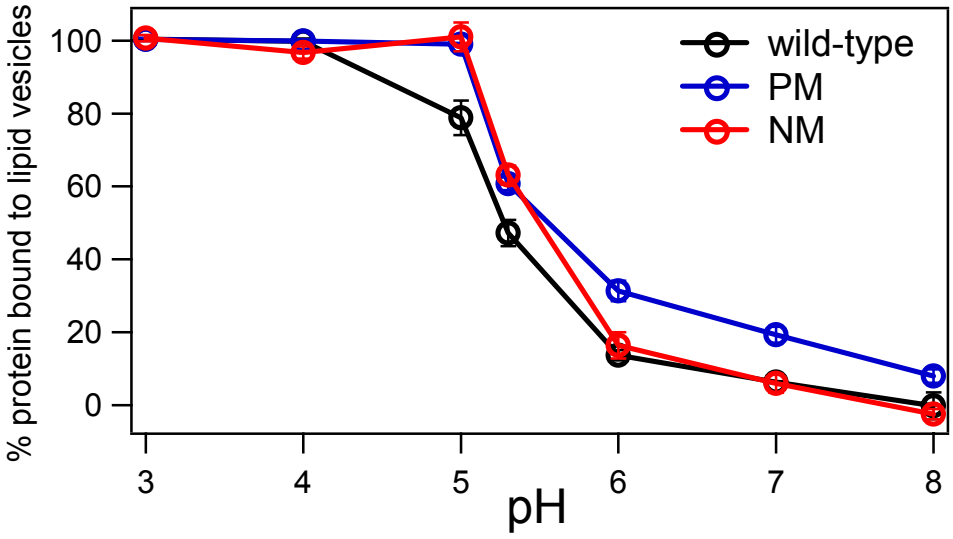

Figure 5.6 Sedimentation assay shows E153Q/D156N to have a pH-dependence profile different from that of the wild-type protein. The lines are drawn just as a guide for the eye and do not represent a fit to any equation.

Reversibility of insertion with pH

Our thermodynamic cycle as depicted in Figure 5.2, assumes the pH-dependent binding of Bcl-X_LΔTM to lipid vesicles is completely reversible, which is rarely the case with membrane proteins. Therefore, we tested whether the pH-dependent binding to lipid vesicles was reversible in order to be able to apply equilibrium thermodynamic equations

to model this system. We tested for the reversibility of Bcl-$X_L\Delta$TM binding to lipid vesicles in two different ways. First, we measured the binding of Bcl-$X_L\Delta$TM to lipid vesicles under different pH conditions using the sedimentation assay. We observed that in a sample of Bcl-$X_L\Delta$TM incubated with lipid vesicles at pH 4.0, we observed almost 100% binding. However, a similar sample that was titrated back up to pH 7.0, displayed almost no binding of Bcl-$X_L\Delta$TM to lipid vesicles. These observations suggest that while almost all of the protein was associated with lipid vesicles at pH 4.0, it was released from the vesicles upon titration back to pH 7.0 (Figure 5.7). This indicated that the process of association mediated by low pH was reversed by increasing the pH back up to neutral conditions. The wild-type and mutants (PM, NM) were all found to be reversibly bound to lipid vesicles at acidic pH conditions.

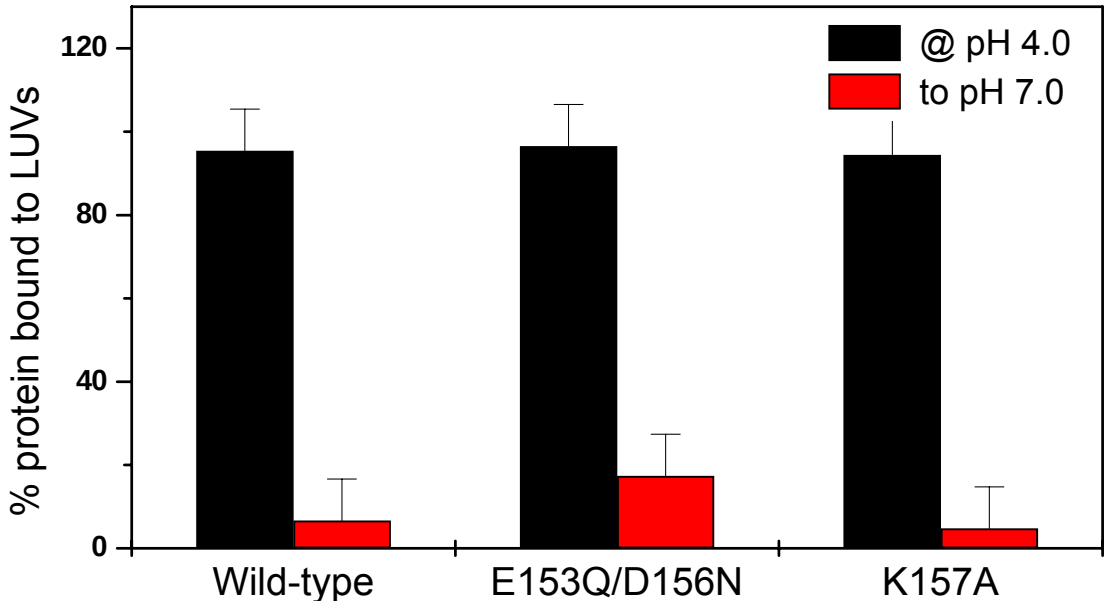

Figure 5.7 Binding of wild-type and mutant Bcl-$X_L\Delta$TM to lipid vesicles is reversible by pH as observed using the vesicle sedimentation assay.

To confirm this reversibility, we prepared an NMR sample of Bcl-$X_L\Delta TM$ in the presence of lipid vesicles and collected a ^{15}N-^{1}H HSQC spectrum at neutral conditions (Figure 5.8a). The sample was titrated down to pH 4.65 by the addition of small amounts of 0.1 of hydrochloric acid and a HSQC spectrum was collected under these acidic conditions (Figure 5.8b). The sample was titrated back up to neutral pH conditions, pH 7.4, and another HSQC spectrum was collected (Figure 5.8c). All the spectra were collected after equilibration for at least two hours under new conditions. An overlay of the three spectra is shown in Figure 5.8d, with the HSQC spectra in Figures 5.8 a, b and c represented as black, red and cyan respectively.

An analysis of the three ^{15}N-^{1}H HSQC spectra indicates the following: (i) The association of Bcl-$X_L\Delta TM$ with lipid vesicles at low pH could be reversed by increasing the pH to neutral conditions (ii) An increase in pH disassociates Bcl-$X_L\Delta TM$ from lipid vesicles and the Bcl-$X_L\Delta TM$ released into solution returns back to its original native structure in solution albeit in a slow process. A comparison of the intensity of resonances in the two samples at pH 7.4 (before and after acidification) indicates that there is a slight reduction (~ 10%) in peak intensity in the sample after acidification. This could be due to three reasons: (i) a decrease in concentration due to a volume increase during titration (ii) a series of ^{15}N-^{1}H HSQC spectra collected on this sample displayed a time-dependent increase in peak intensities suggesting a slow kinetic process (data not shown). (iii) the process is not completely reversible. Based on our observations and understanding the slow kinetics of the process, we think the process is almost completely reversible. This dramatic conformational change that is reversible could be essential for Bcl-X_L to act as a switch controlling the critical regulatory steps in apoptosis.

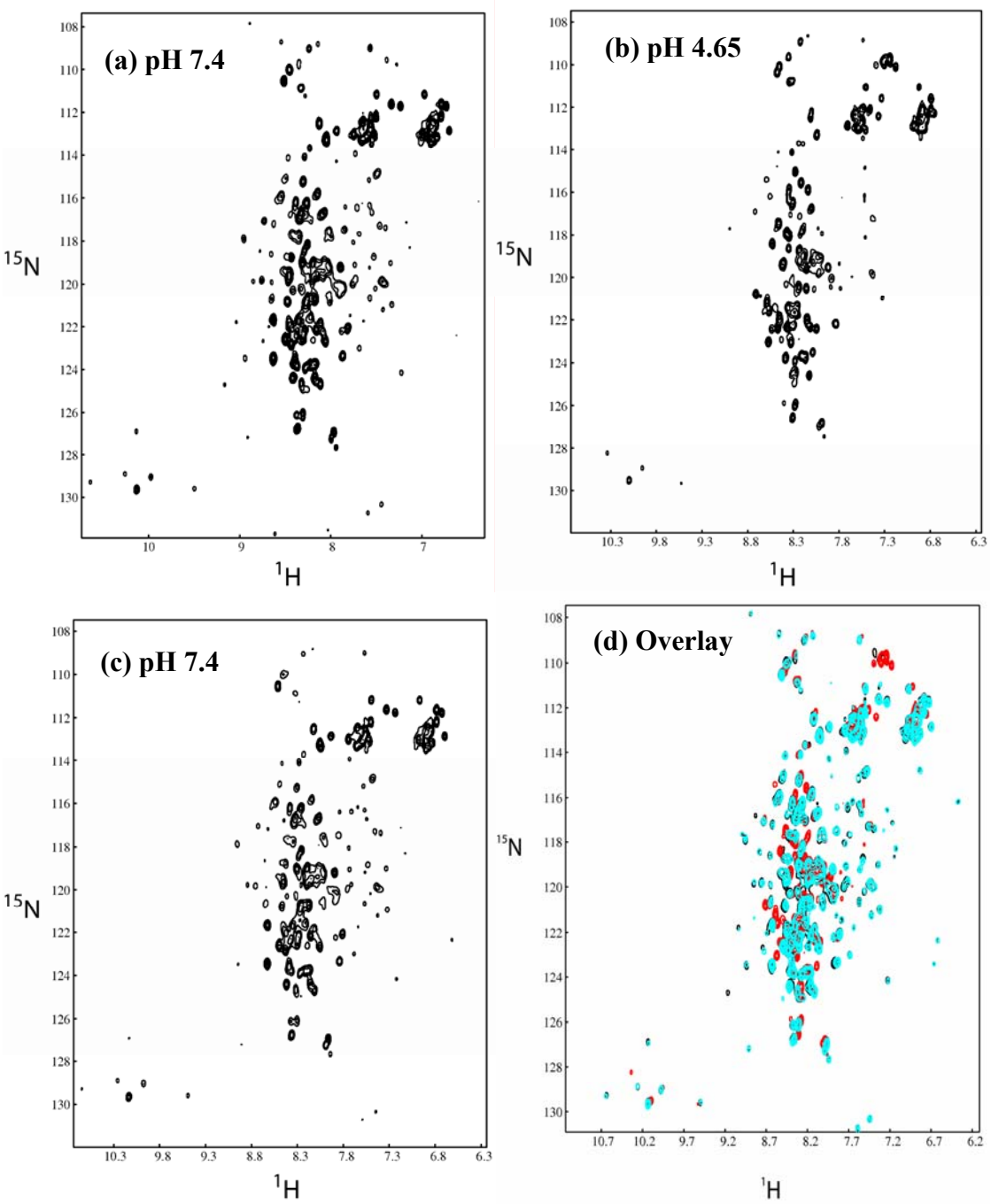

Figure 5.8 Reversibility of Bcl-$X_L\Delta$TM insertion into lipid vesicles as observed using ^{15}N-^{1}H HSQC. The spectra were collected using a P:L ratio of 1:200 with a protein concentration around 60 μM and lipid concentration around 12 mM. Individual spectra are displayed in (a), (b) and (c) and the overlay in (d). The spectrum in (a) and in black in (d) was the first one collected at pH 7.4, the pH was reduced to pH 4.65 by the addition of small amounts of 0.1 N HCl and another spectra was collected and is displayed in (b) and in red in (d). The pH was then increased to 7.4 by the addition of small amounts of 0.1 N NaOH and the spectra collected under these conditions is shown in (c) and in cyan in (d).

Thermodynamic model and data from the vesicle sedimentation assay estimate thermodynamic parameters of the solution-to-membrane conformational change

Having proved the reversibility of the system, we developed the thermodynamic model coupling the protonation equilibrium to the partitioning into the membrane. The important observations about this thermodynamic model (Figure 5.2) are:

(i) there are only three protein populations, two forms in solution, a protonated form and a deprotonated form and one that is bound to the lipid vesicles.

(ii) there is no deprotonation in the membrane bound form.

(iii) the deprotonated form does not bind to the membrane.

The details of this model and the development of the final equation are described in the materials and methods section. The data for the pH dependent binding of the wild-type Bcl-$X_L\Delta$TM to lipid vesicles obtained using the sedimentation assay is now fit to this model using the non-linear curve fitting algorithm (an implementation of the Levenberg-Marquardt algorithm) in Igor Pro.

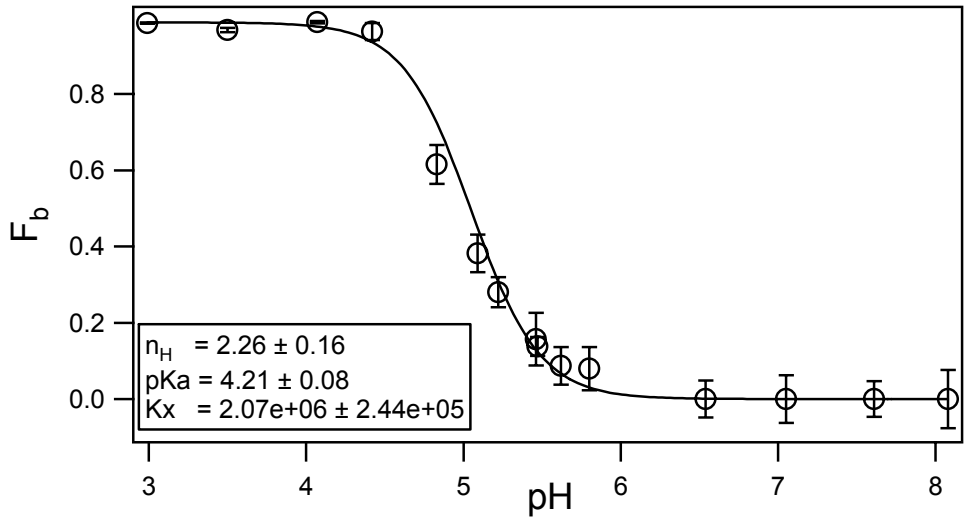

Figure 5.9 Representative data fits to the thermodynamic model described above for wild-type Bcl-$X_L\Delta$TM. Estimated values for the parameters, n_H, pKa and Kx are also displayed on the plot.

The fits (Figure 5.9) generated estimates for the following values when all the parameters were allowed to float, n_H = 2.26, pKa = 4.21 and Kx = 2.07 e^{+06}. Since the value of n_H was around 2, we decided to refine the model to include two protonation sites which are unequal and have different pKa values, pK_1 and pK_2 (Figure 5.4). The details of this model and the thermodynamic equilibria used are discussed in detail in the materials and methods section. The data when fit to the refined model with all the parameters let to float, did not converge to reasonable values for pK_1 and pK_2. This arises from the parameters Kx, pK_1 and pK_2 being interdependent. Therefore, a priori knowledge of at least one parameter is essential to get an accurate description of the other parameters. Fixing the pKa values at reasonable values of pK_1 = 3.9 and pK_2 = 4.3 (assuming the canonical pKa values for exposed Asp and Glu), we obtained reasonable fits to the data (Figure 5.10).

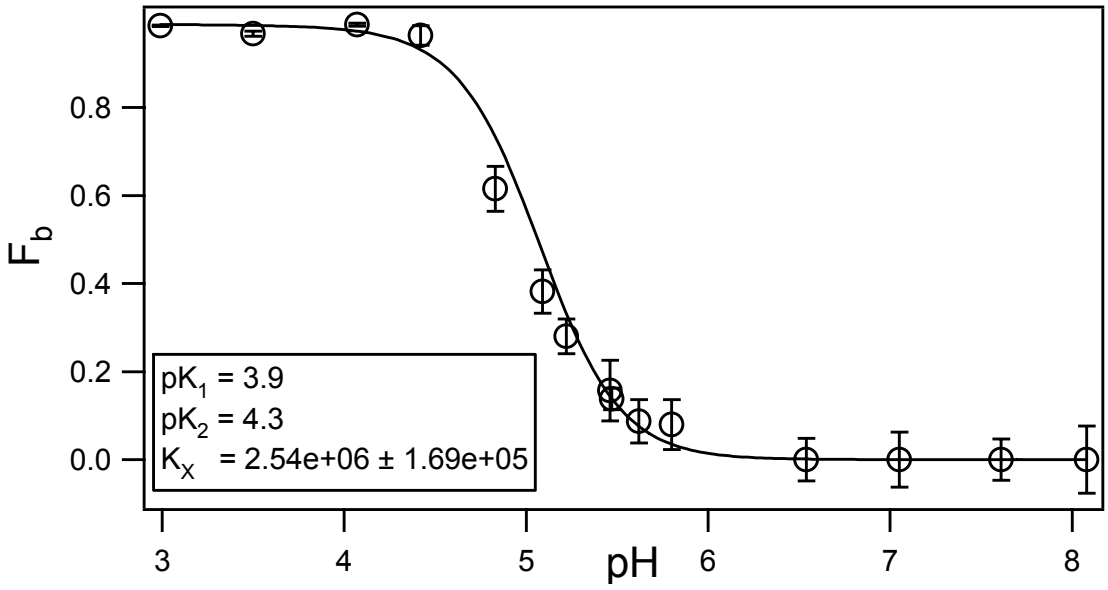

Figure 5.10 Representative data fits to the refined thermodynamic model described above for wild-type Bcl-$X_L\Delta$TM. Estimated values for the parameters, pK_1, pK_2 and Kx are also displayed on the plot.

These fits are still incomplete owing to the inadequacy of the model in explicitly representing the electrostatic attraction between the protein and the membrane surface. A clearer picture will emerge once we have a better understanding of the electrostatic interactions and the protonation equilibria of the key residues at the surface of the membrane.

Electrostatic mutant, PM, inserts even at pH 7.0 and displays increased inhibition of Bax-induced dextran release

To investigate whether the altered pH-dependent binding to lipid vesicles translates into altered membrane insertion properties, we provided protein samples to Dr. Gorka Basanez and a graduate student in his lab at the University of Bilbao, Oihana Terrones to explicitly estimate insertion into membrane layers using the monolayer insertion assay (Figure 5.11). The results from the monolayer insertion assay suggested that at pH 5.0, the wild-type, PM and NM proteins inserted into the monolayer. At neutral pH conditions, there was no insertion of the wild-type and NM, but PM inserted at pH 7.0 suggesting the presence of an electrostatic interaction under neutral pH conditions (data not shown). This observation of insertion at pH 7.0 follows from our observation of binding at pH 7.0 from the vesicle sedimentation assay, but is in contrast with the predictions from MPEx which do not predict insertion of the protein into the membrane under neutral pH conditions.

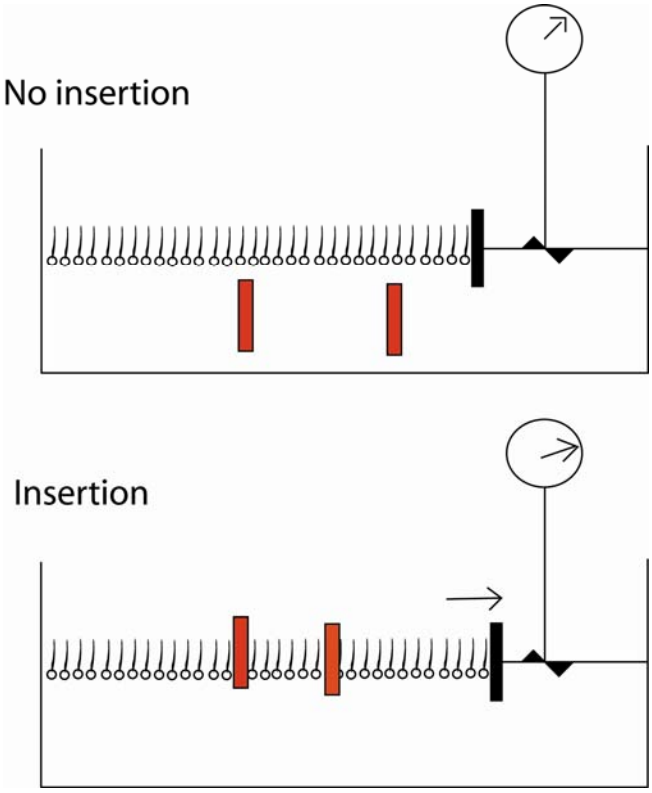

Figure 5.11 A schematic representation of the surface pressure change assay to measure insertion of Bcl-$X_L\Delta TM$ into a lipid monolayer. Upon insertion of the protein (in red) into the monolayer at the air-water interface, there is an increase in surface pressure that indicates insertion.

Since the observations from the monolayer insertion assay confirmed the results from the vesicle sedimentation assay, we hypothesized that the mutation would also alter its potential biological activity at the membrane. We tested this using a biochemical assay that reconstitutes the inhibition of Bax-induced release of cytochrome c from the mitochondria into the cytosol. *In vitro*, this function is tested using a FD-70 dextran release assay, by monitoring the inhibitory role of Bcl-X_L on the Bax (t-Bid activated) induced release of FD-70 from FD-70 encapsulated vesicles (Figure 5.12).

Wild-type Bcl-$X_L\Delta TM$, inhibited the release of FD-70 dextrans as monitored by a decrease in the fluorescence of the non-lipid fraction relative to the control with no Bcl-$X_L\Delta TM$. We also observed that while NM inhibited to the same amount as the wild-type, PM displayed an enhanced inhibition of dextran release relative to wild-type Bcl-$X_L\Delta TM$, suggesting that an alteration of the membrane properties could cause an

apparent anti-apoptotic activity *in vivo*. All these observations taken together suggest the importance of electrostatic interactions between Bcl-$X_L\Delta$TM and the membrane in driving the solution to membrane conformational change and regulating the apparent biological activity.

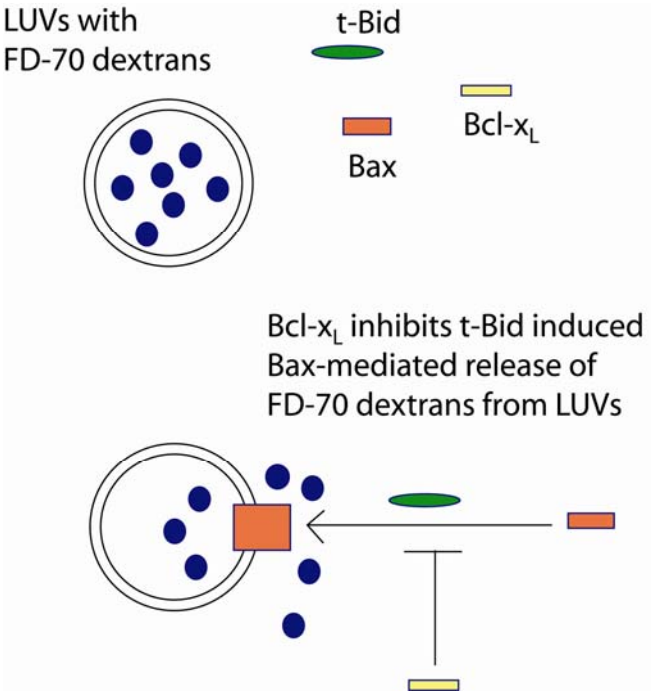

Figure 5.12 A schematic representation of the dextran-release assay to measure the apparent anti-apoptotic activity of Bcl-$X_L\Delta$TM in an *in vitro* context. The release of FD-70 dextrans (blue) from lipid vesicles is caused by the activation of Bax (orange) in the presence of t-Bid (green). Bcl-$X_L\Delta$TM (yellow) inhibites this release, presumably mimicking its effect in preventing cytochrome c *in vivo*.

Discussion

Our previous studies have implicated electrostatic interactions as being able to mediate the binding of the protein to the membrane (Chapter 4). To test this hypothesis, we designed mutants of Bcl-$X_L\Delta$TM that we predicted would have altered electrostatic surface profiles, and tested their ability to bind and insert into lipid vesicles. Our results are consistent with the tip of the hydrophobic helical hairpin engaging in electrostatic interactions with the membrane surface. The structural similarity between Bcl-$X_L\Delta$TM and bacterial toxins like colicins and diphtheria toxin T-domain suggested the importance of the hydrophobic helical hairpin in the membrane insertion process (Lakey et al., 1992; Lesieur et al., 1997; Zakharov and Cramer, 2002b). Using the Membrane Protein Explorer (MPEx) program, we were able to identify charged residues at the tip of the hairpin that were predicted to not affect its partitioning into the membrane. The importance of these charged residues is corroborated by the fact that they are highly conserved among pro-survival members of the Bcl-2 family and diphtheria toxin as shown in Figure 5.13.

```
Bcl-x H.s.  151 - CVESVDKEM - 159
Bcl-x M.m.  151 - CVESVDKEM - 159
Bcl-x R.n.  151 - CVESVDKEM - 159
Bcl-x S.s.  151 - CVESVDKEM - 159
Bcl-x G.g.  147 - CVESVDKEM - 155
Bcl-2 H.s.  158 - CVESVNREM - 164
Bcl-w H.s.  107 - CAESVNKEM - 115
Ced-9 C.e.  185 - MMESVELQG - 193
Ced-9 C.b.  180 - MMESAELQG - 188
AR1   X.l.  142 - CAESVNKEM - 150
AR11  X.l.  123 - CVESANKEM - 131
NR13  C.j.  100 - LAESACEEG - 108
DTX-beta    347 - VGELVDIGF - 355
DTX-omega   347 - VGELVDIGF - 355
```

Figure 5.13 Sequence analysis of the tip of the hydrophobic helical hairpin from various pro-survival members of the Bcl-2 family and diphtheria toxin.

The conserved pattern of charged residues at the tip of the hairpin could be due to its essential role in the electrostatic interactions in mediating insertion into the membrane. Our hypothesis states that the protonation of the negatively charged residues at the tip of the hydrophobic helical hairpin results in the formation of a positively charged surface that could interact with the negatively charged membrane giving rise to the pH-dependent conformational change. This hypothesis is bolstered by an analysis of the electrostatic surface potential of Bcl-X_L (Figure 5.1). The overwhelming negative charge is not at the tip of the hydrophobic helical hairpin suggesting that the surface potential directs the orientation of the protein for a productive interaction between the tip of the hairpin and the membrane surface. The mutants, PM and NM were designed to explicitly test this hypothesis and the expectations were as follows: PM, which displays a more positively charged surface due to the replacement of the two negative charges on E153 and D156, would be able to interact with lipid vesicles even at higher pH conditions where protonation is not expected. NM, on the other hand, with the only positively charged residue removed, will be able to interact with lipid vesicles only when all the negative charges are protonated. The results of the vesicle binding assay suggested that PM displayed a pH profile of vesicle binding as was predicted based on our hypothesis of an electrostatic interaction between the tip of the hydrophobic helical hairpin and the negatively charged membrane surface. However, the other mutant, NM exhibited a pH-dependence profile that was contrary to our expectations. This could be due to its possible involvement in a salt bridge that makes it less valuable to the electrostatic interaction relative to a free charge that readily interacts with a charged membrane

surface. These results suggest that there is a significant electrostatic contribution from the tip of the hydrophobic helical hairpin that was perturbed by the mutation of charged residues to uncharged residues. Similar work on the mutational analysis of charged residues in diphtheria toxin suggested that most mutations were "insensitive", exhibiting pH-titration profiles for membrane association similar to the wild-type (Kaul et al., 1996; Silverman et al., 1994). However, it was also observed that certain mutations like E349K and D352K prevented membrane permeabilization at low pH and also abrogated the biological activity of the toxin in inhibiting protein synthesis (Kaul et al., 1996; Silverman et al., 1994). Interestingly, another mutant, D352N, exhibited diminished pH-dependent membrane permeabilization (assayed by $^{86}Rb^{+}$ release) relative to wild-type while the biological activity was unaffected (Kaul et al., 1996; Silverman et al., 1994). This was explained as due to formation of channels with reduced conductance but at the same rate as wild-type resulting in unaltered biological activity. This data contrasts with our observations, and could be due to the differences in the intracellular localization and biological activity required in vivo for Bcl-X_L and diphtheria toxin. The above statement is corroborated by the observation that the tip of the hairpin of Bax has a profile similar to the E349K/D352K mutant of diphtheria toxin but while the mutant diphtheria toxin does not permeabilize membranes, Bax has been observed to form pores on the membrane capable of causing cytochrome c release.

To understand the pH-dependence of the Bcl-$X_L\Delta TM$ solution-to-membrane conformational change in detail, we built a simple thermodynamic cycle that coupled the protonation equilibrium of ionizable residues on the protein surface with that of the partitioning equilibrium into the membrane. This thermodynamic model requires the pH

dependent insertion into membranes to be reversible. It has been observed with diphtheria toxin that the insertion of toxin into lipid vesicles mediated by a decrease in pH was reversed upon an increase in pH back to neutral pH conditions (Ladokhin et al., 2004). The reversibility of membrane insertion of Bcl-$X_L\Delta TM$ with pH was established using two different methods, a low resolution method using the vesicle binding assay and a high resolution method using NMR. These experiments suggested that upon a decrease in pH, there is a pH-dependent conformational solution from solution to membrane. Returning the pH to neutral conditions causes the membrane inserted protein to return to solution and fold into the native form in solution as observed by NMR. Such reversibility could be important *in vivo*. In the case of Bcl-X_L, a dynamic change in localization from the cytosol to membrane has been observed and might require a reversible association with the mitochondrial outer membrane for a tight control over the critical steps leading up to the initiation of apoptosis (Hsu et al., 1997).

The application of the thermodynamic model to the experimental data has led to an estimation of pKa, Kx and n_H. The estimation of an n_H value equal to 2, suggests that there are two critical residues whose protonation is coupled to the solution-to-membrane conformational change. The slope of the pH-dependence profile is similar for both wild-type and PM suggesting that the E153 and D156 do not play a direct role in modulating the pH dependence. The refined model that assumes two unequal protonation sites is well described using pKa values of 3.9 and 4.3 which are the canonical pKa values for solvent exposed Asp and Glu residues in proteins. However, this could also be due to the coupling between the pKa and Kx values that leads to an incorrect estimation of the thermodynamic parameters.

Since a priori estimation of either Kx or pKa would help in a more accurate description of the other parameter, we have been collaborating with Dr. Diana Murray at Cornell Medical School to use the finite non-linear Poisson Boltzmann algorithm to estimate the pKa values of ionizable groups on the protein when present near the membrane surface.

Previous experiments with salt dependence of binding of Bcl-$X_L\Delta$TM to lipid vesicles (Chapter 4) suggested that there might be a significant hydrophobic contribution to the interaction between Bcl-$X_L\Delta$TM and the membrane. It is possible that Bcl-X_L, in a manner akin to myristoylated proteins like MARCKS etc., exploits electrostatic interactions to provide a regulatory switch that mediates the solution-to-membrane conformational change (McLaughlin and Aderem, 1995). Similar to the myristoylated tail of MARCKS, the C-terminal TM segment of Bcl-X_L could anchor the protein and promote a strong interaction with the membrane but not be enough to insert the protein completely into the membrane until the pH switch triggers insertion.

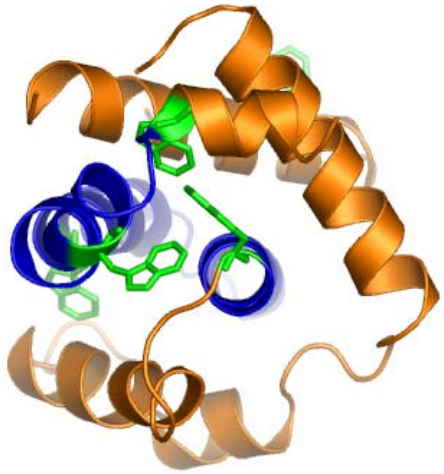

Figure 5.14 Structure of Bcl-X_L showing the positioning of Trp residues (green), especially W137, W181 and W188 that lie at the top of the hydrophobic helical hairpin highlighted in blue.

A closer look at the structure of Bcl-X_L suggests various possibilities for roles of different residues in stabilizing the inserted form. The tryptophan residues are typically found in the interfacial region of the membrane bilayer (the interface between the highly hydrophobic hydrocarbon core and the bulk aqueous solution)

to help stabilize the membrane form. The preference of Trp residues for the interfacial region is due to the balancing effect of the hydrophobic forces that drive it out of water and complex electrostatic forces that stabilize its presence in the hydrated headgroup region (White and Wimley, 1999; Yau et al., 1998). Assuming helices 5 and 6 insert into the bilayer, this would place the three tryptophans, W137, W181 and W188 right at the interface hopefully increasing the stability of the membrane inserted form (Figure 5.14). It is interesting to note that these residues are highly conserved among structurally similar Bcl-2 family members and we believe the conservation is due to their role in stabilizing the biologically relevant membrane form (Figure 5.15). Thus the protein has evolved features that help it exist in two very stable conformations that could be switched from one to the other depending on the biological context.

```
BCLX h.s. 136 NWGRI...IAAWMATYLNDHLEP-WIQENGGW 188
BCL2 h.s. 143 NWGRI...IALWMTEYLNRHLHT-WIQDNGGW 195
BCLW h.s.  92 NWGRL...VQEWMVAYLETRLAD-WIHSSGGW 144
AR1  X.l. 127 NWGRI...IQDWMVTYLETNLRD-WIQSNGGW 179
BAK  h.s. 124 NWGRV...VTRFVVDFMLHHCIARWIAQRGGW 177
BAK2 h.s. 124 NWGRV...VTRFVVDFMLHHCIARWIAQRGGW 177
BAXA h.s. 106 NWGRV...IMGWTLDFLRERLLG-WIQDQGGW 158
BAXB h.s. 106 NWGRV...IMGWTLDFLRERLLG-WIQDQGGW 158
NR13 C.j.  82 NWGRL...LAAALTAYLAEEQGE-WMEEHGGW 134
CED9 C.e. 167 SYGRL...LFVYTSLFIKTRIRNNWKEHNRSW 221
```

Figure 5.15 Sequence alignment of the hydrophobic helical hairpin region of Bcl-X_L with similar regions from other Bcl-2 proteins indicating conservation of the tryptophans.

The results of the monolayer insertion assay were in agreement with the observations from the vesicle sedimentation assay. Wild-type and NM Bcl-$X_L\Delta$TM exhibit an increase in surface pressure (indicating insertion) only at pH 5.0 and not at pH 7.0 as expected. PM does insert at pH 7.0 and at pH 5.0 as suggested by the data from

the sedimentation assay. This alteration in membrane insertion properties also translates to an enhanced inhibitory role for PM in blocking the dextran release induced by t-Bid activated Bax. The results of the dextran release assay that presumably mimics the biological activity of Bcl-X_L to inhibit Bax mediated release of cytochrome c, suggests that the alteration in the membrane association property might play a key role in Bcl-$X_L\Delta$TM eliciting its pro-survival activity *in vivo*. Since at the tip of the hairpin region do not affect the ability of Bcl-X_L to interact with Bax, the increased inhibition of Bax in the dextran release assay by PM suggest that Bcl-X_L might be binding and inhibiting the activity of Bax in the membrane. This is a significant result that confirms the importance of the membrane conformation in apoptosis.

References

Agmon, N. 1995a. The Grotthuss Mechanism. *Abstracts of Papers of the American Chemical Society* 210:328-PHYS.

Agmon, N. 1995b. The Grotthuss Mechanism. *Chemical Physics Letters* 244(5-6):456-462.

Cevc, G., and D. Marsh. 1987. Phospholipid Bilayers: Physical Principles and Models. John Wiley & Sons.

Chapman, D.L. 1913. A contribution to the theory of electrocapillarity. *Philos. Mag.* 25(475.).

Eisenberg, M., T. Gresalfi, T. Riccio, and S. Mclaughlin. 1979. Adsorption of Mono-Valent Cations to Bilayer Membranes Containing Negative Phospholipids. *Biochemistry* 18(23):5213-5223.

Garcia-Saez, A.J., I. Mingarro, E. Perez-Paya, and J. Salgado. 2004. Membrane-insertion fragments of Bcl-xL, Bax, and Bid. *Biochemistry* 43(34):10930-10943.

Gouy, M. 1910. Sur la constitution de la charge électrique a la surface d'un électrolyte. *J. Phys. Theor. Appl.* 9(455-468.).

Hsu, Y.T., K.G. Wolter, and R.J. Youle. 1997. Cytosol-to-membrane redistribution of Bax and Bcl-X(L) during apoptosis. *Proc Natl Acad Sci U S A* 94(8):3668-3672.

Jaysinghe, S., K. Hristova, and S.H. White. 2000. http://blanco.biomol.uci.edu/mpex.

Kaul, P., J. Silverman, W.H. Shen, S.R. Blanke, P.D. Huynh, A. Finkelstein, and R.J. Collier. 1996. Roles of Glu 349 and Asp 352 in membrane insertion and translocation by diphtheria toxin. *Protein Science* 5(4):687-692.

Ladokhin, A.S., R. Legmann, R.J. Collier, and S.H. White. 2004. Reversible refolding of the diphtheria toxin T-domain on lipid membranes. *Biochemistry* 43(23):7451-7458.

Lakey, J.H., J.M. Gonzalez-Manas, F.G. van der Goot, and F. Pattus. 1992. The membrane insertion of colicins. *FEBS Lett* 307(1):26-29.

Lesieur, C., B. Vecsey-Semjen, L. Abrami, M. Fivaz, and F. Gisou van der Goot. 1997. Membrane insertion: The strategies of toxins (review). *Mol Membr Biol* 14(2):45-64.

Losonczi, J.A., E.T. Olejniczak, S.F. Betz, J.E. Harlan, J. Mack, and S.W. Fesik. 2000. NMR studies of the anti-apoptotic protein Bcl-xL in micelles. *Biochemistry* 39(36):11024-11033.

Mclaughlin, S. 1983. Experimental Tests of the Gouy-Chapman-Stern Theory. *Abstracts of Papers of the American Chemical Society* 186(Aug):69-Coll.

McLaughlin, S. 1989. The electrostatic properties of membranes. *Annu Rev Biophys Biophys Chem* 18:113-136.

McLaughlin, S., and A. Aderem. 1995. The myristoyl-electrostatic switch: a modulator of reversible protein-membrane interactions. *Trends Biochem Sci* 20(7):272-276.

Mclaughlin, S., and M. Eisenberg. 1979. Adsorption of Alkali-Metal Cations to Bilayer Membranes Containing Phosphatidyl Serine. *Biophysical Journal* 25(2):A262-a262.

Perrin, D.D. 1963. Buffers of Low Ionic Strength for Spectrophotometric Pk Determinations. *Australian Journal of Chemistry* 16(4):572-&.

Silverman, J.A., J.A. Mindell, A. Finkelstein, W.H. Shen, and R.J. Collier. 1994. Mutational Analysis of the Helical Hairpin Region of Diphtheria-Toxin Transmembrane Domain. *Journal of Biological Chemistry* 269(36):22524-22532.

van der Goot, F.G., J.M. Gonzalez-Manas, J.H. Lakey, and F. Pattus. 1991. A 'molten-globule' membrane-insertion intermediate of the pore-forming domain of colicin A. *Nature* 354(6352):408-410.

White, S.H., and W.C. Wimley. 1999. Membrane protein folding and stability: Physical principles. *Annual Review of Biophysics and Biomolecular Structure* 28:319-365.

Wimley, W.C., T.P. Creamer, and S.H. White. 1996. Experimentally determined hydrophobicity scales for membrane proteins. *Biophysical Journal* 70(2):Tuam1-Tuam1.

Wimley, W.C., and S.H. White. 1996. Experimentally determined hydrophobicity scale for proteins at membrane interfaces. *Nature Structural Biology* 3(10):842-848.

Yau, W.M., W.C. Wimley, K. Gawrisch, and S.H. White. 1998. The preference of tryptophan for membrane interfaces. *Biochemistry* 37(42):14713-14718.

Zakharov, S.D., and W.A. Cramer. 2002. Insertion intermediates of pore-forming colicins in membrane two-dimensional space. *Biochimie* 84(5-6):465-475.

Chapter 6

Conclusions

The observations detailed in Chapters 2, 3, 4 and 5 have led us to propose a model for our current understanding of the solution to membrane conformational change. This model is described in the following figure.

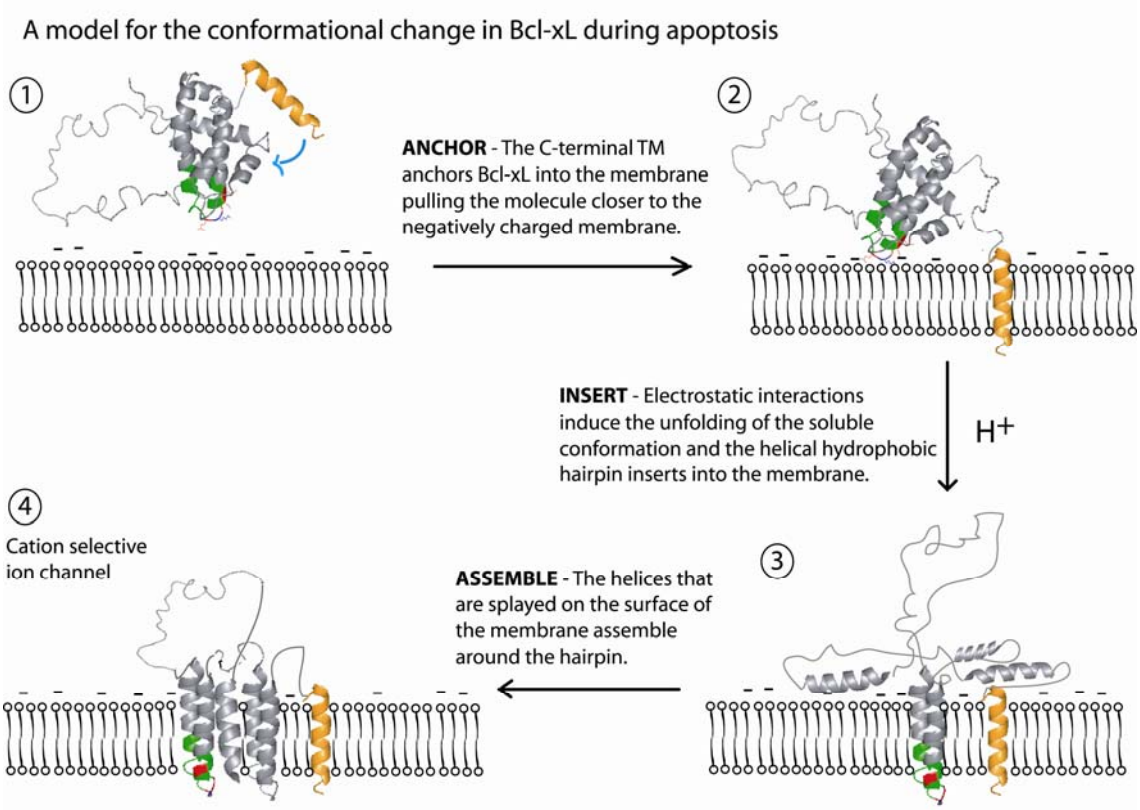

Figure 6.1 A schematic representation of our current understanding of the solution to membrane conformational change of Bcl-$X_L\Delta$TM. This three step process proceeds a solution conformation to a membrane-inserted conformation that functions as an ion channel in the membrane, with the critical step being the second one, the insertion of the hydrophobic helical hairpin forming the umbrella intermediate, #3.

In this model the solution to membrane conformational change is composed of three distinct steps. In the first step, the C-terminal TM segment of Bcl-X_L becomes exposed, resulting in a favorable hydrophobic partitioning into the membrane, thereby anchoring the protein on to the mitochondrial outer membrane. As shown in Chapter 3, this step could be promoted by pH-dependent changes in the dynamics of the loop region preceding the C-terminal TM segment. The second step is a pH-dependent triggering of

the electrostatic switch, which results in an interaction between the protein and the membrane surface. Data presented in Chapter 2 and 4 suggest that this pH-dependence is not due to an acid-induced destabilization of the solution conformation but rather due to a pH-dependent alteration of the electrostatic surface of Bcl-X_L that results in a productive electrostatic interaction between the protein and the negatively charged membrane surface. The shift in the pH profile of the binding of E153Q/D156N mutant, relative to wild-type, suggested electrostatic interactions between the tip of the hydrophobic helical hairpin of Bcl-X_L and the negatively charged membrane surface. The binding energy of this interaction provides the thrust that destabilizes the native solution conformation, exposing the hydrophobic helical hairpin that then inserts into the membrane bilayer to form the "umbrella intermediate". The insertion of the hairpin is inferred from the fluorescence quenching of tryptophans by phospholipids brominated at positions deep in to the bilayer (Chapter 4). The hairpin in the solution conformation has one tryptophan in the middle of helix 6, W169 that would be placed in the environment as suggested by the fluorescence quenching data.

Although our experiments do not explicitly differentiate the intermediate vs. the final membrane-inserted form, we believe that there is an additional step that represents the assembly of the other amphipathic helices of Bcl-X_L around the hydrophobic helical hairpin. This results in the formation of the final membrane inserted conformation, which presumably functions as an ion channel. Although the determination of the oligomeric state of this membrane conformation was beyond the scope of this work, it is worth mentioning that electrophysiological studies have suggested that Bcl-X_L exists as a monomer in the membrane. Although this observation is similar to that of colicins and

diphtheria toxin, it is still difficult to rationalize how a monomer of Bcl-X_L in the membrane would form a pore that would function as an ion channel (Bruggemann and Kayalar, 1986; Peterson and Cramer, 1987; Schein et al., 1978; Slatin, 1988). Bax on the other hand forms an oligomeric membrane conformation that has been observed to conduct ions and other large molecules across the mitochondrial outer membrane (Antonsson et al., 2001b). However, it has been observed that the Bcl-2 proteins alter the properties of the membrane and form lipidic pores (Basanez et al., 2001a; Terrones et al., 2004). It is possible that such an alteration of the membrane might help the protein function as an ion channel in the monomeric form.

The understanding of the steps of this conformational change would be aided by small molecules or other factors that might stabilize the different forms including the intermediate state. Since stabilization of the intermediate state would prevent the solution-to-membrane conformational change, these small molecules would be ideal starting candidates for inhibiting the pro-survival activity of the protein. Thus the intermediate state presents itself as an ideal target for therapeutic intervention. I also believe that these findings will help advance the understanding of molecular features that define structural plasticity of an amino acid sequence being able to adopt a solution conformation and a membrane inserted conformation, modulated by a change in pH.

I would like to wrap things up with a feeling that I have worked on a worthwhile problem and hope that I have lived up to the words of Richard Feynman, who once wrote, "The worthwhile problems are the ones you can really solve or help solve, the ones you can really contribute something to."

References

Antonsson, B., S. Montessuit, B. Sanchez, and J.C. Martinou. 2001. Bax is present as a high molecular weight oligomer/complex in the mitochondrial membrane of apoptotic cells. *Journal of Biological Chemistry* 276(15):11615-11623.

Basanez, G., T.A. Brandt, J.M. Hardwick, and J. Zimmerberg. 2001. Apoptogenic forms of Bcl-x(L) permeabilize pure lipid bilayers through a mechanism sensitive to membrane curvature. *Molecular Biology of the Cell* 12:417A-417A.

Bruggemann, E.P., and C. Kayalar. 1986. Determination of the Molecularity of the Colicin-E1 Channel by Stopped-Flow Ion Flux Kinetics. *Proceedings of the National Academy of Sciences of the United States of America* 83(12):4273-4276.

Peterson, A.A., and W.A. Cramer. 1987. Voltage-Dependent, Monomeric Channel Activity of Colicin-E1 in Artificial Membrane-Vesicles. *Journal of Membrane Biology* 99(3):197-204.

Schein, S.J., B.L. Kagan, and A. Finkelstein. 1978. Colicin-K Acts by Forming Voltage-Dependent Channels in Phospholipid Bilayer Membranes. *Nature* 276(5684):159-163.

Slatin, S.L. 1988. Channels Formed by Colicin E1 in Planar Lipid Bilayers Are Monomers. *Biophysical Journal* 53(2):A155-a155.

Terrones, O., B. Antonsson, H. Yamaguchi, H.G. Wang, J.H. Liu, R.M. Lee, A. Herrmann, and G. Basanez. 2004. Lipidic pore formation by the concerted action of proapoptotic BAX and tBID. *Journal of Biological Chemistry* 279(29):30081-30091.

Guru R Thuduppathy

Mudd Hall #4, 3400 N Charles Street,
Baltimore MD 21218
(443) 854-5018
guru@jhu.edu

EDUCATION

Ph.D. (Biology), Johns Hopkins University, Department of Biology, Baltimore, MD
2000 - 2005

M.S. (Microbial Engg.), University of Minnesota, Bioprocess Technology Institute, Twin Cities, MN
1998 - 2000

B.Tech. (Industrial Biotechnology), Anna University, Center for Biotechnology, Chennai, INDIA
1996 - 1998

HONORS

International Conference for Magnetic Resonance in Biological Systems, **Award for Young Scientists**, 2005.
Biophysical Society, **SRAA (Student research achievement award),** 2004.
Millipore Foundation, **Dmitri V. d'Arbeloff fellowship**, 2002.
Anna University, **University Gold Medal**, 1998.
Jawaharlal Nehru Centre for Advanced Scientific Research, **Rajiv Gandhi Research fellowship**, 1997.
National Council for Education, Research and Training, **National Talent Search Scholarship**, 1992.

RESEARCH EXPERIENCE

Graduate Student, **Advised by Dr. Blake**
September 2000-October 2005
Department of Biology, Johns Hopkins University**,** Baltimore, MD
Research description:

- Initiated and planned this project from conception and discovered that the conformational transition of Bcl-x_L, a clinically important protein, from the solution to the membrane is driven by electrostatic interactions between the protein and the membrane.
- Developed a thermodynamic model that describes the experimental data.
- Designed mutants that have altered membrane binding properties and validated the model.

- Applied extensive biophysical, structural and modeling tools including Circular Dichroism (CD), fluorescence, Nuclear Magnetic Resonance (NMR) spectroscopy, Analytical Ultracentrifugation (AUC) and membrane vesicle (LUV) binding assays to understand the process of conformational transition of Bcl-$x_{L.}$

Graduate Research Assistant, **Advised by Dr. Carston Wagner**
March 1999- August 2000
Department of Medicinal Chemistry, University of Minnesota**,** MN
Research description:

- Initiated this inter-disciplinary project, collaborated with a team of chemists and developed gene-therapy based approaches towards cancer using chemical dimerizers of *E.coli* dihydrofolate reductase.
- Evaluated the activity and efficacy of these dimerizers to bind and dimerize *E.coli* and mouse dihydrofolate reductase using size exclusion chromatography and enzyme inhibition assays.
- Developed an *in vivo* three hybrid based dimerization assay to evaluate dimerization in mammalian cells.

Undergraduate Research Student, **Advised by Dr. Guhan Jayaraman**
January 1998-May 1998
Center for Biotechnology**,** Anna University**,** Chennai INDIA
Research description:

- Worked in tandem with a colleague to develop a computational tool that helped maximize insecticidal crystal protein production from *Bacillus thuringiensis*, an environmentally friendly insecticide against lepidopteran and dipteran insects.
- The metabolic flux analysis tool developed in a MATLAB platform used an understanding of the metabolic pathways of *B. thuringiensis* and *E.coli* to identify the best nutrient sources to maximize protein production.

Summer Research Fellow, **Advised by Dr. Dinakar Salunke**
June- August 1997
Structural Biology Unit, National Institute of Immunology, New Delhi INDIA
Research description:

- Designed and developed peptide mimetics of nucleic acid molecules to help understand the auto-immune response against nucleic acids that result in auto-immune disorders.
- Peptides were developed using Ribonuclease A as the molecular template and their ability to mimic the nucleic acid template was evaluated.

PUBLICATIONS

Carlson JC, Kanter A, **Thuduppathy GR**, Cody V, Pineda PE, McIvor RS, Wagner CR. Designing protein dimerizers: the importance of ligand conformational equilibria. *J. Am. Chem. Soc.* (2003) 1125(6):1501-7.

Thuduppathy GR and Hill RB. Applications of NMR spin relaxation methods for measuring biological motions. *Meth. Enzymol.* (2004) 384:243-64.
Annis, DA et al. An affinity selection-mass spectrometry method for the identification of small molecule ligands from self-encoded combinatorial libraries: Discovery of a novel antagonist of E.coli dihydrofolate reductase. *Intl. J. Mass Spec.* (2004) 238(2):77-83.
Thuduppathy GR and Hill RB. Evidence that Bcl-x_L inserts into membranes by a different mechanism than the structurally homologous, pore-forming domain from Diphtheria toxin. (accepted to *Protein Science*)
Thuduppathy GR, Craig JW, Terrones O, Basanez G and Hill RB. Electrostatics plays a key role in the insertion of Bcl-x_L into membranes. (manuscript in preparation)
Thuduppathy GR, Casares S, Monahan AC and Hill RB. Presence of equilibrium folding intermediates during the folding of the B1 domain of streptococcal protein G. (manuscript in preparation)

ACTIVITIES

2004-2005 **Biophysical Society**, ***member***
2004 **Protein Society**, ***member***
2001-present **Co-founder, Student Seminar Series**, Department of Biology, The Johns Hopkins University
Co-founded a seminar series for students to provide a platform for free discussion of ideas related to the biosciences, including historical, ethical, social, evolutionary and career-oriented perspectives into science.
1997-1998 **Treasurer, Rotaract Club** of A.C. College of Technology, Anna University INDIA
Managed a $2000 budget for the Club and played a pivotal role in organizing an entrepreneurship development workshop for students
1999-2003 **Teaching Assistant**, University of Minnesota & Johns Hopkins University
Taught undergraduate laboratory courses in Biochemistry and Cell Biology. Served as a teaching assistant for the advanced graduate level course on Methods in Molecular Biophysics.

SKILLS

Software : Hold a 2-year Diploma in Software technology and Systems Management from NIIT, India with proficiency in BASIC, Pascal, C, C++, Python and databases
Operating Systems : Windows and Linux platforms
Scientific software : NMRpipe, NMRView, MATLAB, Mathematica, Origin, IgorPro.
Other : MS Office, Adobe Photoshop and Illustrator

Technical : **Upstream processing :**
Setup, configuration and operation of **fermentors (2L) and HPLC** systems.
Broad expertise in **Molecular Biological techniques for protein expression, mutagenesis** and analysis in prokaryotes.

Familiarity with **mammalian cell culture**, genetic manipulation and cytotoxicity assays.

Downstream processing :
Familiarity with **expression and purification** of membrane proteins and proteins that form inclusion bodies.
Expertise in complex **protein purification** techniques including refolding.

Protein chemistry and characterization :
Extensive experience in biochemical and biophysical characterization of proteins using **circular dichroism (CD) spectropolarimetry, fluorescence spectroscopy and calorimetry.**
Expertise in studying protein oligomerization using **Analytical Ultracentrifugation (AUC)**.
Expertise in the application of **Nuclear magnetic resonance (NMR) spectroscopy** based techniques to study protein dynamics and function.

Assay development and modeling:
Experience in scientific modeling exercises including **metabolic, thermodynamic and kinetic** analysis.
Experience in working with **membrane systems** like large unilamellar lipid vesicles and development of assays to quantitate protein binding and insertion into lipid vesicles.
Expertise in protein quantitation and activity assays including **enzymology**.
